Thermal/moisture-related stresses and fracture behaviour in solid wood members during forced drying.

– Modelling and experimental study.

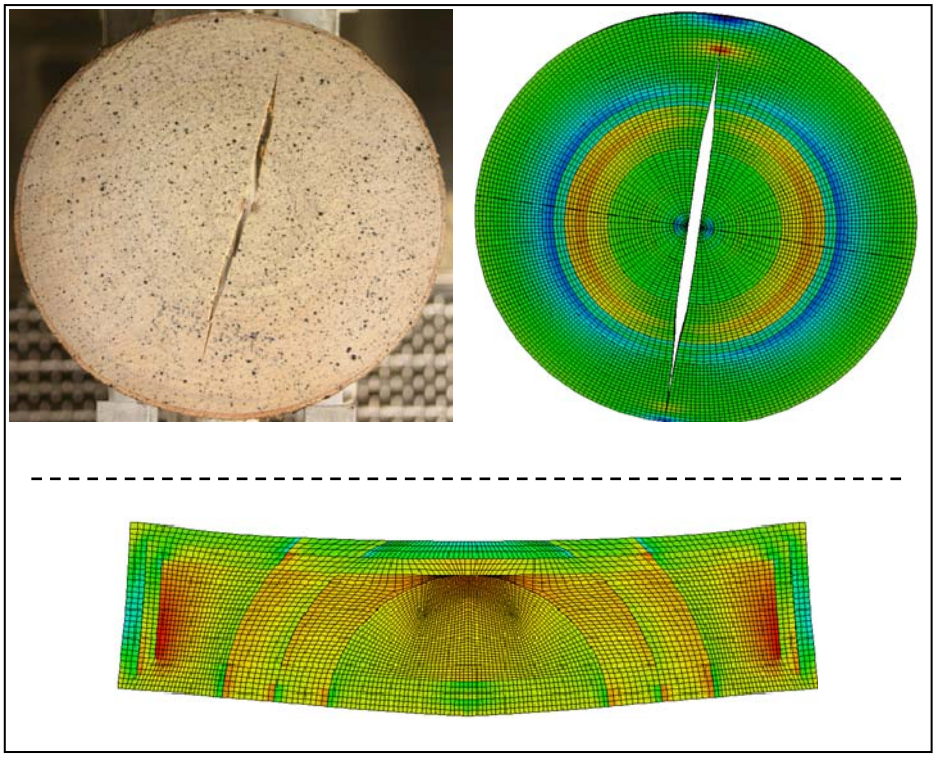

Finn Larsen

Ph.D. Thesis

Department of Civil Engineering
Technical University of Denmark

2012

Thermal/moisture-related stresses and fracture behaviour of solid wood members during forced drying.
– Modelling and experimental study.

Printed by DTU-Tryk
Department of Civil Engineering
Technical University of Denmark
ISBN: 9788778773531
ISSN: 1601-2917
Report no. R-270

Preface

This thesis is submitted in partial fulfilment of the requirements for the Danish Ph.D. degree. The first part introduces the research field, highlights the major findings and provides an overview of the work done, together with a discussion of the results. The second part is a collection of papers that constitute the basis of the work and describe in greater detail the work reported.

Kgs. Lyngby 7st September 2012

Finn Larsen

Preface to published version of thesis

The thesis was defended at a public defence on ?????????. Official opponents were ?????????????, Technical University of Denmark, ????????????????? and ??????????????????????.

A number of minor editorial corrections of the original version of the thesis that was submitted have been implemented and the status of some of the papers on which the thesis is based has changed from submitted to accepted or from accepted to published.

Lyngby, XXth Xxxx 2012

Finn Larsen

Acknowledgement

I gratefully acknowledge the support provided me by my supervising team: associate professor Sigurdur Ormarsson as head supervisor and associate professor John Forbes Olesen as sub supervisor, both from the Department of Civil Engineering, Section for Structural Engineering at the Technical University of Denmark.

I also thank the students, Jesper and Ejnar, who performed tensile strength tests useful for the crack simulations.

I gratefully acknowledge the funding of the project by the Danish Forest and Nature Agency, Haraldsgade 51, 2100 København Ø and the donation from the Velux Foundation of a new and advanced climate chamber that has been highly important for my project by.

I thank Andreas Bergstedt from KU life for the supply of freshly felled Norway spruce logs used in the experimental studies.

Finally, the proofreading of the manuscripts by Robert Goldsmith is greatly acknowledged.

I wish also to thank my family, Annette, Katrine and Sofie for the patience they have shown and the support they have given me throughout the project as a whole and I wish to thank my brother (Poul-Erik) and his wife (Jette) for the moral and practical support they have given during the project.

Abstract

The acclimation and kiln-drying of wood is an important process in the manufacture of all wood products. Those working in the woodworking industry and dealing with the wood used in manufactured products are well aware of the difficulties encountered in the proper removal of the moisture content of wood without injury to the timber itself. When solid wood products are dried from a green condition down to an average moisture content level close to the service life conditions of the final product, significant moisture-induced stresses and related fracturing can occur. The drying stresses arise because of internal constraints that are strongly affected by the annual ring pattern, the moisture gradient over the cross section, differential shrinkage and the inhomogeneity of the material.

The objective of the work reported here was to investigate the behaviour of softwood during drying, in particular the stress and cracking that take place during kiln-drying. Both experimental and numerical work was carried out so as to obtain knowledge regarding stress, strain, mechano-sorption and crack behaviours in wood during drying. The investigations aimed also at revealing how drying damage can best be reduced through appropriable adjustments at the kiln-drying process and identification of the parameters adjustable in this context. Since kiln-drying is usually performed at temperatures of 40 to 90 °C, knowledge of how temperature and moisture affect the elastic, visco elastic and crack behaviours of wood are of paramount importance.

The studies were carried out in several steps, each step providing knowledge used in connection with the further steps, the experimental results being used, for example, for verifying the numerical model, and vice versa. The major highlights of the thesis can be described as follows:

Disc drying was investigated experimentally by measuring the strain field over the cross section as a whole throughout the drying period. A non-contact optical 3D deformation measuring system called Aramis was used to measure the strain field. The strains were measured, along with a drying history that was generated, to verify a model that was used to simulate disc samples of the same type. The stresses were analyzed so as to clarify whether and when critical stress states were encountered during the drying process. The reversibility of the mechano-sorptive strains, i.e. the possibility of driving mechano-sorptive strains back to their original state, was studied then by use of the verified model.

Kiln-drying experiments were carried out, in a specially designed climate chamber under well-defined climatic conditions, allowing the climatic variation limits for crack initiation to be identified. The critical tensile stresses were determined by means of simulations and were compared with the levels of tensile strength found in tests of tensile strength carried out at the same temperature levels. Tensile strength is highly dependent upon the temperature!

Water flux in the tangential and in the radial direction at three different temperatures, and for three different humidities at each temperature, was studied. This provided information regarding the expected drying times under different climatic conditions. In addition data from

these studies were used to simulate three timber boards differing in the location of the pith. The boards behaved quite differently during the drying as regards both deformations and stresses. The variations in the initial (green) moisture content of the timber boards had a significant effect on the final stress state present after drying.

Resumé

Akklimatisering og ovntørring af træ er en vigtig proces ved fremstilling af alle træ produkter. Alle, der er forbundet med træindustrien og med træ i forarbejdede produkter, er ganske klar over de vanskeligheder, der er i fjernelse af vand fra træ uden at skade dette. Når massivt træ tørrer fra en grøn tilstand til et fugtindhold anvendeligt for yderligere forarbejdning, kan fugt-relaterede revner og spændinger forekomme. Tøjninger på grund af tørring opstår på grund af interne deformationsbegrænsninger, som er stærkt afhængig af tværsnittets forskellige svind grundet fugtgradienter og inhomogenitet af materialet.

Formålet med dette projekt er at undersøge nåletræs (softwood) adfærd ved tørring, med fokus på spændinger og revnedannelse ved forceret tørring (kiln drying). Såvel eksperimenter, som numeriske modeller er brugt som værktøjer for at få viden om spændings-, tøjnings-, mechano-sorptive og revne-udviklinger i træ under tørring. Undersøgelserne skal bruges til at belyse hvordan tørringsskader kan reduceres ved justering af tørringsforløbene og til at afdække hvilke parametre, der er justerbare i dette sammenhæng. I forbindelse med forceret tørring, som oftest sker ved temperaturer mellem 40 og 90 °C, er kendskab til temperatur og fugtafhængige elastiske, mechano-sorptive og revnemæssige egenskaber af afgørende betydning.

Undersøgelserne blev foretaget i flere trin, hvor hvert trin afdækkede viden, som blev anvendt til de næste trin, hvor eksperimentelle resultater bruges til at verificere numeriske modeller og vice versa. Denne afhandlings væsentligste hovedpunkter er:

Træskivers tørring blev eksperimentelt undersøgt ved måling af hele skivers tøjningsfelt i hele tørringsperioden. Et kontaktfrit optisk 3D deformations målesystem, kaldet Aramis, blev anvendt til at måle tøjningsfeltet. Målingerne af tøjninger blev, sammen med en genereret tørringshistorik, brugt til at verificere en model, der simulerede samme tørringsforløb. Spændinger blev uddraget af simuleringerne og analyseret for at belyse hvorvidt og hvornår kritiske spændingstilstande optræder under et tørringsforløb. Med den verificerede model blev reversibiliteten af mechano-sorptive tøjninger undersøgt, dvs. evnen til at føre tøjninger tilbage til oprindelig tilstand.

Forcerede tørringsforsøg blev udført i veldefinerede klimatiske forhold i et specieldesignet klimakammer, hvor de klimatiske grænser for revnedannelse blev identificeret. Ved simuleringer blev de kritiske trækspændingen fundet og sammenholdt med brudstyrker fundet ved trækforsøg under samme temperaturforhold: Trækstyrken er stærk afhængig af temperatur!

Undersøgelse af nåletræets tørringshastighed (vand fluks) i tangentielle og radial retning er undersøgt ved tre forskellige temperaturer og tre forskellige luftfugtigheder ved hver temperatur. Resultatet fra disse undersøgelser giver information om forventede tørringstider ved forskellige klimatiske forhold. Derudover blev oplysningerne fra disse undersøgelser brugt til at simulere tørring af tre planker, hvor marven lå forskellige steder. Plankerne opførte sig vidt forskelligt både deformations og spændingsmæssigt. Tørringsforløbet blev

derved forskelligt ved de tre modeller og variationen af begyndelsesfugt i tømmer har stor indflydelse på den endelige spændingstilstand i træet efter tørring.

List of Symbols

The following is a list of the symbols employed in the thesis in the order they are presented:

Symbols	Unit	Description
FSP	%	Fibre saturation point, the maximum amount of chemically bounded moisture that can be contained within the cell walls.
MC	%	Moisture content of the wood.
EMC	%	Equivalent moisture content, the acclimatized MC.
RH	%	Relative humidity, the percentage of saturation of the humidity.
SVD	g/m^3	Saturated vapour density.
VD	g/m^3	Vapour density in the air.
SVP	Pa	Saturated vapour pressure.
T, T_c	°C	Temperature in degrees Celsius.
T_0	°C	Reference temperature, 20 °Celsius.
m	g	Mass of the wooden sample, including both the wood and the moisture mass.
m_0	g	Oven dried mass of the wood.
w_{f0}		Fibre saturation point at 20 °C.
w_{f0}	$°C^{-1}$	Parameter describing the effect of the temperature on FSP.
h		Relative humidity.
K, K_1, K_2, W		Hailwood and Horrobin coefficients.
E_l, E_r, E_t	MPa	Elastic moduli in the longitudinal, radial and tangential directions.
G_l, G_r, G_t	MPa	Shear moduli in the longitudinal, radial and tangential directions.
E_{l0}, E_{r0}, E_{t0}	MPa	Basic elastic moduli in the longitudinal, radial and tangential direction.
$G_{lr0}, G_{lt0}, G_{rt0}$	MPa	Basic shear moduli in longitudinal, radial and tangential direction.
E_{lT}, E_{rT}, E_{tT}	$°C^{-1}$	Parameter describing the effect of temperature on the elastic moduli.
$G_{lrT}, G_{ltT}, G_{rtT}$	$°C^{-1}$	Parameter describing the effect of temperature on the shear moduli.
E_{lw}, E_{rw}, E_{tw}	MPa	Parameter describing the effect of moisture on the elastic moduli
$G_{lrw}, G_{lrw}, G_{rtw}$	MPa	Parameter describing the effect of moisture on the shear moduli
ν_{lr}, ν_{lt}, ν_{rt},		Poisson's ratios
m_{l0}, m_{r0}, m_{t0}	MPa^{-1}	Basic mechano-sorption parameters in the longitudinal, radial and tangential directions.
$m_{lrw}, m_{ltw}, m_{rtw}$	MPa^{-1}	Basic mechano-sorption parameters in shear.
m_{lT}, m_{rT}, m_{tT}	$°C^{-1}$	Parameter describing the effect of the temperature influence on mechano-sorption behaviour
$m_{lrT}, m_{ltT}, m_{rtT}$	$°C^{-1}$	Parameter describing the effect of the temperature on mechano-sorption behaviour.
α_l, α_r, α_t		Shrinkage coefficients in the longitudinal, radial and tangential

		directions.
ε, ε_e, $\varepsilon_{w\sigma}$, ε_w		Total, elastic, mechano-sorptive and moisture strains.
G_F	J/m^2	Fracture energy.
w	mm	Crack opening.
w_c	mm	Ultimate crack opening.
f_t	MPa	Tensile strength.

Symbols	Unit	Description
f_b	MPa	Tensile strength when changing from micro-cracking to fibre-bridging.
σ	MPa	Stresses.
v	kg/m^{2}h	Water flux.
A	m^2	Area, surface area.
t	min,h	Time in minutes or in hours.
ρ	kg/m^3	Density.

		Important indices
$_l$		Longitudinal direction.
$_r$		Radial direction.
$_t$		Tangential direction.

Additional work:

Larsen F., Ormarsson S. and Olesen J.F.:
"Experimental study of moisture-driven distortion and fracture in solid wood"
Proceedings of the 11th International IUFRO Wood Drying Conference, 2010. 137-144, Luleå University of Technology, Skellefteå, Sweden.

Larsen F., Ormarsson S. and Olesen J.F.:
"EXPERIMENTAL INVESTIGATION OF MOISTURE DRIVEN FRACTURE IN SOLID WOOD"
Proceedings of the 11th World Conference on Timber Engineering, 2010. 449-451, Riva del Garda, Italy.

Larsen F. and Ormarsson S.
"A NUMERICAL AND EXPERIMENTAL STUDY OF STRESS AND CRACK DEVELOPMENT IN KILN-DRIED WOOD"
Proceedings of the 12th World Conference on Timber Engineering, 2012.
Auckland, New Zealand.

Part 1

Introduction and summary

Chapter 1

1. Introduction

1.1 Wood drying in general

Wood was probably the first material used by man for construction purposes. With use of it, shelters were built, simple benches and tables were made and trees were cut down and placed across a stream to form the first bridge. Vessels were built of wood materials, for transporting people and materials along and across both rivers and seas; thus down through the ages and on to the present time, wood has continued to be one of the most widely used materials of all.

Lack of knowledge regarding its use, nature and functionality still exists, however, despite wood having been in use for so long and so universally. Accordingly, it is sometimes treated and used in a faulty and wasteful manner. One reason for this imperfect use lies in the fact that wood has a complicated and variable structure, such that one piece can behave quite differently from another, even if they are both cut from the same tree. The butt cut differs, for example, from the cut of the top log; the heartwood differs from the sapwood, et cetera. Also, the way in which the tree is cut, dried and kept affects both the behaviour and the quality of the wood product.

Although the importance of drying wood before using it to manufacture objects was recognized very early, the drying techniques employed were for centuries limited to air drying and sand drying, which were very slow and highly uncontrollable processes. Near the end of the 17th century, methods for accelerating the drying process making use of solar panels were discovered and were employed on a small scale, but it was not until the beginning of the 18th century that kiln-drying systems involving use of heated chamber were built and were employed on a larger scale. Many different drying techniques have since been developed to accelerate the drying process, ranging from the dipping of wood into boiling oil, to the use of pressure, electric induction, microwaves, freezing processes, compression, heated air or the presence of a vacuum, for example, and various combinations of these methods, (see e.g. [9]).

The choice of drying methods often depends on the wood species involved, the sizes and quantities of items, facilities and energy resources available. Methods suitable for one species may damage other species and vice versa, large items and large quantities often requiring large facilities, and the costs of the energy source available for heating can markedly affect the drying methods selected. Damaged wood with visible growth defects, such as cracks,

loose or large knots, rottenness, the presence of foreign objects or damages caused by insects are normally sorted out as soon as discovered, already before a drying process has started, the attempt being made in this way to only use drying energy for the drying of sound products. Moisture-induced defects, such as fractures, cracks and lack of shape stability in solid wood products, that come about during the drying process can likewise cause material losses, through material of this sort needing to be sorted out after drying has been completed. Thus, defects detected after drying can represent either already existing, but hidden or undiscovered failures that first become visible after drying, or defects caused by how the drying process was carried out.

Manufactures are concerned about the manner in which their timber is treated after felling. This includes the felling of the trees, handling them, then cutting them into timber logs, the sorting of logs prior to sawing, the sorting of boards after sawing, the drying process and further treatments and processing of the solid timber before storing or delivering it to customers. The drying process is probably the most critical phase in the manufacture of solid wood products. Knowledge regarding it is to a large extent based on experience collected over the centuries in working with wood drying. As requirements that wood products become more uniform in quality were gradually raised, well-defined kiln-drying systems were developed and drying-schedules designed for particular species were adjusted to the specific kiln-drying systems involved; see e.g. [54]. Various systems and schedules are developed in efforts to reduce waste due to distortions and cracks, yet even with centuries of experiences, cracks are apparently still inevitable. Cracking caused by kiln-drying of solid timber is extremely difficult to predict due to the strong orthotropic and non-homogeneous characteristics of the material in combination with considerable numbers of microscopic defects that can act as crack initiators.

The nature and the behaviour of wood exposed to kiln-drying and to climate changes in general are still not fully explored, but efforts are being made to further research and expand knowledge in this field.

1.2 **Study motivation**

Softwoods, such as Scots pine (Pinus sylvestris) and Norway spruce (Picea abies) are by far the two most common wood species in northern Europe. For example, approximately 80-85 % of the forests in Sweden consist about an equal extent of pine and spruce, and Swedish sawmills produce between 15 to 18 mill m^3 of sawn timber yearly; (see [53]), about 66% of the forests in Germany and 75% of those in Poland consist of these two species, and 2.6 mill m^3 of wood are felled yearly in Denmark, half of this being used as firewood or for paper production. Besides Denmark's own production of wood, approximately 7-8 mill m^3 of wood are imported yearly, large parts of this being softwood used as construction wood and for furniture manufacture. This large amount of natural material will also serve in the future as an important building material, as well as a material for use in the furniture industry, where it is important that wood material be free of defects, cracks or distortions. The drying process is a major cause of cracking and distortions in structural timber. Research regarding this process

is highly relevant and questions concerning it are far from fully explored. The thesis work deals with stresses, distortions and crack propagation caused by drying. The wood species studied is Norway spruce, which is highly representative of softwood generally.

Knowledge of how changes in moisture can generate stresses in wood is of great importance when constructions of wood are analysed, particularly since such stresses can be considerable intensity and be critical additions to the stresses that already exist from external loads on the constructions involved.

1.3 Research methods

The research presented in the thesis involved a combination of modelling and experimental work. The experimental results are used both to accumulate input for the modelling work and to verify the finite element model [37]. In addition, the verified model is used to trace the development of stress, strain and cracks in timber log discs during drying. The results of this combined work are then used to simulate the drying stresses of solid timber boards. These boards have strong initial moisture gradients under green conditions and completely different pith locations.

1.4 Structure of the thesis (aim and scope of the study)

The thesis is based on experimental and modelling work dealing with the drying of softwood, work carried out by the author, and supplemented with the help of two students who carried out experimental investigations of some of the model parameters. The aim of the thesis is to contribute to a better understanding and an optimization of the kiln drying of wood, to develop existing stress models further and to enhance already existing knowledge within this research field. The levels of the studies possible within the area of moisture and moisture related deformation and stresses in wood are many, as shown in Figure 1.1, these ranging from the microscopic level to the structural and product level. The thesis work deals primarily with clear wood and with different structural levels during the kiln drying of wood.

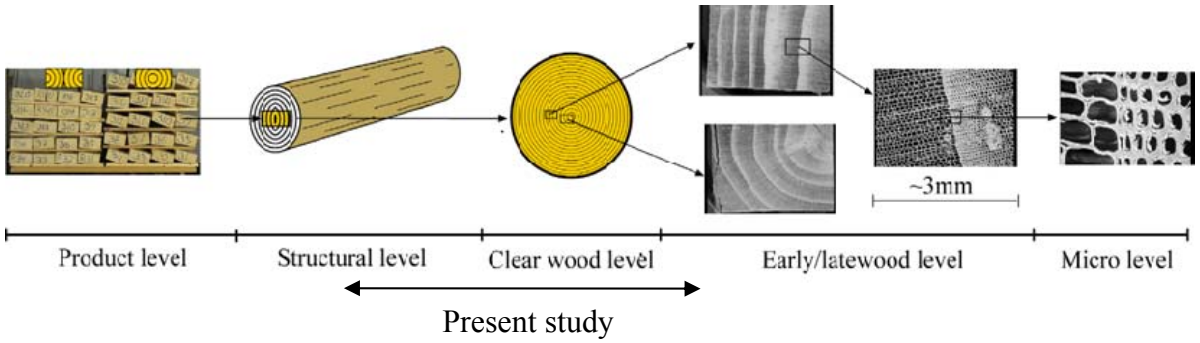

Figure 1.1: *Different levels of research in the field, indicating the relative scope of the present study.*

Part I of the thesis contains seven chapters and five appendices, whereas Part II consists of four appended Papers. Chapter 1 provides a brief and general account of wood drying in a history perspective, the reasons for undertaking the present research and an overview of the thesis itself. Chapter 2 is a summary of research done in the field of wood drying, a general description of softwood and a summary of how variations in climatic conditions affect the moisture content of softwood. Chapter 3 provides a description of the model parameters used in the simulations, of the simulated geometries employed and of the manner in which experimental results are used to generate data for the modelling work. Chapter 4 is a description of the experimental specimens and of the setup used in the experiments. Chapter 5 presents the results of the experiments, of the simulations carried out, and of the combination of the different research approaches employed; determination of the moisture content over a cross section, determination of tangential tensile strength, model verifications, the study of stress crack development in discs during drying, determination of the water flux above the fibre saturation point, study of the dependency at results on the climatic conditions present, and simulations of the kiln-drying of timber boards having different annual ring patterns. Chapter 6 presents the conclusions based on the results. Chapter 7 presents various proposals for future work. The appendices contain supplemental materials, such as an account of different crack testing methods, of tangential tensile strength measurements, various data from the climate chamber and matter of critical stresses and related MC values.

Chapter 2

2. Softwood – basic features

This chapter provides a general account of the internal structure of the softwood material, the moisture content of wood and of the effect of climatic conditions in the surroundings on the moisture content of timber. Most focus is on wood drying and on kiln drying in particular.

2.1 Softwood

The stem of a tree has three physical functions, those of supporting the crown, conducting minerals upwards from the roots to the crown, and storing manufactured nutrients until these are needed. Whereas the entire stem contributes to the support of the crown, the outer circumference is the only part used for conduction and storage. This part is referred to as sapwood, whereas the remaining part is referred to as heartwood, (see Figure 2.1).

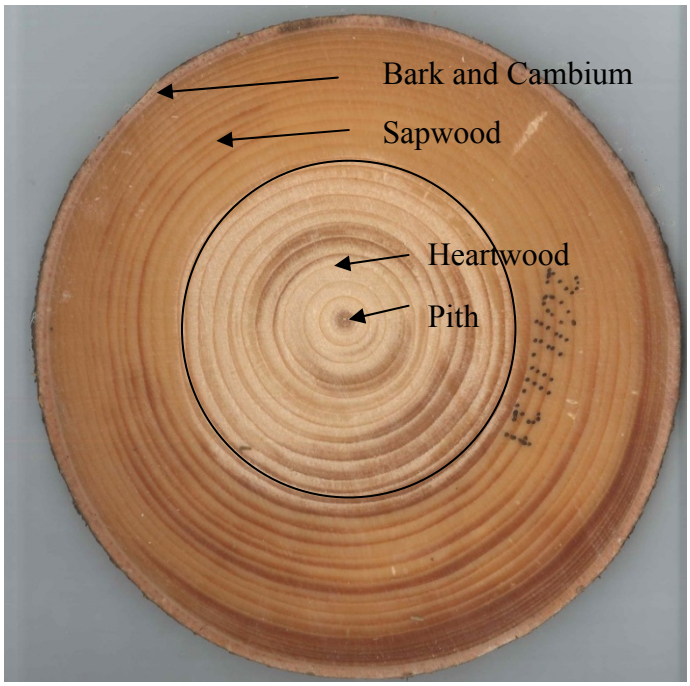

Figure 2.1: *The cross section of a softwood stem.*

Wood consists of wood cells that primarily are cells orientated in the longitudinal direction, often referred to as tracheids. Their function is to support the stem and make fluid transport from root to crown possible. Another type of cells radiates from the pith to the bark, those cells being referred to as ray cells; their function is mainly to store nutrients. The tracheids themselves being in the form of long hollow fibres, the cell walls having pits in both the radial and the tangential direction, the major part of these being oriented in the tangential direction. The pits and the ray cells allow fluid transport in tangential and radial directions to take place, whereas longitudinal fluid transport occurs through pits in the ends of the tracheids; see Figure 2.2. The radial growth of a tree takes place in a thin cambium layer between the outer periphery of the wood stem and the bark. During the growth period, the cambium produces wood fibres inwards and bark cells outwards. The wood fibres form cylindrical layers of varying density dependent upon the growth season; usually one earlywood and one latewood layer are produced yearly, the latewood normally being of higher density than the earlywood.

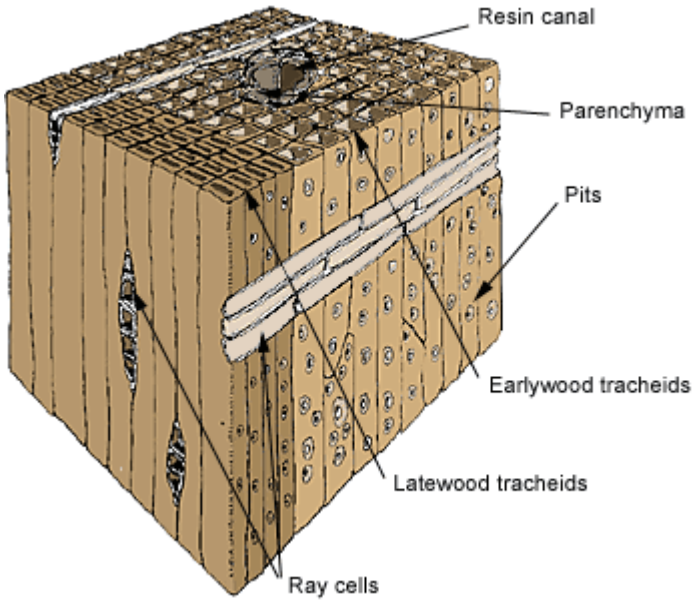

Figure 2.2: *The cell structure of softwood,* [**43**].

2.1.1 The moisture content of wood

A newly felled tree stem (green wood) consists of a considerable amount of moisture, the weight of which often exceeds the weight of the solid material. The weight of the moisture in green sapwood can be double the weight of the dry wood material. The moisture in green wood consists of free and chemically bound water, the free water being stored in the cavity of the cells and the chemically bound water being in the cell walls. The fibre saturation point (FSP) is defined as the state of the moisture content (MC) in which the wood material is saturated by chemically bound water located in the cell walls but has no free water in the cell lumen; see Figure 2.3. The MC at FSP is approximately 30% at a temperature of 20 °C. The bound water is more difficult to remove from the wood during drying. The wood material shrinks, for example, when the bound water is in the process of leaving the cell wall, whereas

the shape of the wood is unchanged during removal of the free water. The size and shape of all timber products are thus dependent upon the MC below FSP.

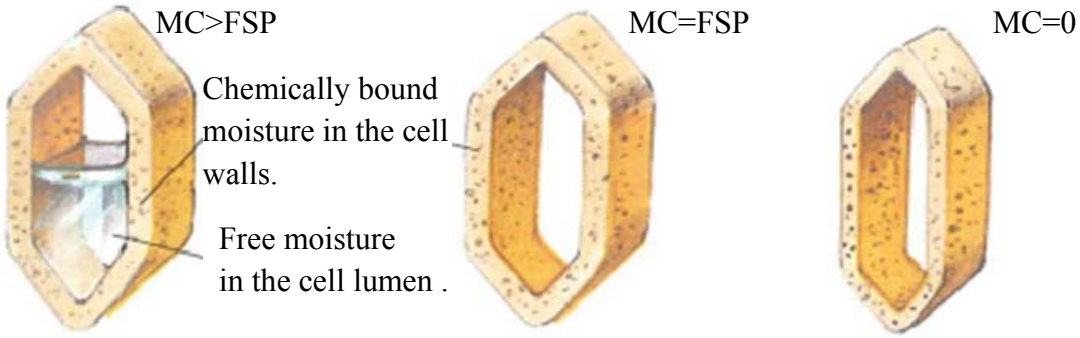

Figure 2.3: *Schematic diagram showing the free and the bound water in wood cells,* [54].

2.2 Climatic conditions and the moisture content of wood

Climate (the air temperature and the humidity), ventilation around the surfaces of the material and timber geometry are some of the important factors that affect the wood drying process. The climatic condition under which wood is dried has a major effect on the drying velocity, the moisture gradients and the moisture level of which the moisture content stabilises (equilibrium moisture content [EMC]).

2.2.1 Relative humidity (RH)

The amount of water vapour in the air at any given time is usually less than that required to saturate the air. The relative humidity [RH] is the percentage of saturated humidity, often calculated in relation to the saturated vapour density [SVD]. The saturated vapour density is a concept closely tied to the saturated vapour pressure. It is useful for getting the exact quantity of water vapour in the air from the relative humidity RH. Given an RH percentage, the density of water in the air is given by RH • SVD = Vapour Density [VD]. Alternatively, RH can be found by RH = VD/SVD. Since RH is a percentage, VD can be given in different units as [g/m^3] or [kg/m^3]. For temperatures below 125 °C, SVD can be approximated from the saturated vapour pressure [SVP] by the ideal gas law: $PV = nRT$, where P is the pressure [Pa], V is the volume [m^3], n is the number of moles, which is related to density by $n = M/m$, where M is the mass of water present and m is the molar mass of the water (18.01528 g/mol), R is the gas constant (8.3145 J/mol K) and T is the temperature. Thus, setting V equal to 1 m^3, the density is found as $P*m/(R*T) = M/V$ = density. Correlations between the saturated vapour densities and the temperature were obtained through experiments. [20] summarised results obtained in atmospheric pressure and made a fitting equation for SVD as

$$SVD = 6.335 + 6718 \cdot T_C - 2.0887 \cdot 10^{-2} \cdot T_C^{\,2} + 7.3095 \cdot 10^{-4} \cdot T_C^{\,3} \qquad (2.1)$$

where T_C is the temperature in [°C]. The vapour densities at different RHs and the temperatures can be calculated on the basis of an extension of eq. 2.1. Figure 2.4 shows the variation of VD with the temperatures for selected RHs.

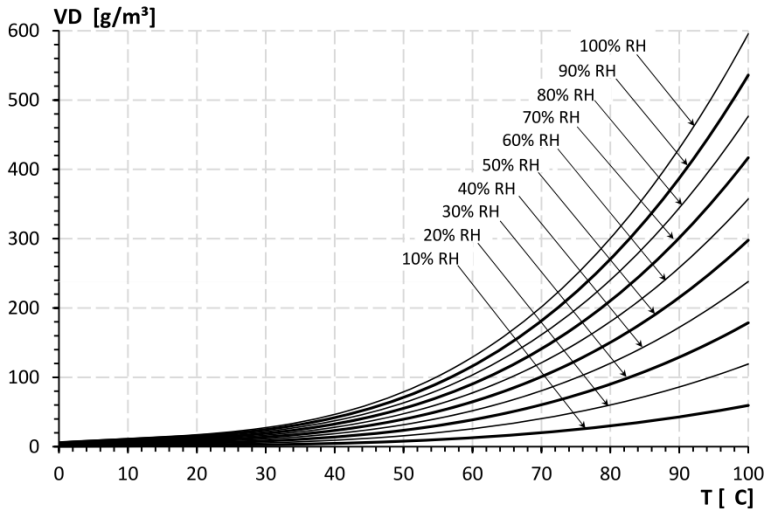

Figure 2.4: *Relationship between the vapour density and the temperature at different relative humidities,*[**54**].

For a constant RH, the VD increases markedly when the temperature rises. For RH=90%, for example, VD is 16 g/m^3 at 20 °C, 116 g/m^3 at 60 °C and 387 g/m^3 at 90 °C. The temperatures involved are highly important for evaluating a drying process, partly because of the material properties being depended upon the temperature and partly because of the drying costs. The costs of a drying process consist of the consumption of water needed to establish the humidity arrived at, the energy consumption needed to heat the wood, air and water, the energy needed to evaporate the water, the energy loss caused by convection to the surroundings, and the costs of the ventilation needed to remove the moisture. Although the drying costs are not discussed further in the thesis, these must be borne in mind in designing drying schedules. The temperature-dependent properties involved are discussed in the thesis.

2.2.2 Moisture content (MC) and fibre saturation point (FSP)

The MC is defined as

$$MC = \frac{(m - m_0) \cdot 100}{m_0} [\%] \tag{2.2}$$

where m is the moist mass of the sample and m_0 is the oven dried mass it has. The FSP is defined as the moisture content of the material when all of the free water is gone and the cell walls are saturated with bound water. This point is found to be dependent upon the temperature of the material. The temperature dependence on the FSP is given, on the basis of [7] or [43] by

$$FSP = w_{f0}\left(1 + w_{fT}\left(T_0 - T\right)\right)\cdot 100 \quad [\%] \tag{2.3}$$

$$FSP = 0.3 - 0.001\left(T - T_0\right)\cdot 100 \quad [\%] \tag{2.4}$$

[7] as defined in eq. (2.3), and on basis of [43] being defined in eq. (2.4), where T_0 is the reference temperature 20 °*C*, T is the actual temperature in [°*C*], w_{f0} is the fibre saturation point at T_0, and w_{fT} is the parameter describing the effects of the temperature on FSP. If the parameters are such that w_{f0}=0.3 and w_{fT}=$3.3\cdot10^{-3}$ $°C^{-1}$, the two equations are identical. The effect of the temperature on FSP is illustrated in Figure 2.6.

2.2.3 Equilibrium moisture content (EMC)

Wood is a hygroscopic material having the ability to take in or give off moisture in the form of vapour. The moisture content of wood depends on the RH and on the temperature of the air surrounding it. The moisture content of a wood material, if it remains in a constant climate long enough, comes into equilibrium with the climate. This moisture state value is known as the equilibrium moisture content (EMC). Thus, every combination of temperature and RH has an associated EMC value. An equation from [45] is given in eq. (2.5), where EMC is given as a function of the temperature and the humidity

$$\mathrm{EMC} = \frac{1800}{\mathrm{W}}\left(\frac{Kh}{1-Kh} + \frac{K_1Kh + 2K_1K_2K^2h^2}{1 + K_1Kh + K_1K_2K^2h^2}\right) \tag{2.5}$$

where EMC is in [%], h is RH, W=349+1.29T+0.0135T^2, K=0.805+0.000736T-0.00000273T^2, K_1=*6.27-0.00938T-0.00303T*^{2}, K_2=*1.91+0.0407T-0.000293T*^{2} and T is the temperature in (°C), W, K, K_1 and K_2 being coefficients based on modelling work done by [20]. The relationship between EMC, RH and the temperature is shown in Figure 2.5. Other equations describing the same relations were developed by Day and Nelson in 1965.

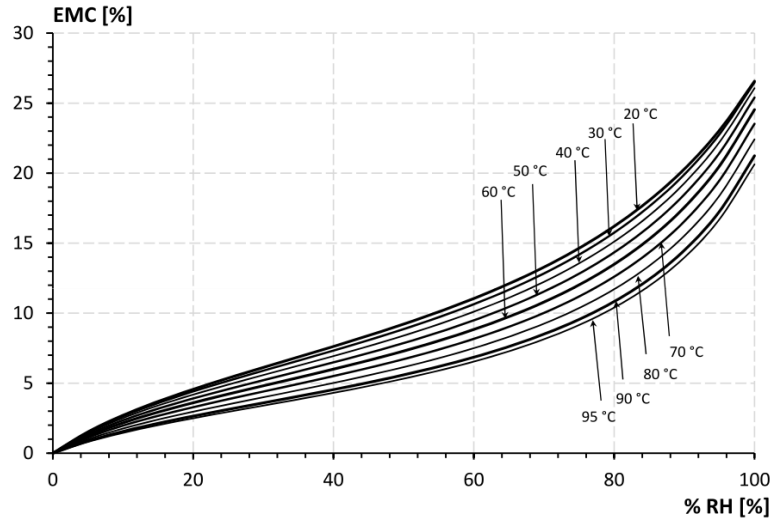

Figure 2.5: *Relationship between EMC and RH at different temperatures,*[**45**].

The Simpson equation (2.5) represents an empirical average fit to tabulated data. It does not account for the slight variations found between different wood species, stress states or for the occurrence of hysteresis. Hysteresis is the phenomenon of the MC level being different at EMC, under constant climatic conditions, regardless of whether the wood loses moisture from a higher MC (desorption) or gains moisture from a lower MC (adsorption). Hysteresis has been studied in a wide variety of investigations; see e.g. [11], [42], [44], [4] and [55]. In [4], the hysteresis effect in Norway spruce was investigated experimentally, and both Simpson's and Day and Nelson's models were used in the attempt to discover possible adjustments to the models that would make the equations appropriate for both the desorptive and the adsorptive paths, yet their results were too few to be able to define a general adjustment parameter. Their investigations showed differences however, in terms of MC at EMC, between desorptive and adsorptive moisture adjustments of up to approximately 1-3%. These results were confirmed by [46], who obtained differences of 0.2-2.5%. Since the EMC curves obtained with use of Eq. (2.5) pertain to adsorption alone, the EMC obtained for drying can be expected to be somewhat higher than those shown in Figure 2.5 and Figure 2.6.

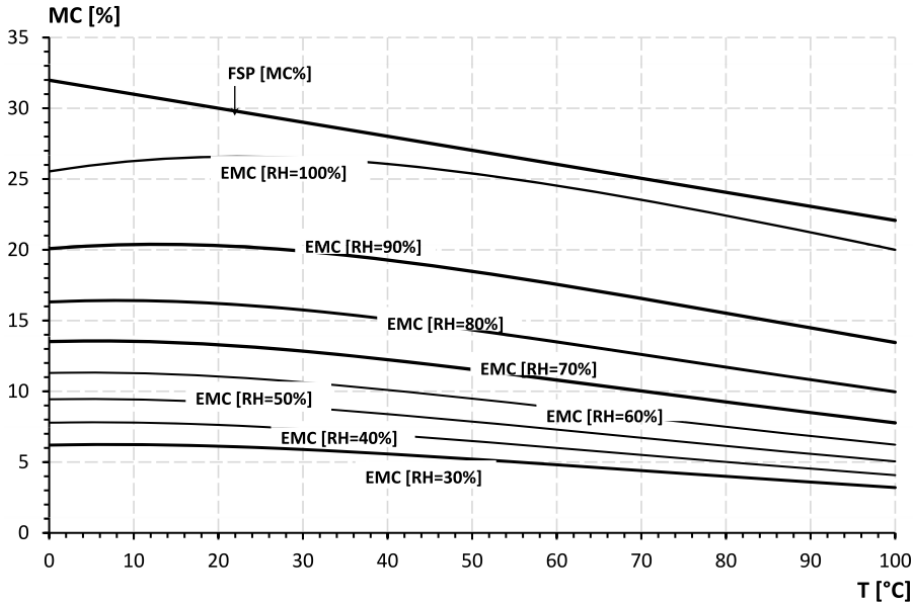

Figure 2.6: *The relationship between temperature and MC for different EMC values,* [**45**] *and at the fibre saturation point, according to* [**37**].

Figure 2.6 shows the relationship between EMC and temperature at fixed RHs, [45]. It also shows the relationship under FSP conditions as described in eq. 2.3. Note that the relationship for the EMC condition at a relative humidity of 100% is not linear, although the two curves should be nearly identical. Both curves are approximations that show the same linear tendency between 40 and 100 °C, especially when one takes into account the fact that Simpson's values were based on adsorption that can be a few percent less than the desorption values. The decrease in FSP with an increase in temperature does not necessarily lead to lesser span between FSP and EMC, since the EMC level also decreases with an increase in temperatures, as is shown in Figure 2.6.

Chapter 3

3. Modelling work

The development of stress in wood during drying is very difficult to predict due to the material inhomogeneity and the moisture gradients over the cross section of the wood samples making it difficult to know where and when the maximum stresses will occur. Models based on experimental results were created to simulate strain, stress and crack development in wood during drying. The simulation model employed involved the use of Abaqus 6.82 [1] (FE software) and of special routines for wood distortion that were developed by [37]. The routines are for solid 3D elements, their taking account of elastic deformation, free shrinkage or swelling and mechano-sorptive deformation. The references employed concerned a local coordinate system (*l,r,t*) representing the longitudinal, radial and tangential directions, respectively, the pith serving as the centre. The changes in MC occurring below the FSP serve as a driving force for the deformation and stress generation that occur.

3.1 Material data for solid wood

The model employed requires use of 45 user-defined material parameters, partly for describing the local stiffness properties (E_l, E_r, E_t, G_l, G_r, and G_t), adjusting these to the moisture and the temperature level involved, together with use of Poisson's ratios, shrinkage parameters, the mechano-sorptive parameters and the adjustments of these to moisture and temperature at hand. All the parameters used are assumed to be representative for Norway spruce. A typical expression for the elastic modulus and the shear modulus and their rate of change as functions of MC and of temperature is given by

$$E_i = E_{i0}(1 + E_{iT}(T_0 - T)) + E_{iw}(w_{f0}(1 + w_{fT}(T_0 - T)) - w_a) \tag{3.1}$$

$$G_i = G_{i0}(1 + G_{iT}(T_0 - T)) + G_{iw}(w_{f0}(1 + w_{fT}(T_0 - T)) - w_a) \tag{3.2}$$

$$\dot{E}_i = E_{iw}(-w_{f0}w_{fT}\dot{T} - \dot{w}_a) - E_{i0}E_{iT}\dot{T} \tag{3.3}$$

$$\dot{G}_i = G_{iw}(-w_{f0}w_{fT}\dot{T} - \dot{w}_a) - G_{i0}G_{iT}\dot{T} \tag{3.4}$$

where the index i represents the material directions (l,r,t), E_{i0} is the basic elastic modulus and G_{i0} is the basic shear modulus, both of these moduli at the reference temperature T_0=20 °C, where E_{iT}, E_{iw}, G_{iT} and G_{iw} represent the effects of the temperature and of the moisture level on the reference modulus. The additional parameters listed in the Table 3.1 are Poisson's ratios v_{ij}, the mechano sorption parameters m_{i0}, m_{iT}, m_{iw}, the coefficients μ_{ij} describing the coupling between the mechano-sorption effect in the different directions, the shrinkage coefficients α_i, the coefficients w_{f0}, and w_{fT}, which represent the fibre saturation point, the coefficient w_a, which represents the moisture content when equal to or below the fibre saturation point (for a moisture content above FSP the value for FSP is employed), the reference temperature T_0, and the temperature T. Table 3.1 shows the material parameters used in the simulations that follow. Both the parameters and the indices refer to notations used in [37].

Table 3.1: *Material parameters used in the simulations*

E_{l0}=9700*MPa*	E_{r0}=400*MPa*	E_{t0}=220*MPa*
E_{lT}=0.013°C^{-1}	E_{rT}=0.013°C^{-1}	E_{tT}=0.013°C^{-1}
E_{lw}=21000*MPa*	E_{rw}=*2200MPa*	E_{tw}=*1300MPa*
v_{lr}=0.35	v_{lt}=0.60	v_{rt}=0.55
G_{lr0}=400*MPa*	G_{lt0}=250*MPa*	G_{rt0}=25*MPa*
G_{lrT}=0.013°C^{-1}	G_{ltT}=0.013°C^{-1}	G_{rtT}=0.013°C^{-1}
G_{lrw}=1163*MPa*	G_{ltw}=122*MPa*	G_{rtw}=72*MPa*
m_{l0}=*0.0001MPa*$^{-1}$	m_{r0}=*0.15MPa*$^{-1}$	m_{t0}=*0.2MPa*$^{-1}$
m_{lT}=-0.01° C^{-1}	m_{rT}=-0.01° C^{-1}	m_{tT}=-0.01° C^{-1}
m_{lrT}=-0.01° C^{-1}	m_{ltT}=-0.01° C^{-1}	m_{rtT}=-0.01° C^{-1}
m_{lrw}=0.008*MPa*$^{-1}$	m_{ltw}=0.008*MPa*$^{-1}$	m_{rtw}=-0.8*MPa*$^{-1}$
μ_{lr}=0.0	μ_{lt}=0.0	μ_{rt}=1.0
α_l=0.0071	α_{r_heart}=0.10	α_{t_heart}=0.20
α_{slope}=-0.038	α_{r_sap}=0.17	α_{t_sap}=0.35
T_0=20°*C*	w_{f0}=0.30	w_{fT}=0.0033
T [°C]	$w_{init}\geq$0.30	E_{l0_slope}=0.0

The difference between the radial shrinkage coefficients for heartwood and for sapwood being the same as was predicted experimentally by both [27] and [39]. The tangential shrinkage coefficient (α_t) was assumed to be twice as large as the radial coefficient (α_r), both for heartwood and for sapwood.

Figure 3.1 presents an example of the relationships between temperature, MC and the elastic modulus in the tangential direction, showing how the latter is linearly related to the temperature when the MC is constant. Similar linear relationships exist between stiffness properties and MC at constant temperatures. The curves in Figure 3.1 show that at 20% MC

and temperatures close to 100 °C the elastic modulus is reduced to a level close to zero, although that it is reduced completely to zero does not seem likely, since some stiffness can be expected at these high temperatures. The equations presented were verified up to 80 °C and to a MC level up to a FSP governed by the temperature (see Figure 2.5). The range of 80 - 100 °C are to be regarded as an extrapolation of the relationship from 0 - 80 °C, which is not necessarily adequate all the way to 100 °C. In these investigations, however, the temperature, MC and the elastic modulus relationships were expanded from 0–80 to 0-90 °C.

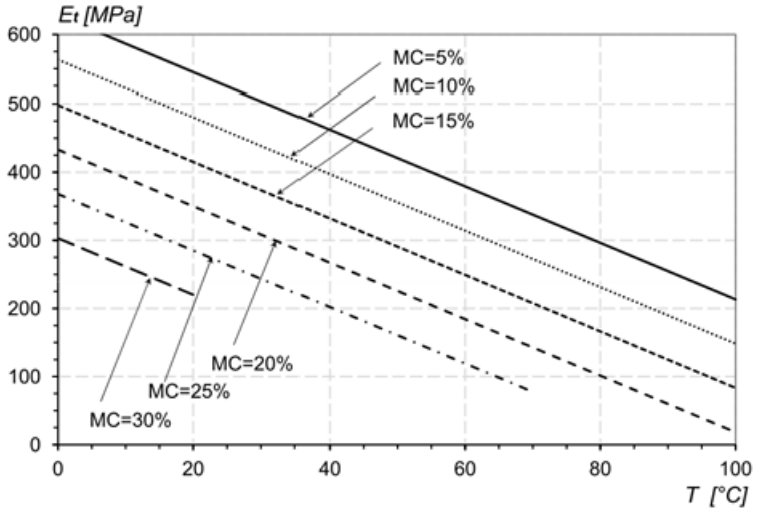

Figure 3.1: *Relationship between elastic modulus in the tangential direction and the temperature for different MC levels.*

All of the parameters concerned with moisture content and with the fibre saturation point were described in section 2.2.2. A relationship similar to that in Figure 3.1 can also be applied in the radial direction.

3.1.1 Strains

The strains in wood that develop are generated not only by stresses caused by external loads, but also by internally generated stresses driven by moisture changes. The strain distribution is also strongly affected by the orthotropy and the inhomogeneity of the wood material.

3.1.1.1 Total strains

The solid wood material model employed takes elastic, free shrinkage, and mechano-sorptive deformation into account. Visco-elastic deformations are not taken account of, however, since according to investigations conducted by [51], drying-related visco-elastic strains represent only a small part of the total strains. Temperature-related strains are not taken into account either because of their being so small in wood generally and the variations of temperature in the simulations being quite limited. The total strain rate is given as

$$\dot{\bar{\varepsilon}} = \dot{\bar{\varepsilon}}_e + \dot{\bar{\varepsilon}}_w + \dot{\bar{\varepsilon}}_{w\sigma} \qquad \textbf{(3.5)}$$

where $\dot{\bar{\varepsilon}}$ is the total strain rate, $\dot{\bar{\varepsilon}}_e$ is the elastic strain rate, $\dot{\bar{\varepsilon}}_{w\sigma}$ is the mechano-sorption strain rate and $\dot{\bar{\varepsilon}}_w$ is the moisture-induced strain rate. Reference is made to the local coordinate system *l*, *r* and *t*.

3.1.1.2 Elastic strain

Elastic strains are related to stresses by Hooke's law

$$\bar{\varepsilon}_e = \bar{C}\bar{\sigma} \tag{3.6}$$

where $\bar{\varepsilon}_e$ and $\bar{\sigma}$ are the elastic strain and the stress column matrices, respectively, and $\bar{C}$ is the compliance matrix ($\bar{C}^{-1} = \bar{D}$, where $\bar{D}$ being the elastic material matrix). The elastic strain rate $\dot{\bar{\varepsilon}}_e$ is given by

$$\dot{\bar{\varepsilon}}_e = \bar{C}\dot{\bar{\sigma}} + \dot{\bar{C}}\bar{\sigma} \tag{3.7}$$

3.1.1.3 Moisture induced strain

The moisture-induced strain rate (representing the free shrinkage or swelling rate) is given by

$$\dot{\bar{\varepsilon}}_w = \alpha \dot{w}_a \tag{3.8}$$

where α is a matrix describing the orthotropic shrinkage properties of wood and $\dot{w}_a$ is the change in moisture content below FSP.

3.1.1.4 The mechano-sorption strain

Mechano-sorption strains develop during the combination of stresses and changes in moisture content. According to [[37]], the mechano-sorption strain rate $\dot{\bar{\varepsilon}}_{wc}$ is defined as

$$\dot{\bar{\varepsilon}}_{wc} = \bar{m}\bar{\sigma}\left|\dot{w}_a\right| \tag{3.9}$$

where $\bar{m}$ is a matrix describing the mechano-sorption properties in the orthotropic material directions, $\bar{\sigma}$ is the stress matrix and $\dot{w}_a$ is the moisture content rate.

The parameters presented here are described more thoroughly in [37].

3.2 **Cracks**

In the course of time, comprehensive efforts have been made to reveal the secrets of cracks in almost all materials. The earliest investigations conducted were for steel and concrete, these still affecting the test methods employed to a large part. Crack developments are generally categorized in terms of three basic fracture modes: Mode I fractures are cracks caused by tensile stresses perpendicular to the crack direction; Mode II fractures are cracks driven by shear stress in the crack plane directed along the direction of the crack, whereas Mode III fractures are cracks driven by shear stress directed out of plane. In addition to these modes, different combinations of Modes I, II and III termed Mixed Modes, are possible. For isotropic

materials the basic modes are quite sufficient, but for strongly orthotropic material such as wood further crack modes are needed to describe the orthotropic behaviour that occurs. Figure 3.2 shows the three basic crack modes and the six possible crack orientations that refer to the orthotropic material axis of the wood.

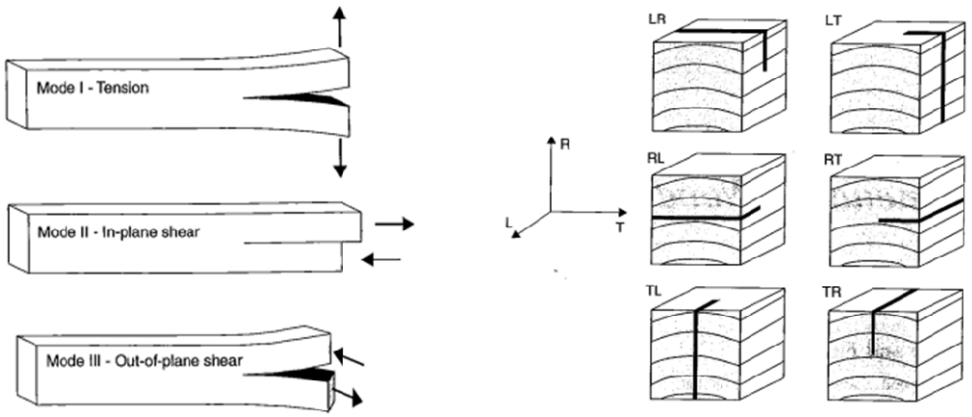

Figure 3.2: *Fracture modes I, II and III and the corresponding crack orientations referring to the wood growth axis,* [46], [56].

The first letter specifying the crack orientation refers to the direction perpendicular to the plane of the crack, and the second specifies the direction of the crack itself *L*, *R* and *T* representing the longitudinal, radial and the tangential directions, respectively. The present study is concerned primarily with crack development in the LR-plane (the TL and TR directions), these directions often being the directions most critical conserning drying-related fractures.

The application of fracture mechanical principles to wood began late in the 1960s, particularly on the basis of Linear Elastic Fracture Mechanics (LEFM), a theory presented by A.A. Griffith, (an engineer with a Doctorate from Liverpool University) already shortly after World War I. From the late 1960s and onwards, strong efforts was made to measure and tabulate fracture toughness so as to verify and supplement the theory, but up until now no standard method for the investigations of cracks has been prescribed. Several different principles for Mode I crack tests are shown in Appendix A, and other test methods can be added. Some of the test methods involved was designed originally for other materials, for example a 50 cm long three-point bending test with a notch, designed for concrete and for other isotropic materials. The three-point bending test would be ideal for crack tests of wood in the LR and LT directions, but is difficult to implement for the other wood-crack directions. Nevertheless, tests in the TL and the TR directions were performed by gluing wood parts together to create a rather acceptable test specimen; see e.g. [14]. The advantage of using standardized test methods is that this makes comparisons between different species of wood easier. Wood crack tests can be exceedingly complex since one need to take into account the fact that the properties of wood depend in part on the temperature and on the moisture content, which is why information regarding climatic conditions is of such great importance

when results are presented. Examples of the problems encountered in comparing different test results will be presented later.

The LEFM theory was found to not take account of all of the physical phenomena associated with wood fracture, since during the fracture tests a fracture process zone (FPZ) was observed ahead of the tip of the crack, one that did not fit with the LEFM approach. Various toughening mechanisms take place within this zone, such as micro-cracking and crack bridging. The fictitious crack model, also called the cohesive crack model, is a good approach for dealing with such physical phenomena.

The basic description of the cohesive crack model is that, for fracture mode I the fracture process zone of a finite crack width can be described by a fictitious crack that transmits normal stress σ. This stress is assumed to be a function of the crack separation variable w (the opening width). When w is equal to zero, the corresponding material point can transmit normal stress σ up to a value equal to the tensile strength of the material, whereas for a material point at which $w=w_c$ the normal stress cannot be transferred at all, which means the complete fracture of a cohesive crack face. The area under the entire softening stress-separation curve represents the fracture energy G_F [J/m^2] required to completely separate the crack faces at a given material point,

$$G_F = \int_o^{w_C} \sigma(w)dw \tag{3.10}$$

The relationship between the stress and the crack width is called the crack softening behaviour. Figure 3.3 shows a typical stress variation along a cohesive crack.

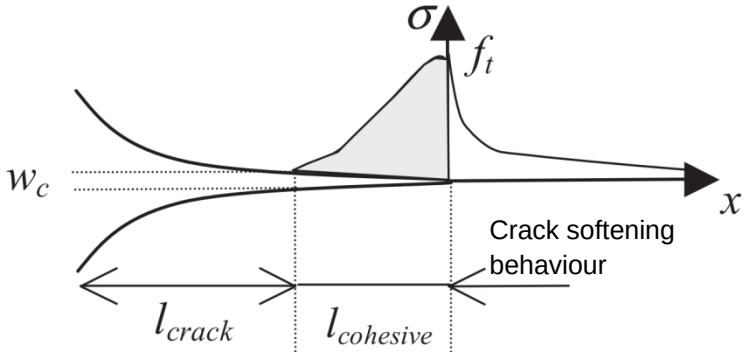

Figure 3.3: *Sketch of a cohesive crack* [[12]].

The softening behaviours obtained in experiments are normally not linear. Polynomial functions are often used to fit the curves obtained, see Figure 3.4(a), that shows three different softening curves for wood (presented in [12]), these having equal fracture energies, G_F=240 J/m^2, but different strength and ultimate crack opening values, (f_t, w_c). Figure 3.4(b) shows softening curves representing different fracture energies and a fixed ultimate crack opening.

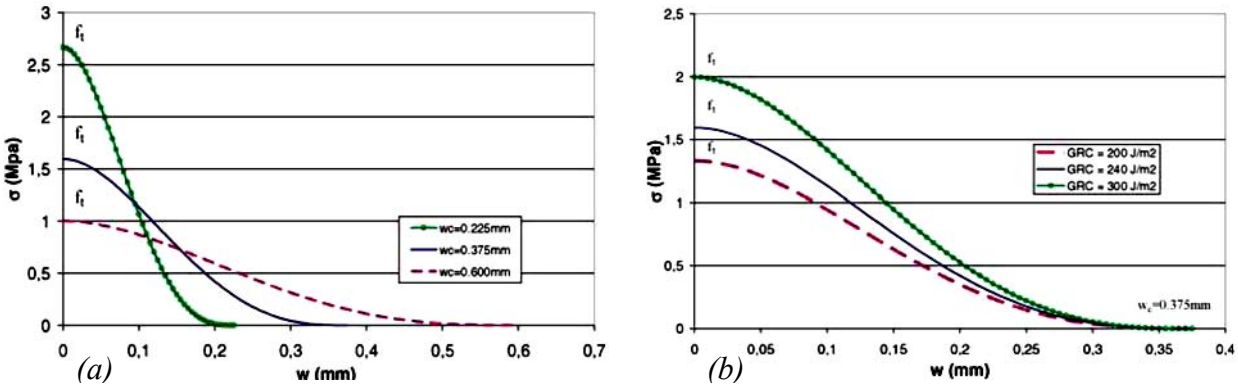

Figure 3.4: *Crack softening behaviours for TR and RT-fractures in wood: (a) Different curves having the same fracture energy G_F = 240 J/m^2, (b) Different curves differing in G_F but having the same ultimate crack width w_c,* [12].

Many investigations of crack development and related softening curves have been carried out in the attempt to describe the fracture behaviour of wood in an easy yet sufficient way. The splitting method used for wood crack testing, presented in 1995 by [47 and 48], introduced a new way of describing crack softening behaviour. It was noted there that, on the basis of microscopic observations of crack generation, crack development could be divided into two phases, starting with a phase in which micro-cracks generated this being followed by a so-called fibre-bridging phase. The existence of such a two phase crack phenomenon was documented by photos taken on a micro-scale. The crack softening behaviour shown in Figure 3.4 is often approximated as being a bilinear behaviour encompassing each of these two fracture phases.

Figure 3.5 shows a typical bilinear crack softening model in which (after the peak-point w_0, f_t) the stress-softening behaviour is defined by two descending lines. The first line spans the peak-point and the break-point (w_b, f_b), the corresponding fracture energy there being characterised by "micro-cracking" (represented by the white triangle); this energy is referred to as the cohesive micro-cracking energy $G_{f\mu}$. The second line extents between the break-point and the ultimate fracture point (w_c, *0*), the fracture energy G_{fb} there being characterised by "fibre-bridging" (represented by the gray triangle). The total area encompassed by this bilinear crack softening model is said to represent cohesive fracture energy $G_F = G_{f\mu}+G_{fb}$.

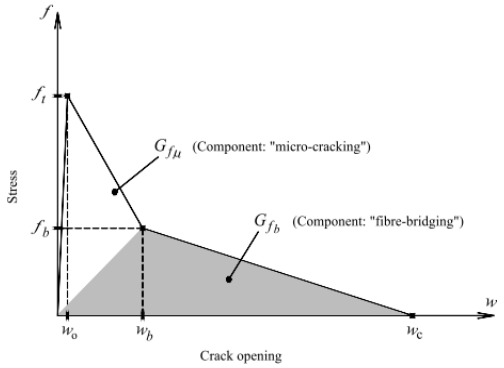

Figure 3.5: *Approximated bilinear softening behaviour in the TR-fracture of wood as described by* [50] *and* [14].

The cohesive fracture energy involved can be written as

$$G_F = \frac{f_t w_b}{2} + \frac{f_b w_c}{2} \tag{3.11}$$

where the value of the triangle *(0,0), (0,f_t), (w_0,f_t)* is neglected.

3.2.1 Fracture energy in crack modelling

Similar to many of the material parameters of wood, its crack-related properties can vary considerably both within a given wood species and between different wood species. The literature study of fracture properties of Norway spruce presented here thus provides only limited information regarding the fracture behaviour of wood in general.

It was noted in the literature that it is quite common for researchers working with wood fracture to fail to distinguish between fractures in the radial (TR) and in the tangential (RT) direction, even though the tensile strength of wood differs markedly in the two directions, a fact suggesting there to be differences between these two directions in the fracture properties as well.

In an experimental investigation (of 12 specimens) by [14] and [15] the TR-fracture energy and the tangential tensile strength of the wood under climatic conditions of 20 °C and 65% RH (MC~12%) were determined. The results were obtained using a three-point bending test setup. The fracture energy, micro-cracking and fibre-bridge cracking respectively, was divided into almost equal parts as shown in Figure 3.6.

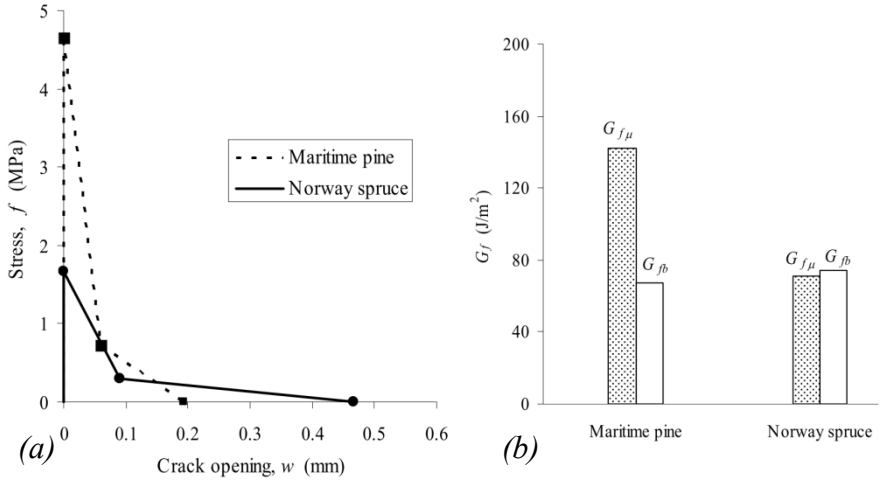

Figure 3.6: *Softening behaviour of Norway spruce and Maritime pine,* [[14]]*, (a) the bilinear relationship of micro-cracking and fibre-bridging, (b) the fracture energies involved.*

In [58] both the RT- and the TR-fracture energy of Norway spruce were determined at each of four different levels of moisture content (6, 12, 16 and 30%), presumably at the same 20 °C temperature throughout. The tensile strength of the wood material was not given in the study. The results were obtained by use of a wedge-splitting technique. The fracture energy of spruce has been reported by [46], although without providing information concerning the

crack orientation, the temperature or the humidity. In [47] the bridging fracture energy was reported to represent only about 10% of the total fracture energy, the experimental tests being performed with use of small end-tapered 'double cantilever beam' specimens. A summary of Mode I test results based primarily on use of the LEFM approach has been presented by [56]. The results of 61 different investigations, involving 11 different species, 9 different test methods and all 6 crack directions were summarised, considerable variations being present in the results. In [19], the tangential tensile strength of Birch, Pine and Spruce were presented, the effect of temperature, moisture and density on the material strength being shown. In addition, the dependency of the fracture energy on the density at 12% MC and presumably at 20 °C was shown. In [38], concerning 15 tests of spruce, the fracture energy of the wood at 20 °C and 12% MC was reported, although without information regarding crack direction or material strength being included. Use was made of a wedge-splitting technique; the load displacement curve obtained being shown in Figure 3.7. In this study, the micro-crack part appeared to be appreciably larger than the fibre-bridging part.

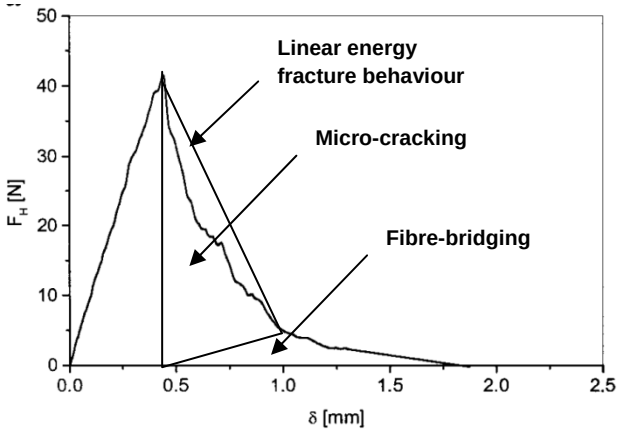

Figure 3.7: *Load displacement curve for fracture in spruce specimens at* 20 *°C and MC =* 12*%,* [38]. *The estimated two-fracture energies (micro-cracking and Fibre-bridging) are shown as the triangles.*

Figure 3.8 provides a summary of fracture energy results for spruce. The results reported by Vasic, summarised there, show the TR-fracture energy to be considerably larger than the RT-fracture energy. The summary also indicates the fracture energy results to display a marked spread. This can be due to different test methods having been used and possibly to differences in the crack orientation.

The variation in fracture energy is due partly also to the significant variation in the tensile strength of the wood. For example, the tensile strength as reported in [14] and [15] was measured to be 1.66 MPa, whereas in [19] the tensile strength obtained under the same conditions was given as being 3.0 MPa.

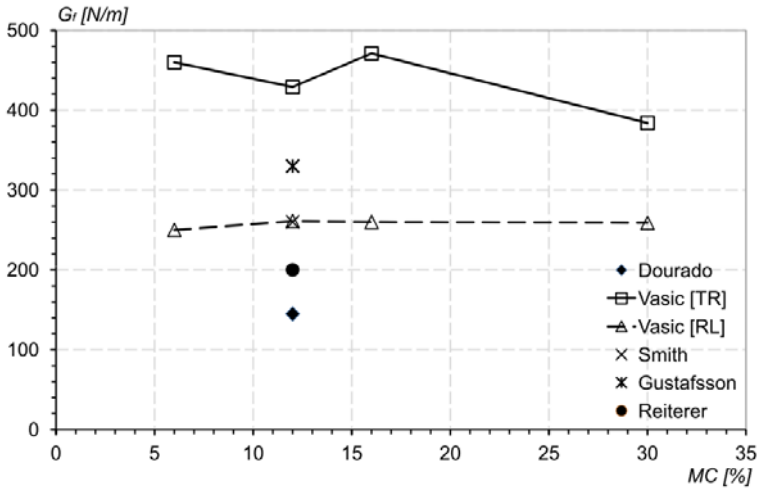

Figure 3.8: *A summary of different fracture energy results for spruce at* 20 *°C.*

Neither the results for the fracture energy, the ratio of the micro-crack to the fibre-bridging energy, nor the results for tensile strength show any completely unambiguous values. The micro-crack energy does seem however, to be markedly larger than the fibre-bridging energy. Only limited results were found concerning the effect of temperature the fracture properties.

The fracture parameters used in the simulations that follow are based mainly on the results presented above obtained from the literature though partly too on my own experimental results. The TR-fracture energy used was set to be 240 J/m^2 (0.00024 MN/m) and it was assumed to be independent of the temperature. The softening curve was designed as a linear damage evolution, the fibre-bridging energy level being assumed to be relatively low as it is also presented as being in Figure 3.7. The tangential tensile strength was found by own experimental study presented in the section 5.2 and 5.5. In the stress simulations, the elastic modulus in the crack zone was adjusted in accordance with the temperature and the moisture content.

3.3 Simulation of disc specimens obtained from timber logs

Solid wood is a hygroscopic, orthotropic and nonhomogeneous material, the stiffness properties of which are strongly affected by the moisture content (MC). Moisture related stress and variations in strain over nonhomogeneous cross sections are quite difficult to predict. Several numerical and experimental investigations taking different approaches to these behaviours have been conducted, their being summarised in Paper II [29]. The MC within a timber log in a green condition varies over the cross section, since the heartwood has a considerably lower initial MC than the sapwood. When a solid piece of lumber consists of both heartwood and sapwood, large stresses can develop during drying because of the large deformation constraints that arise. The heartwood part starts to shrink at an early stage since it reaches FSP much earlier than the sapwood part does. The drying history is likewise complex, through the fact that drying occurs faster above than below the FSP. How fast

softwood dries above FSP was investigated experimentally by [27] and [59], among others, numerical investigations regarding this being presented in [40] and [42].

Drying-related stresses in thin discs taken from timber logs are simulated here because of these providing simple and well-defined moisture histories of the heartwood, the transition wood and the sapwood part, this facilitating adequate calibration of the simulation model. The model is useful in quite a general way since it can easily be used for the simulation of stresses and fractures in kiln dried timber boards.

3.3.1 Geometry and element mesh

Simulations of the disc specimens were performed by use of the FE software Abaqus [1], a 3D stress analysis being carried out using 8-node linear brick elements of type C3D8. The type of specimen studied was a circular 15 mm thick disc from a timber log containing 19 annual rings and a pith. Each annual ring was partitioned into four quarters in order to make a suitable element mesh. The parts were connected by a so-called tie-constraint that allowed the discs to function as an inhomogeneous continuum. Each quarter of the annual rings had its own set of material parameters as well as its own moisture and temperature histories. The disc sample was 232 mm in diameter, which is approximately the same diameter as that of the test specimens used for verification of the simulation model.

To simulate possible crack propagation in the radial direction, four thin fracture parts were created. The parts were oriented from pith to bark in between the quarter parts of the annual rings. The crack elements were 0.2 mm thick cohesive hexahedral elements of type COH3D8. The fracture parts were connected to the solid annual ring parts by a tie-constraint that allowed the disc to work as a continuum until it cracked. Figure 3.9 shows the dimensions, the predefined crack pattern and the element mesh of the disc sample that was studied.

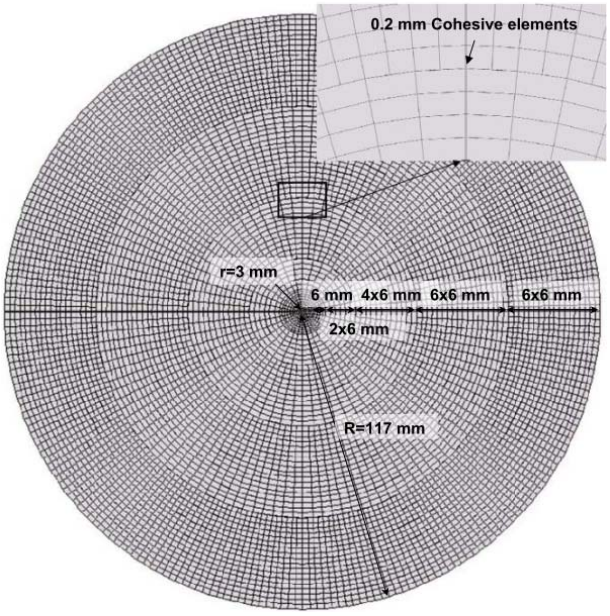

Figure 3.9: *Dimensions, predefined crack pattern and element mesh of the disc sample that was studied.*

Figure 3.9 shows the mesh and the geometry used for the disc simulations. Each annual ring was prescribed as being 6 mm thick and the pith as having a radius of 3 mm. The seven annual rings closest to the pith were defined on the basis of the material parameters involved as being heartwood, whereas the rest of the annual rings were defined by the parameters as being sapwood. The cohesive elements were designed as 0.2 mm thick elements. The solid elements were designed as being quadratic and as being as equal sized as possible, making it necessary to change the seeds of the edges as the radius became larger. The seeds were typically doubled when changes were made, as can be seen on the close up.

3.3.2 Moisture history of the disc samples

The drying history of the disc specimen conceived of as its total weight vs. time was recorded during the drying process as a whole. The total weight as the average of the weight of the sapwood and that of the heartwood was used to calculate the average MC-history of the disc; see Figure 3.10. The sapwood drying history shown in Figure 3.10 was calculated on the basis of the average MC history and the MC in the green condition. From such earlier investigations as [26] and [27] it was observed that the drying history can be considered almost identical for all parts (heartwood, transition wood and sapwood) of the cross section when the drying starts from the green condition. For example, in Figure 3.10, a sapwood part with an initial MC of 195 % needs 350 min to reach the EMC, and transition wood with an initial MC of 70 % needs 175 min to reach the EMC. A further description of these relationships is presented in Paper III [30].

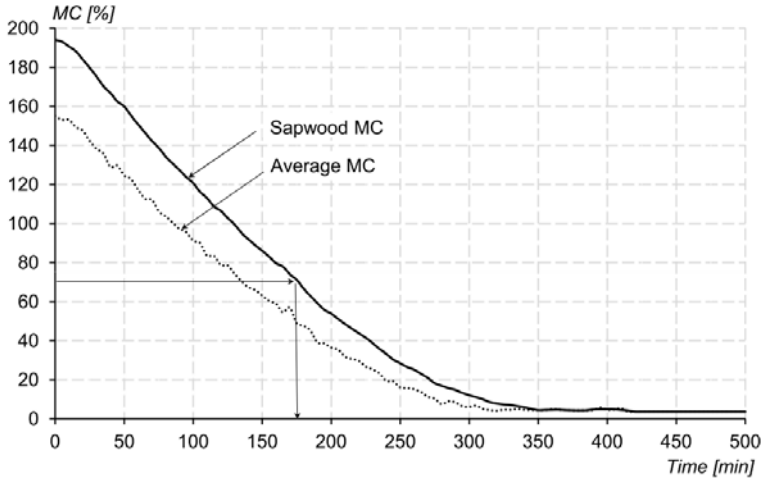

Figure 3.10: *The average MC history of a disc and the calculated sapwood MC history of it at* 90 *°C and* 30*% RH.*

To provide adequate input data for the simulation model, the initial variation in the green MC state (t = 0) together with the MC-history curves over time were obtained along the radius (r) of the discs.

Figure 3.11 present the results of the measured MC-history field of the disc specimen that was studied. In the disc model, the MC-history field is assumed to be axisymmetrically distributed around the pith.

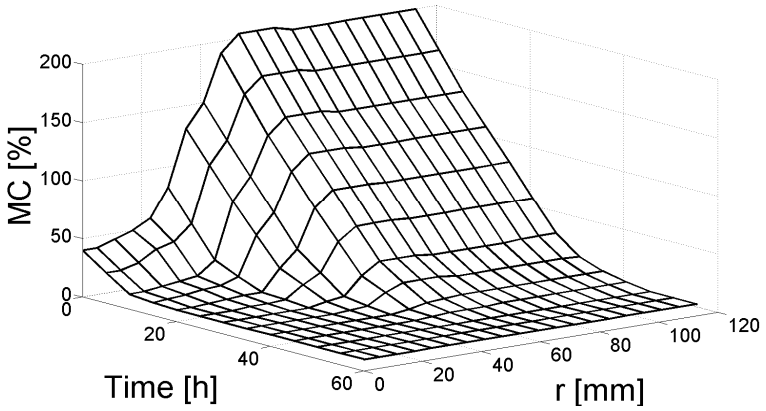

Figure 3.11: *The MC-history field used as input data for stress simulation of a disc specimen at 23 °C and 63% RH, Paper II* [29].

3.4 **Simulation of timber boards**

Timber logs are generally sawn into a number of timber boards before being exposed to kiln drying. The sawing (board) patterns of logs are in most cases determined so as to obtain as much volume of timber as possible. This often results in boards containing both heartwood and sapwood. The drying of timber boards can be said to involve moisture gradients from the surfaces to the centre of the boards, see e.g. [37], [16] and [34]. The moisture gradients that occur due to variations in the initial (green) MC are seldom accounted for when evaluating kiln drying. The log disc drying results presented later shows that initial MC variations have a marked effect on the strain, mechano-sorption, stress and crack development during the drying process. The size of the external surface from which the water evaporates also has a strong effect on the speed of the drying process, since a small surface for a specific volume results in a shorter drying process than a larger surface does, if the climatic conditions are identical. It is assumed here that the moisture in given volume evaporate mainly from the surfaces that belong to the volume in question. The drying process is more difficult to simulate, due to the fact that MC for different volumes can sink beneath the FSP at different times.

3.4.1 **Board geometry and element mesh**

The stress simulation of the timber boards was performed using the same type of analysis as for the disc samples. The board studied had a rectangular cross section consisting of 4 different sub-volumes (parts); one heartwood part, two transition zones and one sapwood part. As before, the parts were connected by the tie-constraint that allowed the board to function as an inhomogeneous continuum. Each part was further divided into two sub-parts close to the surfaces and a centre volume, as shown in Figure 3.12. All the sub-parts can have their own set of material parameters and their own moisture and temperature histories.

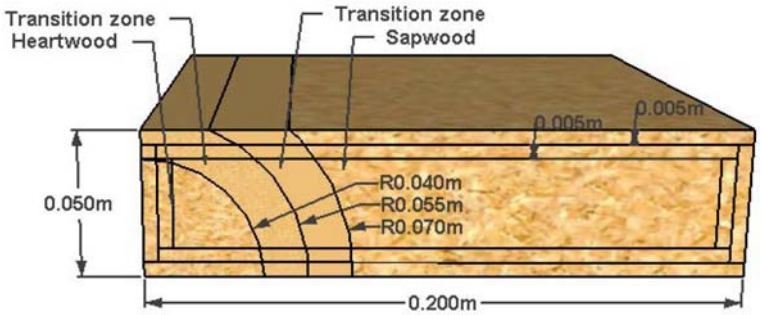

Figure 3.12: *An example of the board dimensions and the sub-volume patterns used to estimate the drying history of the boards, Paper III* [31].

The thin sub-parts close to the surfaces make it possible to simulate the moisture gradient from the surface to the centre of the board. Three different boards of equal outer geometry were analysed to investigate how the sawing pattern affects the stress development during drying. The three boards presented below, differ from one another in where the pith is located. This results in considerable differences between them in the relative volumes of the heart-, transition- and sap-wood. The heartwood volume has a radius of 40 mm and each transition subzone is 15 mm thick. The outer geometry of the boards is one of 50x200 mm, as shown in Figure 3.12. The element mesh of the three boards that were studied is shown in Figure 3.13.

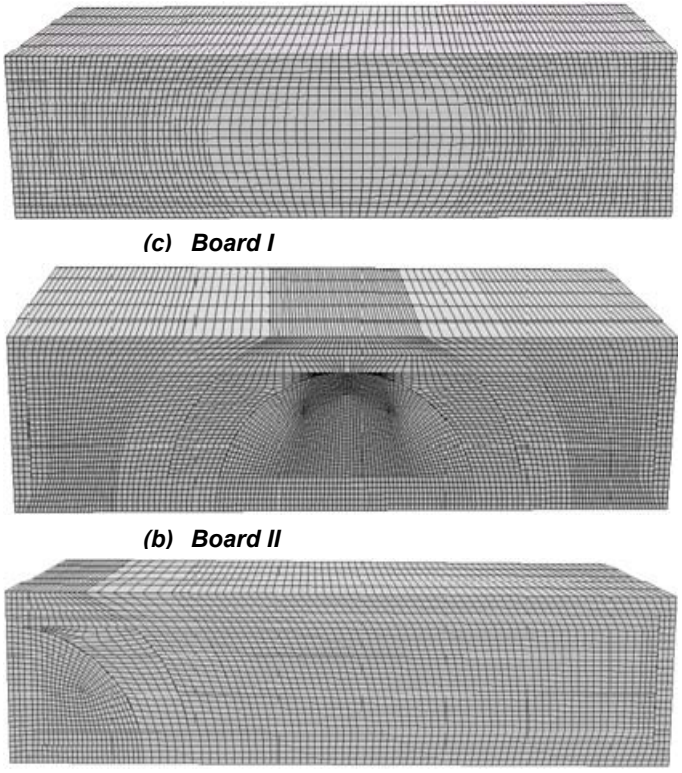

Figure 3.13: *The element mesh of the three timber boards that were studied, the pith of which was located (a) in the centre of the board, (b) at the centre of the bottom surface, (c) at the lower left corner of the board, Paper IV* [31].

Note the fine mesh in the central part of board II. Since the sub-parts close to the heartwood have a thicknesses that reduce down to nil, biased seed was used to reduce singularities and produce a finer mesh in these areas.

3.4.2 Moisture gradients

Many investigations of the drying behaviour of timber boards have been carried out and different models for the transient movement of moisture have been developed. Several moisture transport models dealing with moisture flow below and above the FSP are summarised in [42], for example. The results of one of these models were used as a basis for our simulations aimed at describing MC variations over a cross section. It has been observed in materials having long capillaries that water can move in the form of a film or at the corners of capillaries having polygonal cross-sections. Such a flow phenomenon probably occurs to some degree in wood. This could lead to links between water-filled clusters being formed, increasing the continuity of the liquid phase. Inclusion of film or corner flow in modelling was investigated by [60]. Typical modelling results based on this flow phenomenon are shown in Figure 3.14.

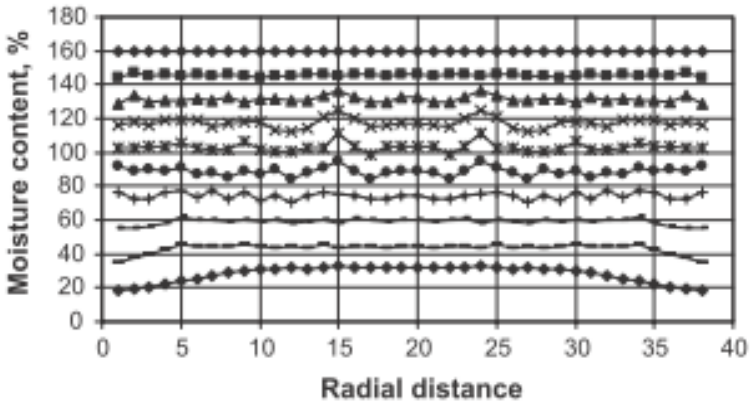

Figure 3.14: *Moisture content profiles simulated with use of a film flow model,* **[42]**.

Figure 3.14 shows the moisture to move to the surface with almost no gradient until the MC becomes approximately 60-70 %; from this stage on a gradient builds up, the MC at the edge being approximately 10-12 % lower than the MC in the central part. The gradient is found down to a depth of approximately 10 mm.

3.4.3 Drying description of the boards

On the basis of the results from the experimental study presented in Chapter 5, the green MC of the heartwood and the sapwood were set to 60 and 165%, respectively, the MCs of the transition zones being assumed to be graduated linearly between the heart- and the sapwood MC values. The material parameters used are those representing Norway spruce, showing a density of 450 kg/m^3 at 12% MC. The moisture gradient history from the surface to the centre was estimated on the basis of the moisture profiles presented in [42], in which use of the film flow theory was made; see Figure 3.14. Each sub-volume of the boards, such as that of the heartwood, the transition wood and the sapwood, has its own external surfaces from which all

of the moisture within the specific volumes involved is expected to evaporate during the drying process. The total water flux v for each sub-volume is calculated on the basis of the measured moisture losses at a constant climate of 60 °C and 80% RH. A further account of how the moisture histories of the different sub-volumes were calculated and how they were used is presented in Paper IV [31]. The results from the simulations are presented later.

Chapter 4

4. Experimental work

The experiments reported on in the thesis were conducted in order to examine the strain and crack development of Norway spruce during kiln drying and to investigate the drying rate or water flux occurring under kiln drying conditions. Three different types of experiments are reported on:

1) Experiments to study strains and fractures in log disc samples under varying climatic conditions.
2) Tangential tensile strength experiments performed under different climatic conditions.
3) Experiment to investigate drying rate for heartwood, transition wood and sapwood.

The experiments involved test specimens and a specially designed climate chamber to determine the climatic conditions needed and the different pieces of equipment to measure strains, forces and weights and to evaluate the experimental results. The different facilities employed in conducting the experiments are described below.

4.1 Climatic conditions

The drying experiments were performed under controlled climate conditions. The first couple of experiments were conducted in a room in which the temperature and the relative humidity were measured online by a hygrometer, a flow of air around the specimens being produced by a ventilator: The average temperature was 23 ºC and the average humidity was approx. 63% RH. The variation in temperature was $\pm$2 ºC and the variation in humidity $\pm$3% RH. All the other experiments were performed in the climate chamber described in the following section.

4.1.1 Climate chamber

The experimental facility used to measure moisture related deformations of the test samples of wood, when varying and well-controlled climatic conditions were needed, was a new and specially designed climate chamber developed at the DTU, Department of Civil Engineering. The chamber is approximately 1.1x1.1x0.9 m in size, and allows the air to circulate freely around the specimens at a velocity of approx. 1 m/s. It has a potential temperature that range of -70 to 180 °C and a controlled humidity range of 10 to 98% RH within the temperature range of 10 to 95 °C. With use of items of up to 25 kg in weight inside the chamber, the rate of temperature change is 5 °C/min, both from low to high temperatures and vice versa. The

chamber has four free sides (top, bottom and two vertical sides), there being bushings that enable load devices to be inserted into the chamber in a horizontal or a vertical direction. The door to the chamber has a special window with a heating arrangement that keeps the window clear of rime, dew and condensation. This arrangement enables cameras to take undisturbed pictures of the test samples during any variations in climate within the chamber.

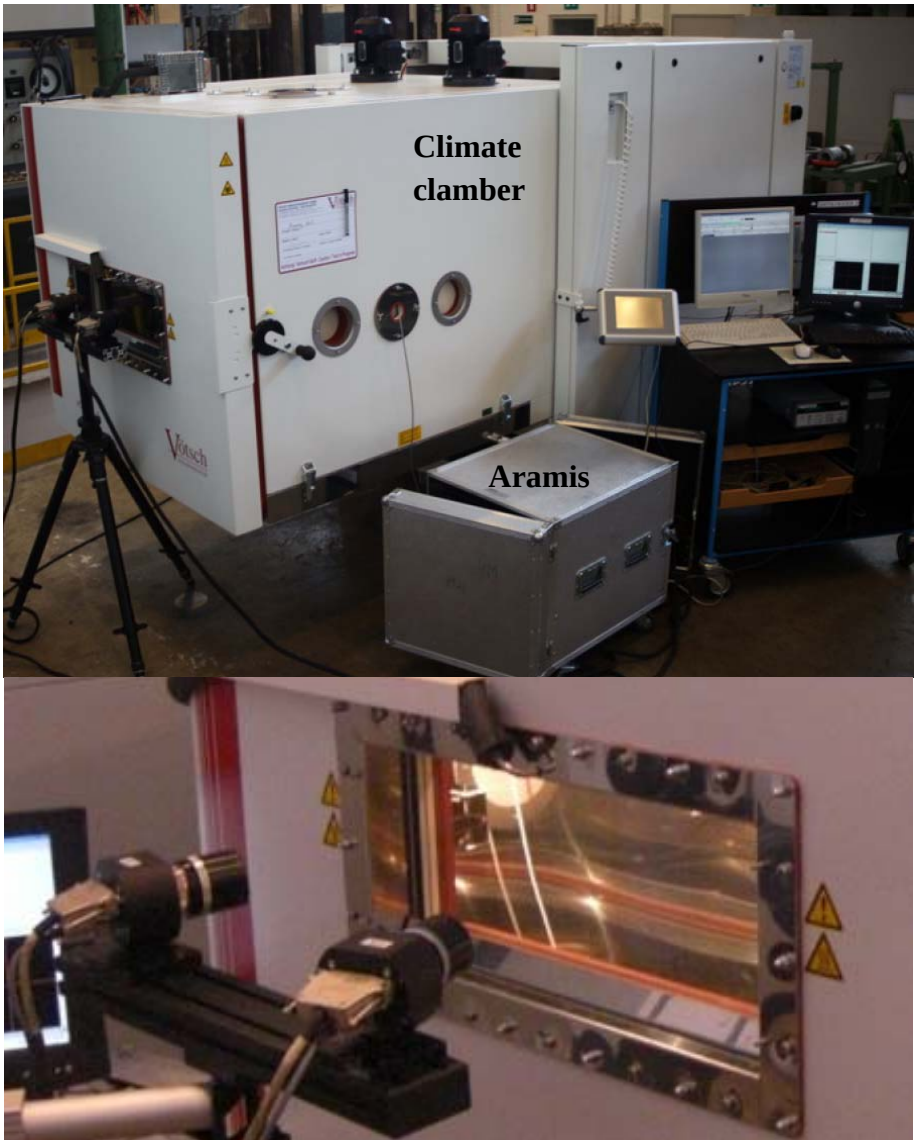

Figure 4.1: *Climate chamber with specially designed window allowing Aramis placed outside the chamber, to measure developments in the strain field for specimens placed inside the chamber.*

The deviations from the preset temperature that can take place are $\pm$0.1-0.3 °C in the centre of the working space $\pm$0.5-1.0 °C within the space. The deviations from the preset humidity that can occur are $\pm$1-3% RH. The general performance of the chamber described in Appendix C. The specimens were placed on online weighting arrangements inside the chamber during the testing process as a whole.

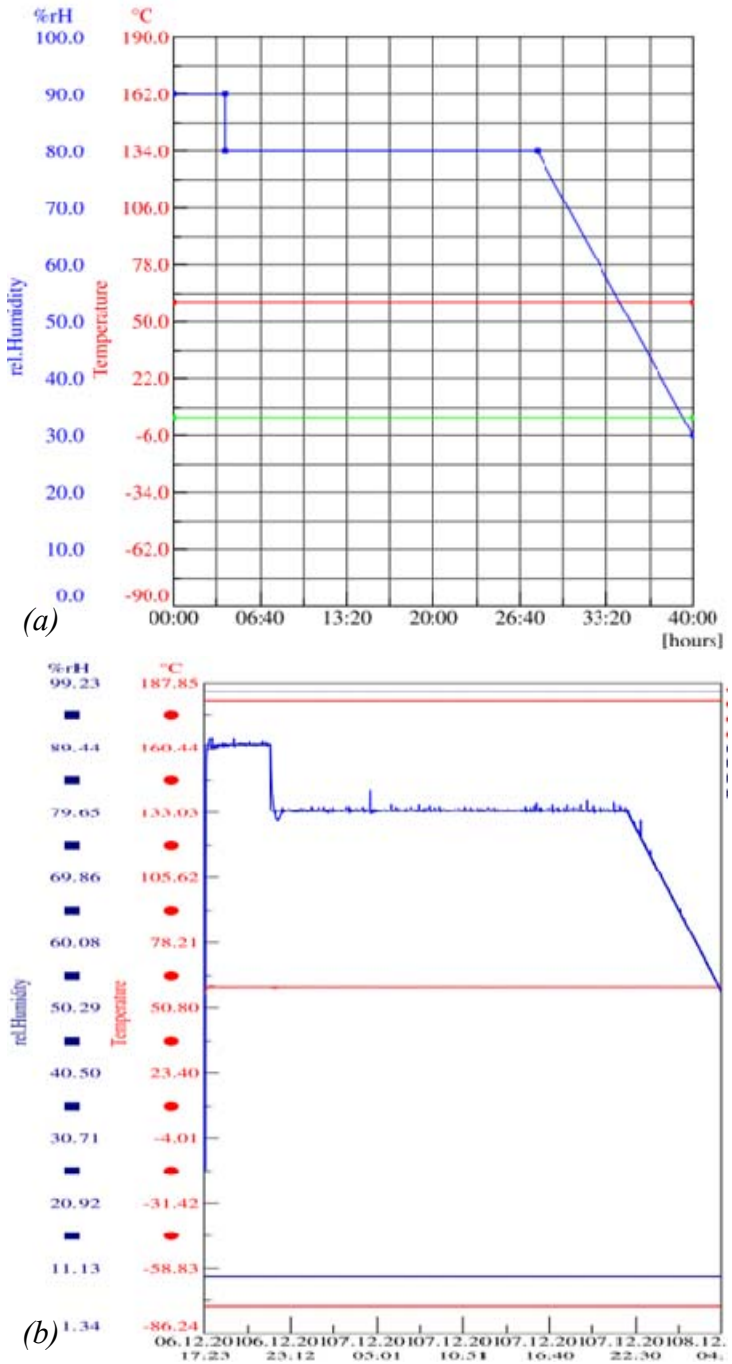

Figure 4.2: *Climate control in the climate chamber: (a) a preset drying schedule involving a constant temperature and varying RH, (b) an activity report showing the current climate conditions in the chamber together with the preset ones.*

The climate conditions within the chamber are controlled by software enabling the temperature and the humidity and the course of any changes in these, such as shown in Figure 4.2(a) to be preset. In the schedule shown (the red line), the temperature is held constant at 60 °C, but the temperature could have any predetermined course between 10 and 95 °C as long as the level of humidity was aimed at was maintained (otherwise the temperature range could

be as extreme as -70-185 °C). The green line represents the level of ventilation in the chamber, but this facility is not made use of here. The blue line is the expected humidity level throughout the experiment, which can be selected to be anywhere between 10 and 95% RH. The activity report is shown in Figure 4.2(b), the red lines at the top and bottom being the ultimate limits of the temperature that can be preset, whereas the line in the middle is the preset course and the actual course (the actual temperature is kept very close to the preset value). The blue lines at the top and bottom are the preset limits of the humidity, whereas the curves in between are the preset course and the actual course (note that the actual course here differs more from the preset course than the temperature). As shown in Figure 4.2, the humidity is the most difficult parameter to adjust to preset values.

4.2 Test samples

The log disc specimens were selected from 20-year old Norway spruce trees from North Zealand in Denmark. The trees were felled in the winter periods of the years 2009-2012, when logs with a diameter of 200-250 mm were removed from the trees. The specimens were selected from areas free of defects. Figure 4.3 shows the principles employed in the selection of disc specimens.

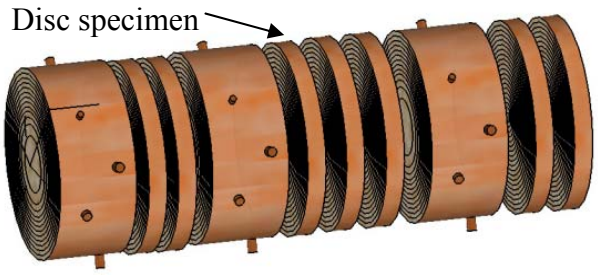

Figure 4.3: *Principle of selection of disc specimens from timber logs, Paper II* [29].

4.2.1 Stick samples used to estimate the green MC

The variation in initial (green) MC was determined by cutting 18x18x65 mm sticks out of the cross section, the sticks being numbered as shown in Figure 4.4.

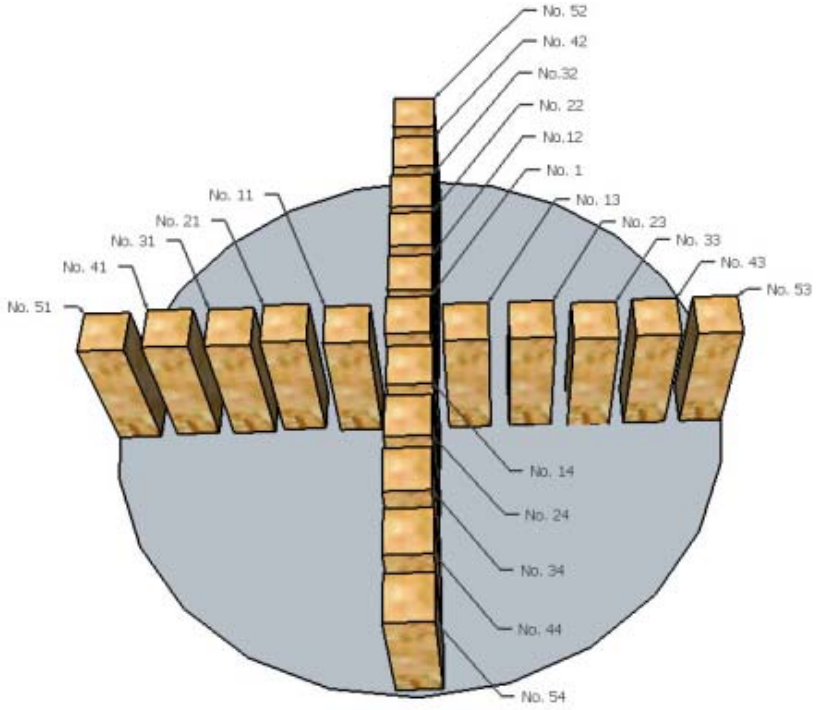

Figure 4.4: *Stick pattern and numbering used for determining the variation found in the green MC from the pith to the bark.*

4.2.2 Disc specimens used for strain and fracture tests

Discs with a thickness of 15 mm were sawn out from the log in a frozen condition, as shown in Figure 4.3. The thickness was determined on the basis of preliminary test results which showed the moisture gradient in the longitudinal direction to be limited; see [26] and Paper I [28] for a more detailed account. The samples were sawn gently by hand to reduce the risk of damage. Each sawn disc was examined for defects, all the discs that had defects being discarded.

4.2.3 Specimens used for tangential tensile strength tests

Test specimens for the tangential tensile strength tests were cut from discs taken from the same logs as the disc specimens. The specimens were cut out slightly oversized in a green condition to ascertain that the specimens were still large enough after the free shrinkage deformations caused by the drying had taken place. The specimens were cut out in a green condition in a size of approximately 18x50x140 mm. The specimens were then acclimatized in a climate chamber to 18% MC at 20 °C and 85% RH before the final shaping was carried out. The climatic conditions were set in accordance with the equilibrium moisture content (EMC) calculations given in [45] and shown in Figure 2.5. The final dimensions of the samples were 15x40x125 mm, these having a curved and narrowing zone in the middle, as shown in Figure 4.5. The smallest area in the centre of the sample, where the failure is expected to occur, is approximately 15x20 mm. The exact geometry was measured for each specimen prior to the start of measurements, all the specimens being kept in a freezer until the tests were carried out.

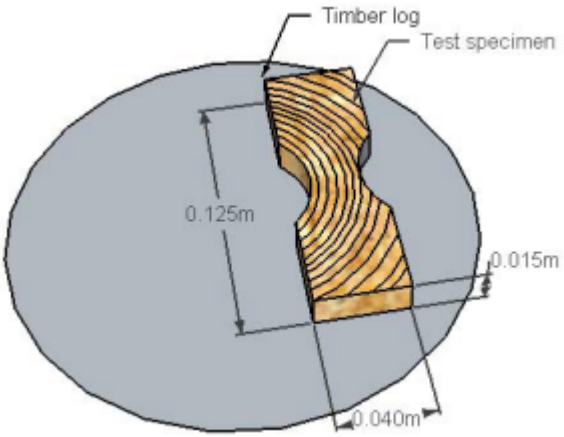

Figure 4.5: *The geometry and the annual ring pattern of the specimens used for the tangential tensile strength tests.*

4.2.4 Specimens for water flux testing

The test specimens were sawn from timber logs having diameters of approximately 200 mm. Figure 4.6 shows the sawing pattern and numbering of the test samples.

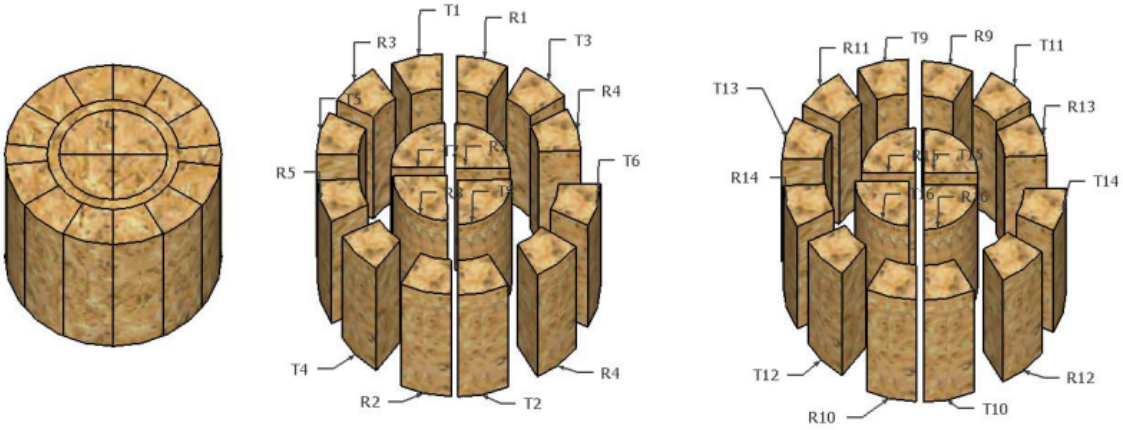

Figure 4.6: *Sawing pattern and the numbering of the specimens used for the water flux experiments.*

The specimens were cut out with a band saw in a frozen condition so as to avoid evaporation from the surfaces, which were sealed with a layer of Conclad. Each specimen in the sapwood area had a length of 150 mm, a thickness of 35 mm in the radial direction, which gave a width of 30 mm closest to pith and 40 mm closest to bark. The specimens referred to as T1-T6 and T9-T14 were sealed with Conclad at the ends and on the RL-surfaces, which allowed evaporation to only take place in the R direction only, whereas the specimens referred to as R1-R6 and R9-R14 were sealed with Conclad at the ends and on the opposite surfaces (TL-surfaces), allowing evaporation to only take place in the T direction. The surface areas in the radial and in the tangential direction were at the same size (0.0105 m²), the average maximal distance from the surfaces to the centre of the samples being 0.0175 m.

4.2.5 Preparation and preservation of the test materials

The spruce logs were brought in to DTU-Byg either the same day or during the next few days after the tree had been felled. The logs were cut into manageable pieces approx. 50 cm in length. The log pieces were kept in a freezer at approximately -10 °C, the log pieces only being brought up to be cut into test specimens, the rest being kept further in the freezer. In this way, the green moisture content was kept intact. The specimens were created in a frozen condition so as to reduce the risk of the evaporation of moisture from the surface during preparation and were brought back to the freezer then until they were used in the experiments.

As mentioned earlier the specimens for the water flux tests were sealed with a layer of Conclad on some of the surfaces so as to stop all evaporation of moisture. Conclad is a two component sealing produced and manufactured by Condor Kemi A/S. The sealing is a waterproof one with a permeability of Pam, which is a value of 21 $m^2h*mm*Hg/g$ according to ASTM C 355. It has a strength of 7.5 MPa, a modulus of elasticity of 5 MPa and a maximum strain before fracture of 260 %. The sealing can be applied at temperatures of 2-35 °C. It has a thickness of 1-1.5 mm. Its considerable strength, together with its low modulus of elasticity makes this coating highly useful, its generating only relatively small stresses when it follows the wood surface during shrinkage deformation. Another quality of Conclad is that it has very good adhesive ability on wet and cold surfaces. The sealing was applied to the surfaces when the temperature of the specimen was approximately 2-3 °C. After the sealing, the specimens were wrapped in a polyethylene film and were placed in a climate at room temperature until the sealing had hardened. After a few hours of hardening, the specimens were brought back to the freezer for further preservation until the experiments were performed. The moisture loss during the defrosting period was eliminated through film being wrapped around the samples.

4.3 Strain measurements

The moisture-related strain fields that developed over the cross section of the disc specimens during drying were measured in two ways. The first was by use of the Aramis system, a non-contact optical 3D deformation measuring system used to measure the strain field; see [2]. This method requires the use of two specially designed cameras that are placed with precision, both in between and towards the studied specimen. The other way of measuring the moisture-related strain fields was by the use of a digital camera; the digital pictures were then imported into the Aramis software, in which 2D strain fields can be generated. Using only one camera seems, from experience, to be more robust and easier to work with than the 3D system, the 2D results also being quite sufficient for these investigations. A third way of measuring geometrical changes is that of a simple scanning of the disc specimens at different stages of drying.

4.3.1 Strains field measurements using Aramis

The drying deformations of disc specimens were studied by use of Aramis, the specimens being placed on a stand containing a digital load cell. An arbitrary pattern of dots, as shown

in Figure 4.7(b), was sprayed on the surface for use in obtaining strain measurements. The entire strain field history of each disc specimen was measured, together with the weight of the test specimen. The climatic conditions were verified by the activity report from the climate chamber described above.

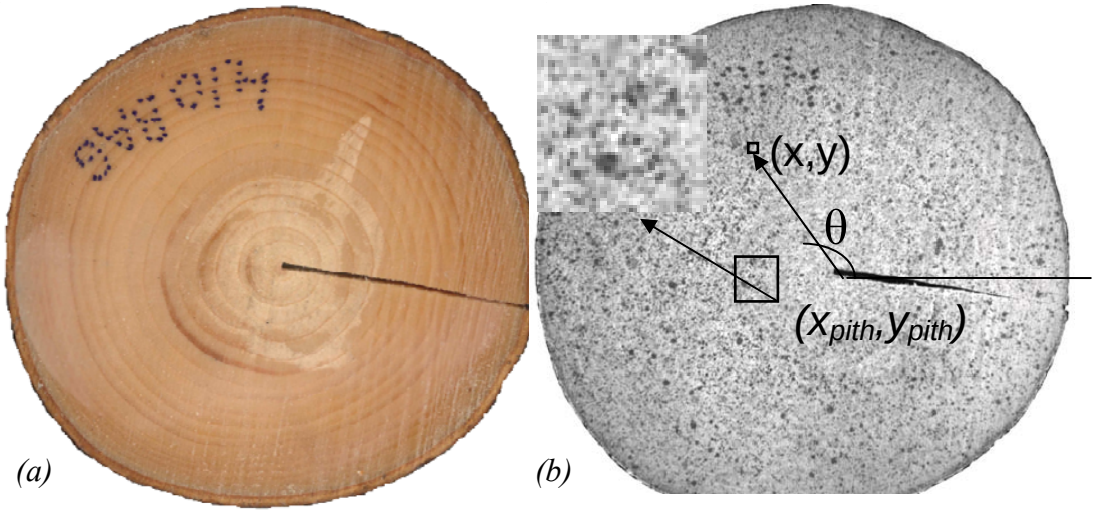

Figure 4.7: *(a) a disc specimen with a slit, (b) a specimen sprayed with a random dot-pattern used for the Aramis measurements.*

The Aramis system recognized the surface pattern of the specimen on the basis of digital images, coordinates being assigned to the pixels of the images. Initial images obtained at the undeformed stage served as the reference state, the image stages thereafter being recorded during the deformation phase of the specimen using fixed intervals. The system computes displacements and strains occurring from one image to another through determining the movement of a square facet as compared with the movement of the neighbour facets. A more detailed description of the strain measurements is presented in Papers I, II and III [28], [29] and [30].

4.3.1.1 Processing of the experimental data

To compare the strains measured by use of Aramis with simulated strains, those strains referring to the (x,y) coordinate system were transformed to a local coordinate system (r,t) of the wood material. The disc specimens studied had nearly circular annual rings, the pith was located close to the centre of the discs, see Figure 4.7(a). An account of how the measured strains were transformed to local radial and tangential strains is found in Paper II [29].

4.3.2 Geometrical changes measured by scanning

The third method of measuring geometry changes of disc samples is a simple scanning by means of an A3 scanner, normally used for scanning documents. The scanned geometries were very precise in size 1:1. The scanning of the specimens was saved as pdf-documents. Results obtained by use of digital measuring equipments were compared with the physical measurements of the specimens that were made, the two being found to correlate very

closely. The scanning was done first on the undeformed geometry of the disc samples (in green condition) just after the samples reached EMC and finally after their being dried down to 0% MC. This enabled the geometry under chosen conditions to be stored, these geometries later being used as a reference together with other data, such as weight. This method was used, for example, for determining the shrinkage coefficients.

4.4 Determination of moisture content

The moisture content of wood can be determined in various ways. The following 3 methods are often used:

1) Use of an electrical resistance meter
2) Dielectric measurement
3) The "Oven dry" method

Measuring of the electric resistance is based on two electrodes being pressed into the timber so that an electric current can pass through the tree along the grain from one to the other electrode. Since the electrical resistance of wood is affected by the MC of the wood, the measured electrical resistance of the wood can be translated into a certain moisture level. An electrical resistance meter is easy and quick to use. It is used mostly for the measurement of moisture content levels between 6 and 28%. The accuracy of this method is approximately ±2% MC.

A dielectric capacity measuring method makes use of a metal conductor, formed as a plate, bracket or a ball, which is placed on the wood surface. This sensor type method is not as accurate as the resistance meter described above. It is more suitable for measuring high MCs below FSP, but is less suitable for the determination of low and exact wood MC values.

A disadvantage of both the methods presented above is that they cannot be used to measure MC above the FSP level. The MC of all the wood specimens was thus determined according to EN 13183-1: *Moisture content of a piece of sawn timber. Part 1: Determination by oven dry method.* This method is the most accurate one available for determining the MC in wood and is the only way of determining MC above FSP. The wood samples were oven dry at 103 ºC ±2 ºC. The samples were weighed every three hours until the weight became constant, i.e. the dry mass m_0 was determined. The accuracy of this method depends on the difference in weight between the last two measurements as compared with the total weight loss. The measurements were stopped when the MC could be determined with a deviation of less than 0.1%.

To study the history of the weight loss of the wood samples during the experiment, a special stand to hold the specimen was built and was placed in the middle of the climate chamber. The changes in weight of the wood sample could then be measured online during the entire experiment with use of a special (mV signal) load cell that was linked to the stand. The weight of the specimen was determined manually as well, immediately before and after the experiments. These two weight measurements were used to check the start and the end values of the online (mV) measurements. On the basis of the online weights and the oven dry

weight, the MC-history could be generated for the experimental process as a whole. The maximum weight capacity of the load cell was 50 N. The setup is shown in section 4.5.2.

4.5 Experimental setup

Use was made of two different experimental setups for obtaining the experimental results needed for the modelling work, one for tangential tensile strength testing and the other for measuring the strain and crack propagation of the log disc samples.

4.5.1 Tensile strength test setup

The tangential tensile strength testing was performed in the setup shown in Figure 4.8. The setup consists of a test frame and two steel rods, one of them connecting the frame with the upper sample clamp and the other connecting the lower sample clamp with the loading device (a load bucket), a deformation device and the test specimen being attached to the two clamps. The load on the specimen was applied by slowly filling metal chips into the load bucket until the specimen broke. The loading was carried out continuously over a period of approximately five minutes. The final weight of the loading plus the weight of the experimental arrangement beneath the specimen was used to calculate the tangential tensile strength of the material.

The tests were conducted primarily under the well-defined climatic conditions in the climate chamber (see 4.1.1).

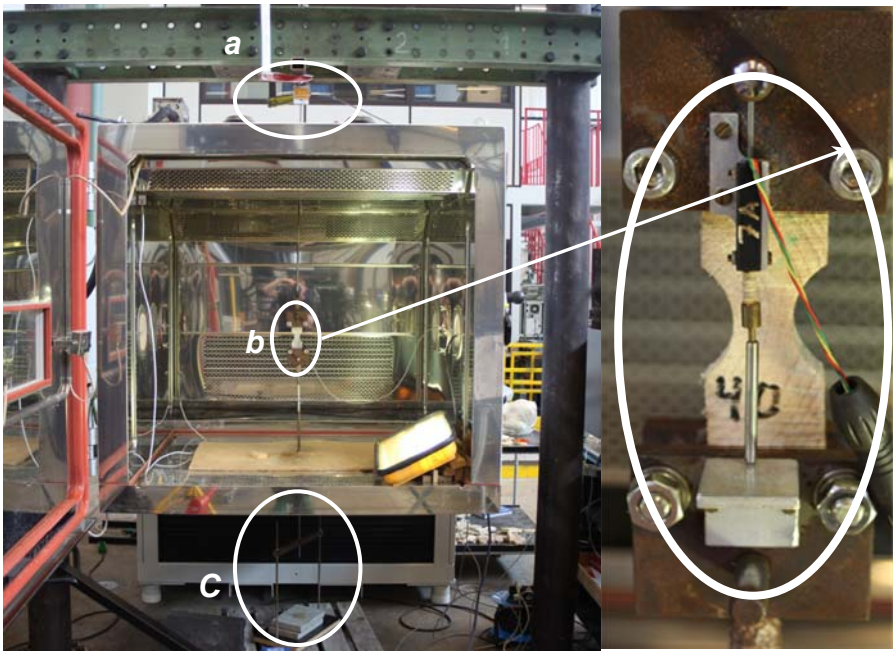

Figure 4.8: *Experimental setup for the tensile strength testing, a: the load cell, b: the specimen with clamps on it, c: the load device (a bucket).*

The test frame was placed outside the chamber, the upper rod passing through a moisture-tight rubber bushing at the top of the chamber and the lower rod going through a small pipe

which also went through a bushing on the bottom side of the chamber, allowing the lower rod to move up and down freely within the pipe. The load bucket was hanging underneath the chamber. This setup made it possible to acclimatize the specimen prior to testing and to perform the testing under different climatic conditions.

4.5.2 Disc sample test setup

The disc sample experiments were conducted in a setup that involved use of the climate chamber (described in section 4.1.1), a specially designed stand, a load cell and the Aramis system (described in 4.3.1). The stand and load cell setup is shown in Figure 4.9. The load cell was built into the stand so as to enable there to be free ventilation around the specimen. The specimen touched the stand at only three points and it was placed at the same height as the heated window, enabling Aramis (or other cameras) to take pictures from outside the chamber during the experimental process. The load cell was connected to a data logger outside the chamber.

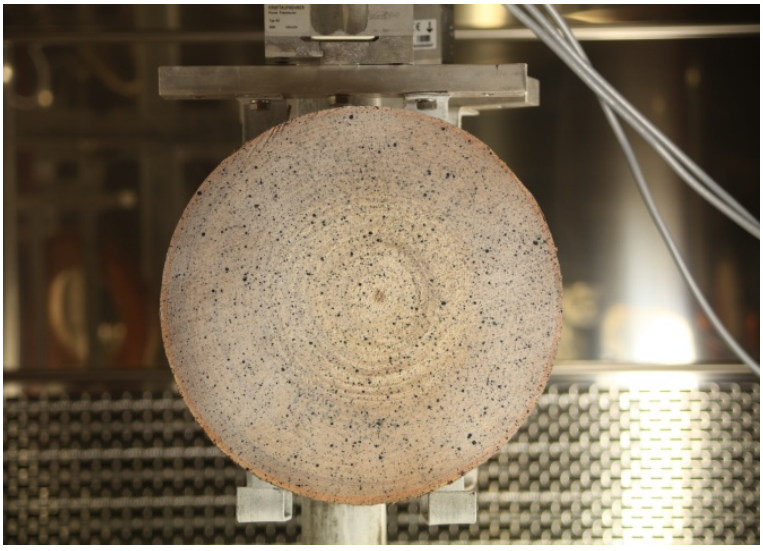

Figure 4.9: *A picture of the experimental setup taken through the heated window by Aramis. The specimen is placed on the stand in the middle of the climate chamber. The stand is mounted on the load cell that is fixed above it.*

Chapter 5

5. Results

5.1 Moisture content

Initial variations in MC under green conditions, (t = 0) as well as history curves over time were obtained for several points along the radius (r) of the disc specimens on the basis of small oven dried sticks from the cross section. The principle involved in the cutting of the sticks is shown in Figure 4.4.

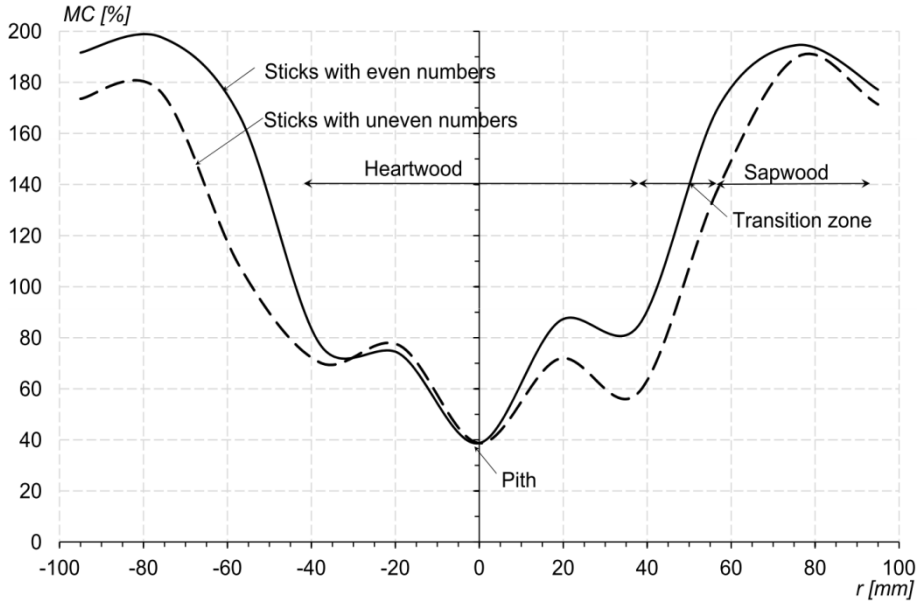

Figure 5.1: *Variations in the green MC from pith to bark, Paper III* [30].

Figure 5.1 shows variations in the green MC from pith to the bark. The four MC paths were not identical, each curve corresponding to a quarter of the disc. On the basis of these different MC path curves under green conditions, moisture histories for the nineteen annual rings and the pith zone, seventy-seven different drying histories in all, were generated in connection with each simulation. Results similar to those presented in Figure 5.1 were reported in [26].

5.2 Tangential tensile strength

The log disc simulations were used to investigate the stress level for crack initiation and crack propagation at different temperatures. The tangential tensile strength is a parameter needed for the cohesive crack simulation model. Tangential tensile strength tests were performed at three different temperatures - 20, 60 and 90 °C - under constant climatic conditions of 20 °C and 85% RH, of 60 °C and 91% RH, and of 90 °C and 96% RH, respectively, coupled with 18% EMC in the wood. The specimens were acclimatized in the chamber for the test climate involved for a period of at least 12 hours, before tests in question started. The results were reported in Paper III [30], but are also summarised in Table 5.1:

Table 5.1: *Effects of the temperature on the tangential tensile strength of Norway spruce at MC=18%.*

Temperature	**20 °C**	**60 °C**	**90 °C**
	$f_{t,90}$ [MPa]	**$f_{t,90}$ [MPa]**	**$f_{t,90}$ [MPa]**
Test no. 1	2.55	1.14	1.20
Test no. 2	2.46	1.58	0.64
Test no. 3	2.25	1.39	0.66
Test no. 4	2.35	1.73	0.85
Test no. 5	2.05	0.75	
Test no. 6		1.27	
Test no. 7		1.47	
Average	2.33	1.33	0.83
Standard derivation	0.20	0.32	0.26

The results presented in Table 5.1 show there to be a marked decrease in strength with an increase in temperature, there being slight variations in the standard deviation from one set of tests to the other. Further discussion and a comparison of these results with those obtained with use of simulated values is to be found in section 5.5.

5.3 Experimental verification of the log disc model

In order to verify the log disc model, two experimental studies under well-controlled climatic conditions were carried out. The first study dealt with a disc having a 1.5 mm wide (initial) slit from bark to pith, the second study dealing with a similar disc without a slit. The first study was also presented in Paper II [29]. The discs were dried from a green MC down to a constant MC of 12%, a constant drying climate at 23 °C and 63% RH being employed during the entire drying process.

5.3.1 Disc with an initial slit

For the disc specimens studied, development of the strain field was measured during the drying process by use of Aramis, the slit opening next to the bark being measured at regular time intervals as well. The correlation between the experimental and the simulated results was assessed for the strain state attained after 25 hours of drying. Figure 4.7(b), Figure 5.2 and Figure 5.3 show the deformation state (after 25 hours of drying) representing the condition of the wood when the heartwood reached an EMC of 12% and the sapwood was still appreciable above the FSP level. Note that the slit shown in Figure 4.7(b), originally 1.5 mm wide, had closed in the sapwood area and become wider in the heartwood area. This occurred because of the tangential shrinkage of the heartwood material tenting to open the slit, at the same time as the opening of it was suppressed by the sapwood, which had not yet started to shrink, while the radial shrinkage in the heartwood area dragged the sapwood towards the pith, resulting in the closing of the slit in the sapwood area.

Figure 5.2 presents a colour plot produced by Aramis showing minor strains and the directions they take. Here all the minor strains were negative, the numerically largest strains representing the limiting values. In most areas, the directions of the strains were nearly tangential, this corresponding closely to the direction of the largest shrinkage coefficient of the wood. In the heartwood area, close to the free edges of the slit in particular, much larger strains occurred than in the remainder of the cross section. The unsymmetrical colour variations that can be seen in Figure 4.7(a), that may possibly indicate certain variations in the moisture level or the material properties at these locations, see the marked areas in Figure 5.2.

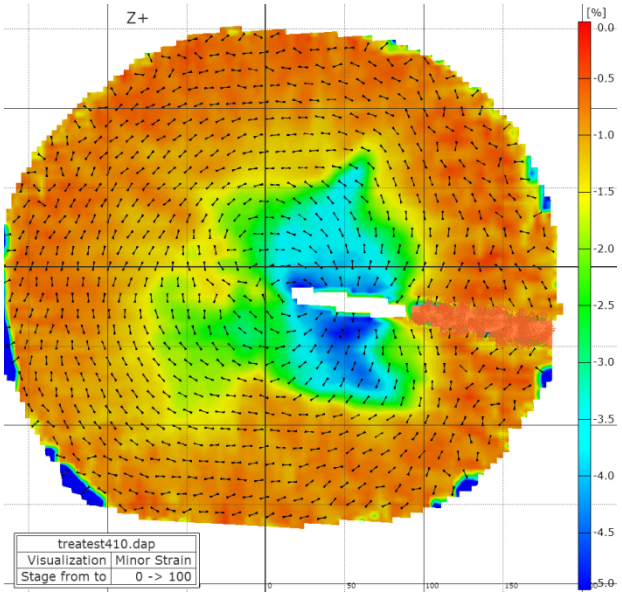

Figure 5.2: *Variations in the minor strains and their directions across the disc specimen after 25 hours of drying.*

To show that the slit was actually closed at this state of drying, the slit in the sapwood area shown in Figure 5.2 and Figure 5.3(a) was repaired slightly. The facets close to the slit could

not be calculated correctly since neighbouring facets were located in the slit and resulted in incorrect values being obtained for the strains close to the edge, which were then discarded.

The global strains (ε_x, ε_y and ε_{xy}), which were measured by Aramis, were transformed into strains in the tangential and the radial directions so as to be comparable to the simulated strains, see Paper II [29]. Figure 5.3 shows the transformed tangential strains together with the simulated strains found at the same point in time. The simulated strain field in Figure 5.3(b) shows tendencies similar to those of the transformed one shown in Figure 5.3(a), except for certain uneven strain variations being present. The path *r* used for comparing experimental and numerical strains with one another in terms of their variation is shown in Figure 5.3((a) and (b)), the results obtained being shown in Figure 5.3(c).

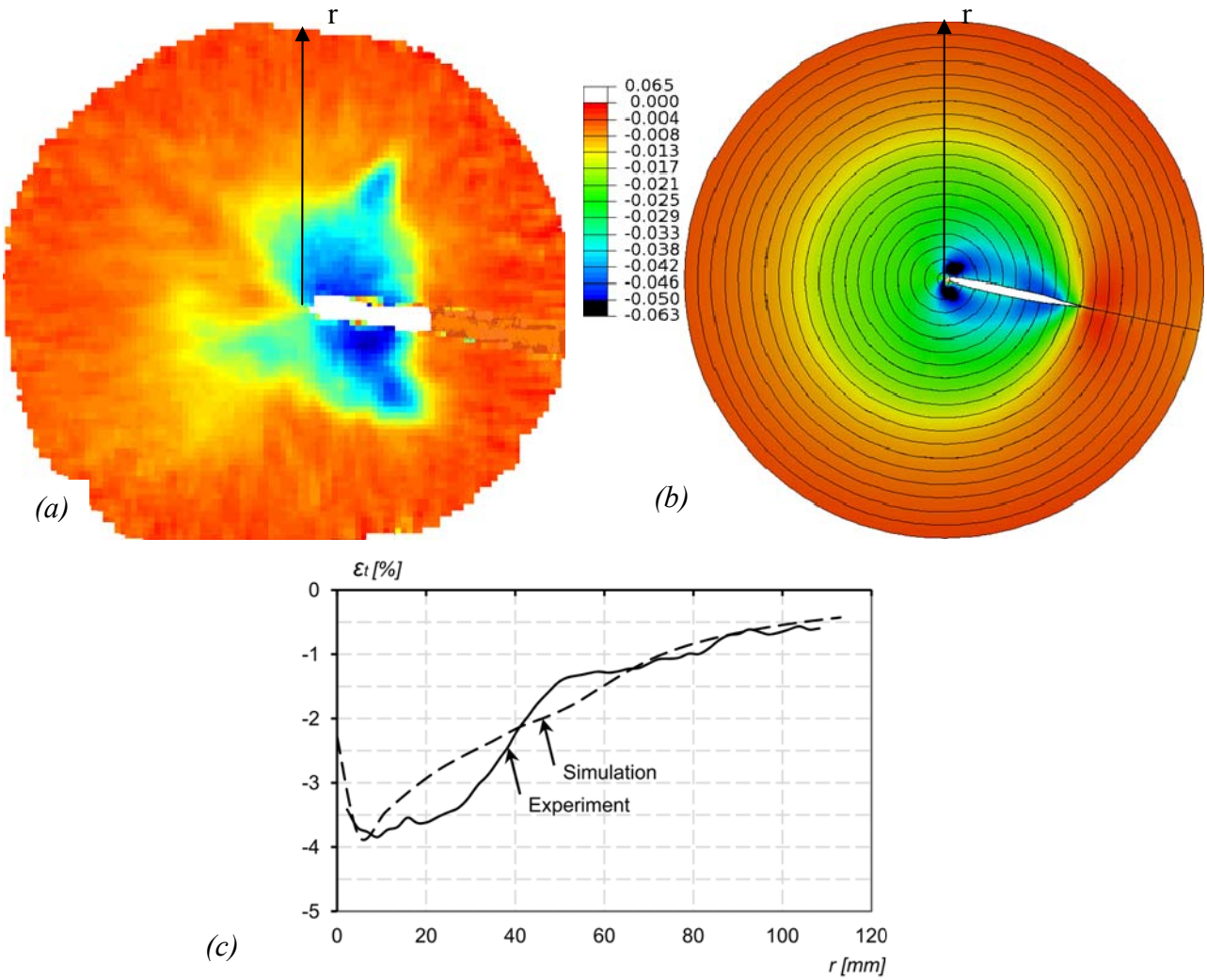

Figure 5.3: *Tangential strain distribution after* 25 *hours of drying: (a) measured strain, (b) simulated strain, (c) variations in strain along the path r, Paper II* [29].

For the variations in strains along path r, an acceptable degree of correspondence was found between the experimental and the simulated results. The measured size of the slit opening found after 25 hours of drying and at the final EMC stage corresponded rather closely in size to that of the simulated opening shown in Figure 5.4. After the model had been verified

experimentally, it was used to investigate the strain, the stress and the development of distortion of the disc specimen during the drying process as a whole.

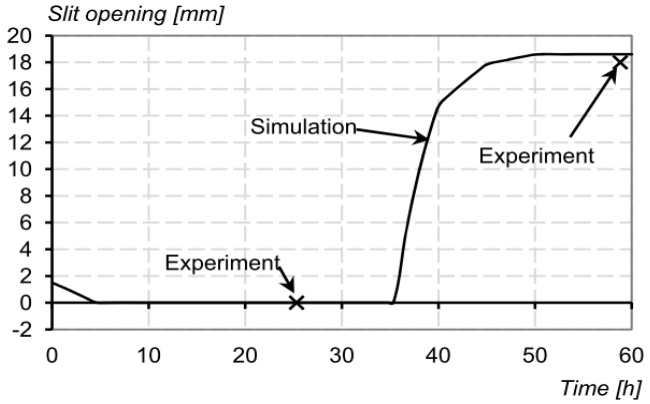

Figure 5.4: *Variations in the slit opening during drying, Paper II* [29].

5.3.2 Discs with closed annual rings

The log discs were studied experimentally (moisture related strain field measurements) to investigate the mechano-sorption behaviour of a closed cross section. One aim here was to examine the reversibility of the mechano-sorption strains.

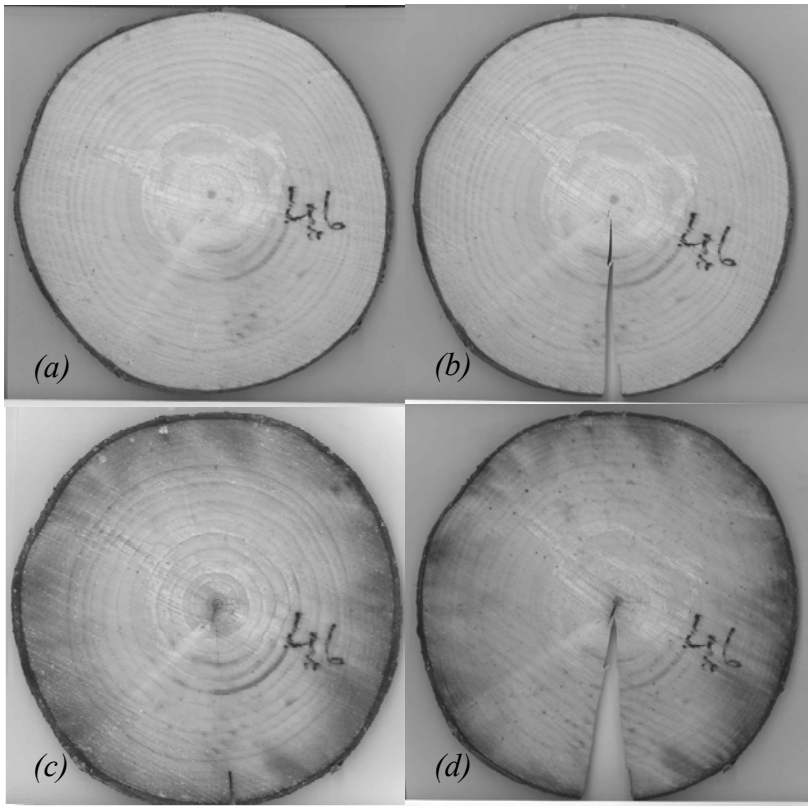

Figure 5.5: *A disc sample exposed to a drying-wetting-drying process: (a) the uncracked geometry of the cross section after the initial drying down to* 12*% EMC, (b) the cracked geometry after crack initiation at* 12*% EMC, (c) the cross section showing a closed crack after wetting up to FSP, (d) a cross section showing a large crack opening after a second drying down to* 12*% EMC.*

Figure 5.5 shows a deformed disc specimen at different stages in time during the drying and wetting processes. The specimen was a 15 mm thick disc without a slit. The first subfigure shows the disc sample in an uncracked condition, and with the moisture history shown in Figure 3.11, after it had been dried from a green condition down to 12% EMC. The second picture shows the disc sample after it has cracked from the bark to the pith. Note that the crack was initiated (at 12% EMC) by sawing a few millimetre radial slit at the periphery of the disc. The crack developed instantly while the slit was being sawn, which indicated there to be a certain amount of tangential stress within the cross section. The immediate opening of the crack at the periphery was 3.2 mm in length, the crack propagating all the way to the pith. The disc was then put into water until FSP was reached 2 days later. The crack closed totally during the wetting, the cross section geometry shown in subfigure (c) becoming similar to that found under green conditions. From this condition a new 24 hours drying period started with homogeneous drying over the cross section that took place until 12% EMC was reached. The maximum crack opening was then 22 mm.

This disc was simulated with exactly the same material and moisture parameters as used for the disc that had a slit. The crack propagation was simulated by removing very thin elements along the path of the crack when EMC had been reached. At this stage the disc worked as a disc would that had a very thin slit from the bark to the pith. Figure 5.6 shows a history plot for simulated crack opening together with measured crack openings after the first drying (inclusive crack initiation), after the wetting period and after the second drying.

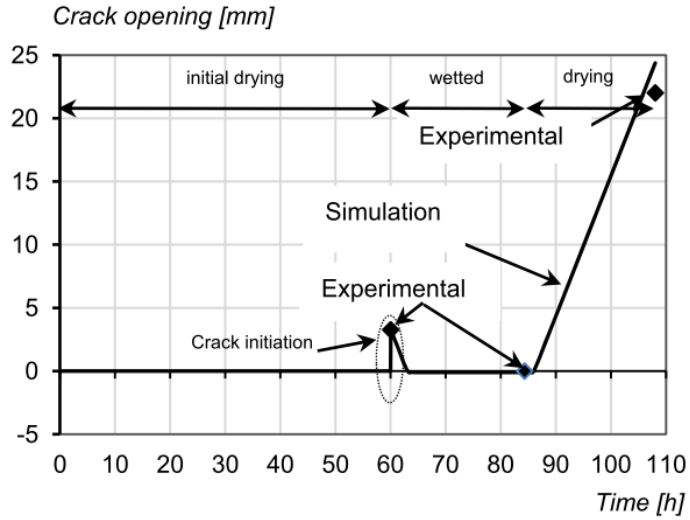

Figure 5.6: *Development of a crack opening during a forced drying-wetting-drying process.*

5.4 Simulation results

5.4.1 Simulations of discs with an initial slit

In order to study in a more detailed way the moisture-related behaviour of the disc specimens, simulation results obtained along the path r were used to investigate how strains and stresses develop during drying. It was the tangential strains and stresses that were studied because of cracks propagating primarily from the pith to the bark occurring because of the tangential stresses exceeding the tensile strength of the material.

5.4.1.1 Strain development

The simulation results presented in Figure 5.7 indicate that strain development in one part of the disc (e.g. in the sapwood) is affected by the moisture history and the shrinkage behaviour in other parts and vice versa. For example, the central part (from the pith on outward to a radius of some 20 mm) displayed material properties and a moisture history for which, in the case of free shrinking behaviour, would have led to the total tangential strain being identical throughout, although under the conditions that were present the surrounding material partly hindered shrinkage, this generating stresses and mechano-sorption strains that led to a reduction in the total value of the tangential strains and variation in them. The same phenomenon could be noted in the sapwood area. By comparison, the strain of free tangential shrinkage was about 5% after 45 hours of drying. The marked curves in Figure 5.7, representing 45 and 55 hours of drying, respectively, show marked elastic and mechano-sorptive strain behaviour. The sapwood closest to the bark was least affected by this mechano-sorptive behaviour.

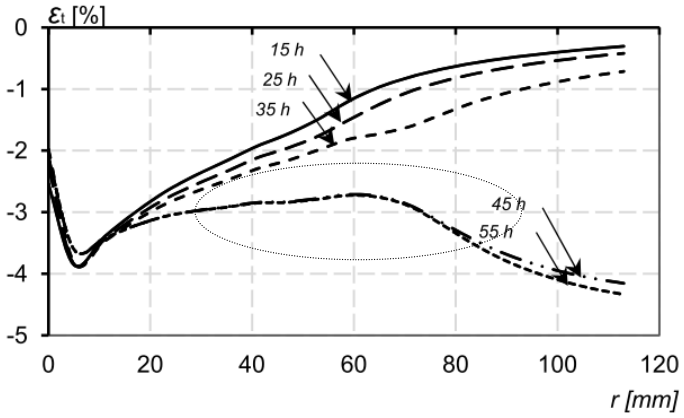

Figure 5.7: *Variation in the (total) tangential strain along path r (at Fig. 5.3(b)) at different times during drying, Paper II* [29].

The tangential strain history is shown in Figure 5.8. Note the marked changes between 2000 and 2500 min due to the changes in MC in the sapwood area and the effect that both the heartwood and the sapwood have on the strain development in the transition zone (around the annual ring number 10). Further discussion of the strain development that takes place is presented in Paper II [29].

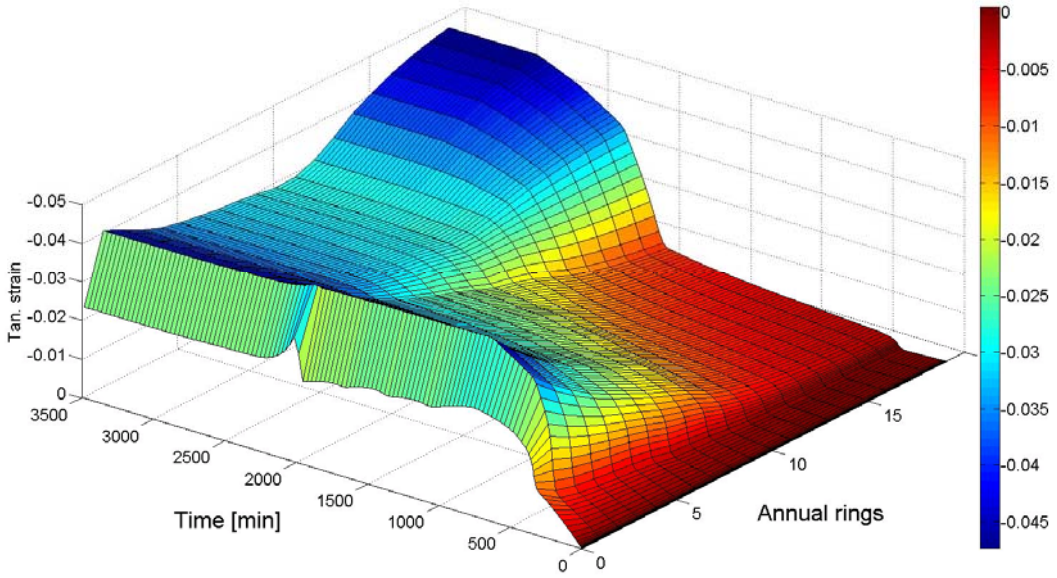

Figure 5.8: *The tangential strain history for a path from pith to bark that a simulated drying process gives rise to.*

5.4.1.2 Stress development

Mechano-sorption effects make stress development difficult to predict. Figure 5.9 and Figure 5.10 present a field plot of the tangential and the radial stress components as functions of the radius r and the drying time. Figure 5.9 shows there to be large variation in stress along r during the entire drying time. The largest stress gradients are to be found close to the pith and within the transition zone between the heartwood and the sapwood. The tensile stress within the transition zone becomes very close in size to the tensile strength of the material. The sapwood begins shrinking after about 35 hours (2100 min.) of drying, as clearly evident both in Figure 5.9 and in Figure 5.10. Shortly after this, the slit starts to open (see Figure 5.4). This changes the stress distribution markedly within the cross section as a whole. The most pronounced changes occur in the transition zone between the heartwood and the sapwood (see annual rings no. 10-12 in Figure 5.9).

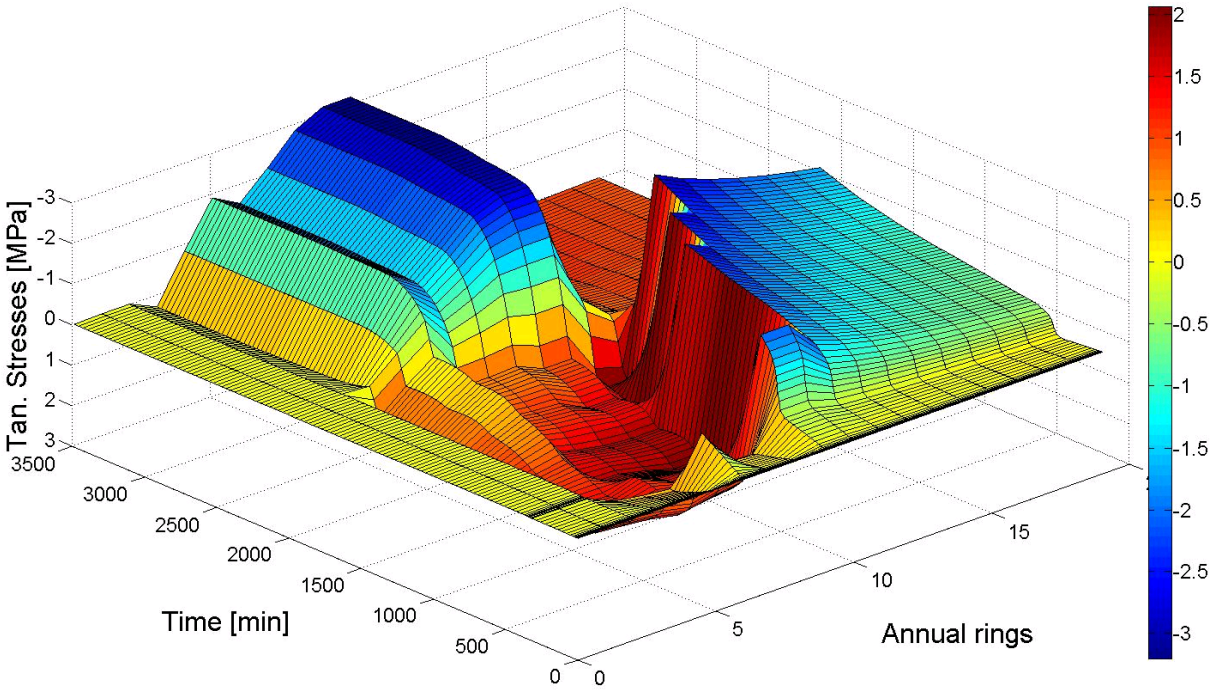

Figure 5.9: *Tangential stress, σ_t, as a function of the radius r and the drying time.*

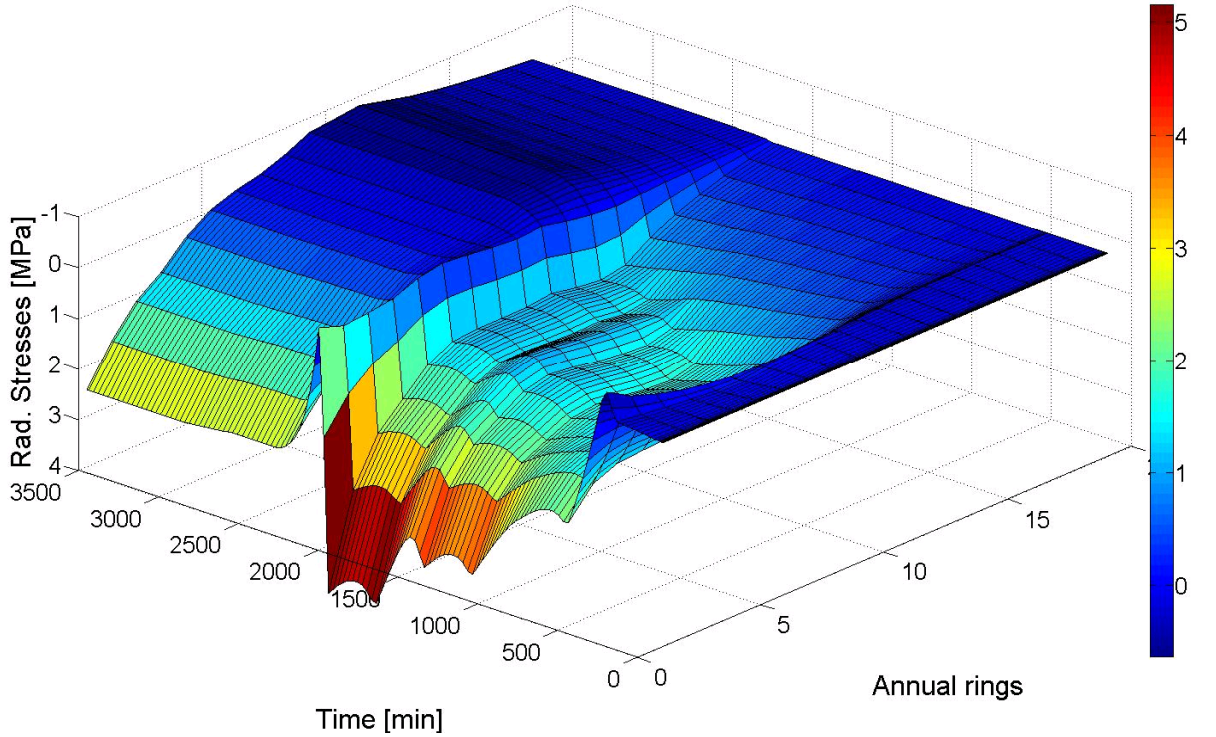

Figure 5.10: *Radial stress, σ_r, as a function of the radius r and the drying time.*

The stress generation in this zone is strongly affected by the early shrinking of the heartwood and the simultaneous resistance of the sapwood, that are followed by shrinking of the sapwood and constraint caused by the heartwood when it has reached EMC. The largest tangential compressive stresses occur in the middle zone near the end of the drying process,

whereas the largest tangential tensile stresses in this zone occur much earlier in the drying process.

In the quest for a better understanding of moisture-related stresses in wood, it is of interest to study how the stress state as a whole (σ_t, σ_r, τ_{rt}) develops at each material point in the course of the drying process. Figure 5.11 and Figure 5.12 show path plots for tangential, radial and shear stresses along path *r* after 15 and 45 hours of drying, respectively. For the transition zone, there is only a slight gradient for the radial stresses and there are almost no changes in the shear stresses. In the heartwood, the radial tensile stresses occur at a rather early stage in the drying process (at 15 hours), their being of the same level as the tangential stresses, although the tangential shrinkage coefficient is twice as large as the radial one.

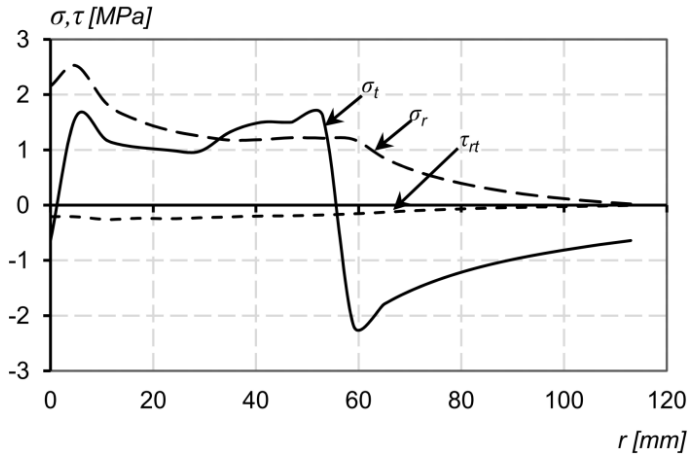

Figure 5.11: *Variations in radial, tangential and shear stress along r after* 15 *h (*900 *min.) of drying.*

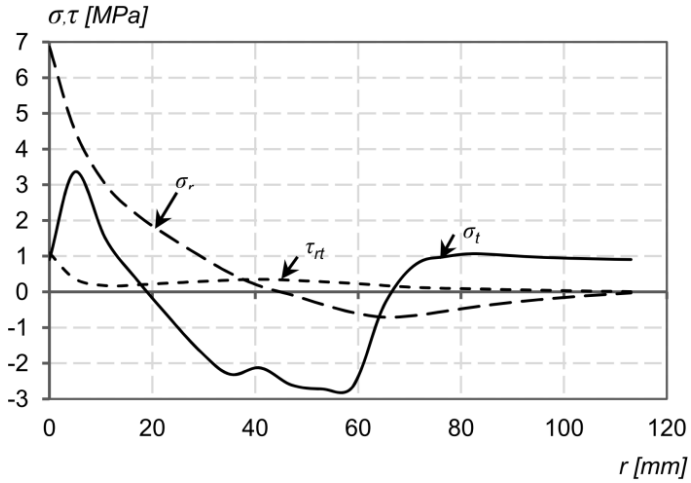

Figure 5.12: *Variations in radial, tangential and shear stress along r after* 45 *h (*2700 *min.) of drying.*

This is due to the internal constraints in these two directions being different, the elastic modulus in the radial direction being almost twice as large as the tangential one. For both the tangential and the radial stresses, the largest stresses along *r* are to be found close to the pith (at the tip of the slit), because of the stress concentrations being governed by the opening of the slit. Throughout the drying process, the shear stresses within the disc are only very slight.

5.4.2 Effects of drying schedules on strain and stress developments

Further numerical investigations were performed to examine how different drying conditions affect the development of strains and of stresses. Instead of using constant climatic conditions, as in the experimental study (63% RH and 23 °C applying there), two variable drying schedules were employed. The first schedule began with a humidity of 95% RH and a temperature of 23 °C, changes in these continuing until the entire cross section had reached 23% EMC (according to the Hailwood-Horrobin equation). From this stage on down to 12% EMC, the drying was simulated on the basis of the moisture history shown by the experimental results. The second drying schedule began with climatic conditions of 95% RH and 60 °C until a 20% EMC was reached in the cross section as a whole, changes that occurred then leading, just as for the first schedule, to conditions of EMC = 12%. During this simulation, the temperature was held at 60 °C. Both of the schedules aimed at removing the free water from the sapwood before the disc specimen as a whole was dried to a lower moisture content level, one that resulted in there being virtually no MC gradient below the EMC, which was reached after the initial drying phase. Each of the three drying schedules lasted for 60 hours and ended at 12% EMC. For each of the schedules, beginning at 95% RH, the course of MC from 40 to 60 (2400-3600 min.) hours was the same.

As shown in Figure 5.9 and Figure 5.12, variations in tangential stress along path *r* can be compared with those caused by each of the two modified moisture histories. Figure 5.13 and Figure 5.14 show variations in the tangential stresses each of the three drying schedules gives rise to after 15 and 45 hours (900 and 2700 min.) of drying, respectively.

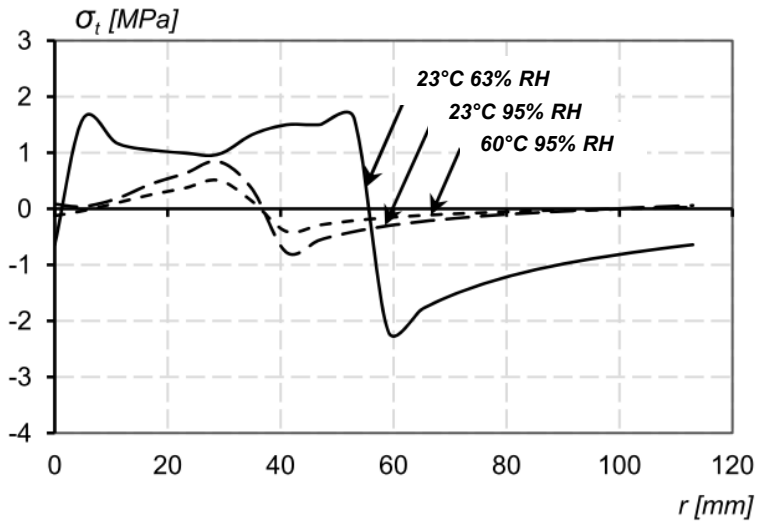

Figure 5.13: *Effects of each of three separate drying schemes on variations in tangential stress along path r after* 15 *hours (*900 *min.) of drying.*

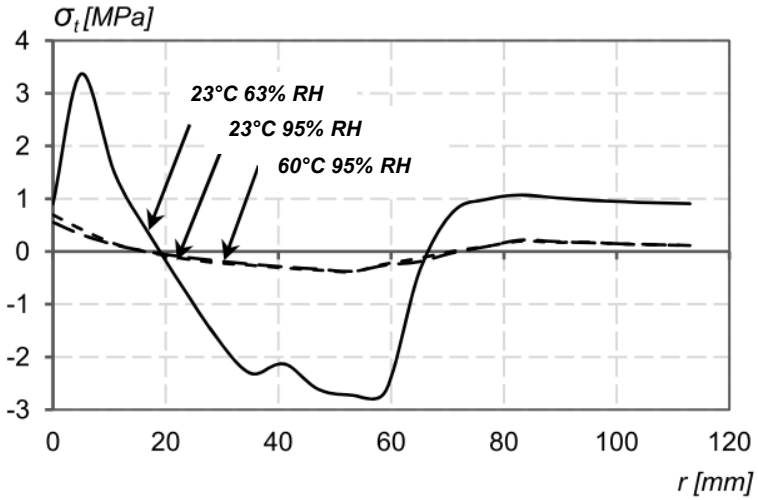

Figure 5.14: *Effects of each of three separate drying schemes on variations of tangential stress along path r after* 45 *hours (*2700 *min) of drying.*

Both Figure 5.13 and Figure 5.14 show there to be substantial reductions in the stresses occurring under the conditions that the modified drying schedules involve. The stress reduction in the diagram for 15 hours of drying (Figure 5.13) was most evident for the schedule with the highest temperature, although at 95% RH the EMC was lower at this temperature. These results indicate the clear effect of temperature on the elasticity and mechano-sorptive properties of the discs. Note that the elastic moduli and the mechano-sorption parameters change markedly from 23 °C to 60 °C; see Paper II [29] for further details. Both a reduction in the elasticity modulus and an increase in the mechano-sorption parameters lead at 60 °C to an increase in the mechano-sorptive strain and a reduction in constraints, this resulting in a lower stress level there.

5.4.3 Simulations of discs with closed annual rings

A number of simulations of the disc samples were performed to study how the strains and stresses develop during the drying-wetting-drying process. One of the major aims here was to study when, and where in the cross section, the cracking occurs under such conditions. Figure 5.15 shows the tangential strain history at different locations along path *r* shown in Figure 5.3. Comparison of the tangential strains for the first 60 hours with those of a disc having a slit shows the strain development to be basically the same, although the closed cross section showed a certain pattern, especially through the sapwood area there, displaying approximately 20% reduction in strains after the initial drying. The strain reduction was related to differential shrinkage that occurred in the tangential and the radial directions, the smaller radial shrinkage serving to hinder free tangential shrinkage from developing in the closed geometry involved. Also, the stress development during the initial drying period showed similarities to that in the disc with a slit. In both cases the heartwood area developed tensile stresses during the first 35 hours, the sapwood area developing compressive stresses during this period. The stresses changed from tensile to compressive, and vice versa, when the sapwood area started to shrink after 35 hours, see Figure 5.16.

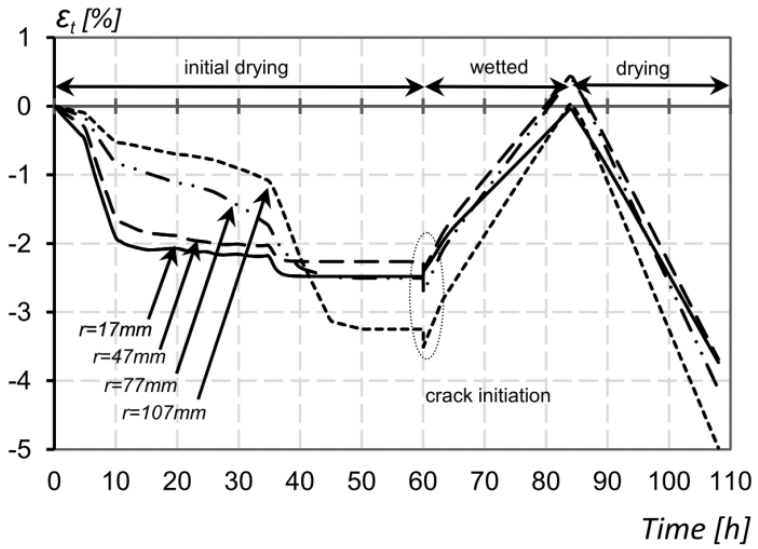

Figure 5.15: *The simulated tangential strain history as found at different distances from pith.*

The elastic strains were released when the crack was initiated; this appears as a jump in the curves at 60 hours in Figure 5.15. Figure 5.16 shows the tensile and the compressive stresses to immediately be reduced to nearly zero when the crack is initiated. The tangential swelling during the wetting period starts as a free swelling until the crack (shown in Figure 5.5) closes, from this point the stresses building up to a level after 10 hours of wetting and remaining constant then until FSP is reached after 24 hours of wetting. The stresses that developed during the wetting period reverse the mechano-sorptive strains developed earlier and bring the wood back into its original shape. The stresses only increase during the early part of the wetting period, whereas the strains continue rising until FSP is reached. The crack opens almost immediately after the second drying period has started and allows almost free tangential shrinking of the disc as a whole to take place. The differences in the shrinkage coefficient between the heartwood and the sapwood in connection with the stresses that are generated, appeared to be strongest in the transition zone (r=47 mm), whereas the effect of this sort close to pith and to bark was only limited. The substantial difference between the initial crack opening and the final crack opening that can be seen in Figure 5.5 shows the effect of the mechano-sorption that occurs on the stress development taking place, this effect being due to the large initial (green) variations in MC over the cross section and the closed geometry of the annual rings.

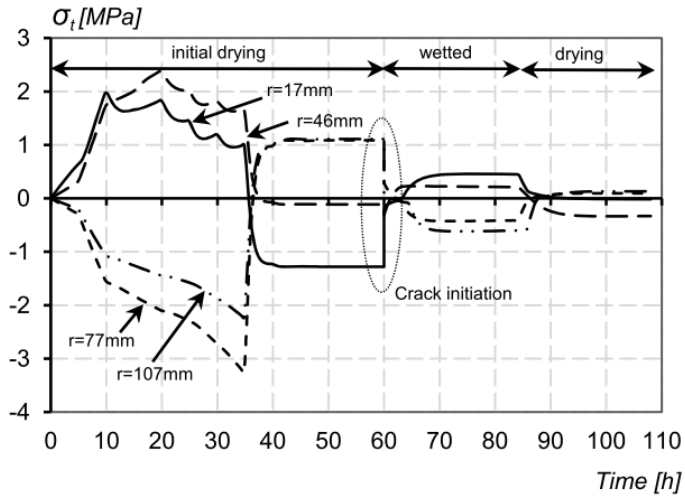

Figure 5.16: *The simulated tangential stress history at different distances from the pith.*

Figure 5.17 shows the tangential stress path plot at different times during drying prior to crack initiation, whereas Figure 5.18 shows the tangential stress path at different times during wetting and during the second drying phase after crack initiation.

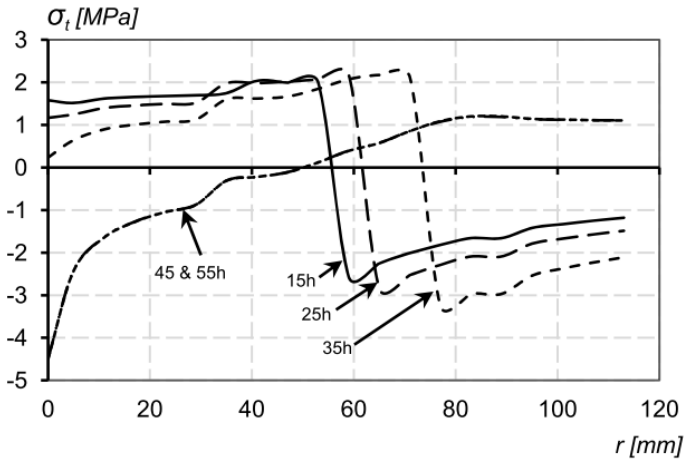

Figure 5.17: *Variations in the simulated tangential stress found along r at different points of time prior to crack initiation.*

The pattern prior to crack initiation showed the tensile stresses to be greatest early in the drying process, the tensile stresses being markedly reduced at the end of initial drying period. Both the tensile and the compressive stresses, except for the stress concentration close to the pith, were considerable less after crack initiation than prior to that.

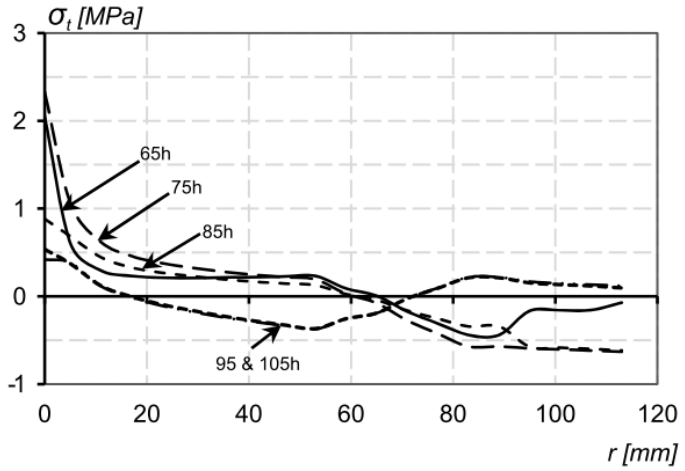

Figure 5.18: *Variations in the simulated tangential stress found along path r at different points of time after crack initiation.*

When the disc was initially dried down, considerable variation in the MC over the cross section gave rise to large stresses and mechano-sorptive strains. The mechano-sorptive strains were found to be totally reversible, however. The tangential stresses could be reduced if the MC was distributed over the cross section homogeneously, both prior to and during the drying process, as described in section 5.4.2, in Figure 5.13 and 5.14.

5.5 Crack developments under different drying conditions

As is known, both the elasticity and the mechano-sorption parameters of wood vary both with the temperature and with the moisture content. The tensile strength is also affected by the temperature, as has been summarised for three different species of wood by [19]. This summary (shown in Figure 5.19) indicates the tangential tensile strength to decreases with increasing temperature and MC, except for spruce, when temperature rises from 20 to 40 °C.

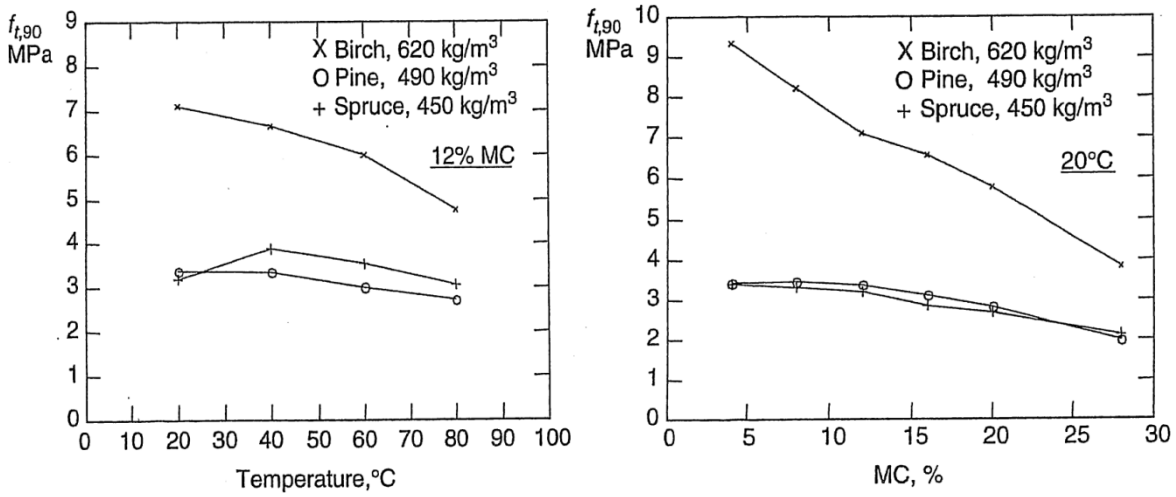

Figure 5.19: *The effect of temperature and of MC on tangential tensile strength in three different wood species,* [19].

The simulations presented in section 5.4.2 revealed a marked stress reduction when the initial (green) moisture gradient between different parts of the wood (e.g. the heartwood and the sapwood) is reduced. The gradient can vary from FSP to EMC, FSP depending upon the temperature and EMC depending both on the temperature and on RH. The MC span between FSP and EMC and the drying velocity both rise when the humidity decreases (see e.g. Figure 2.6).

Experimental investigations were carried out to determine how the temperature affects the tangential tensile strength. Disc specimens cut from the same timber log were dried in the climate chamber under different climatic conditions, each test sample being exposed to a constant temperature and a constant humidity. Tests at a given temperature and at intervals of 10% RH were recorded by means of Aramis and of load cells to observe whether the discs cracked and how and when the cracking occurred. Figure 5.20 provides a summary of the results, also presented in Paper III [30], indicating the test climates involved and whether or not the discs cracked.

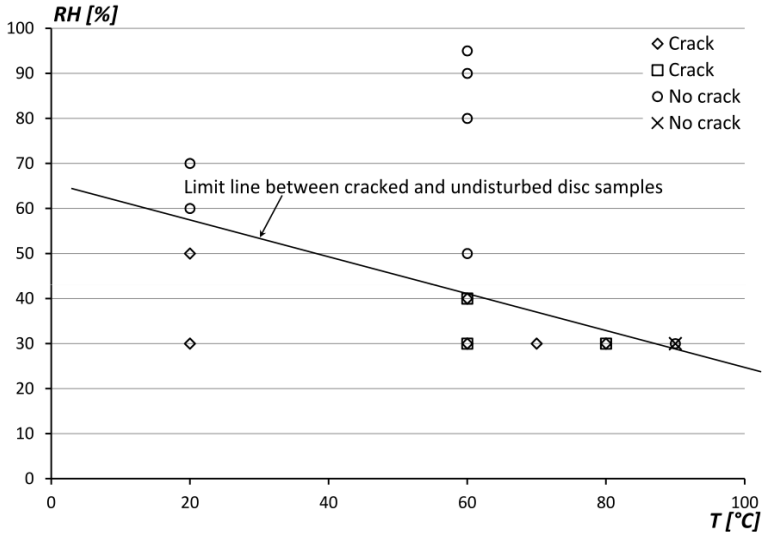

Figure 5.20: *A test result summary showing the relationship between the climate conditions and the cracking of disc specimens* 15 *mm thick, Paper III* [30].

The results presented in Figure 5.20 shows there to be an almost linear relationship between temperature, humidity and crack initiation. As presented in section 3.3.2, a moisture history was generated for each of the test cases, on the basis of the weight recordings obtained and calculations concerning these. The discs closest to the limit line were simulated in Abaqus, in accordance with what was taken up in section 3.3.2, each of the moisture histories and the temperature with each associated being studied. The critical tensile stresses were found for each of the simulations. The stress distribution and the moisture content at the highest stress level is shown in each case in Appendix D. The critical stresses from each of the simulations were then adjusted, in accordance with the relationships presented in Figure 5.19, to a value having a common MC of 18%. The critical stresses involved and the adjusted values are summarized in Paper III [30]. The tangential tensile strength lay somewhere in between the simulated stresses applying to the cracked and uncracked discs, taking the mean

value between those from cracked and uncracked discs at 20 °C and so forth. The simulated values are plotted directly in Figure 5.21 by use of the circular markers there, together with the tensile strength results (x-markers) presented in section 5.2.

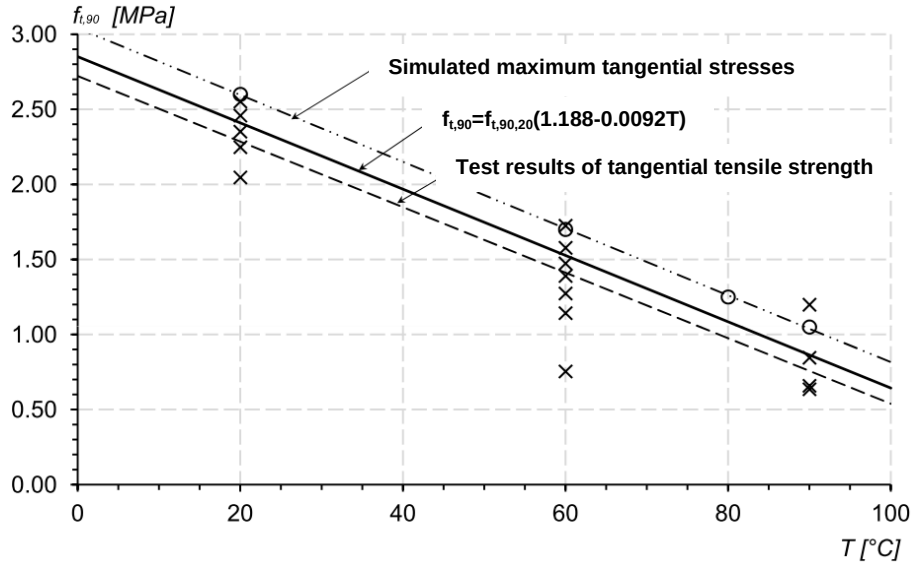

Figure 5.21: *Temperature dependence of the tangential tensile strength of Norway spruce, as obtained for* 15 *mm thick specimens at MC=*18*% on the basis of test and disc simulation results, Paper III* [30].

Figure 5.21 shows there to be a rather close correlation between the simulated and the experimentally obtained values here, despite the two trend lines being slightly displaced relative to one another. Both sets of results indicate the temperature to markedly affect the tangential tensile strength. This temperature/strength relationship can be thought to also occur in the radial and the longitudinal directions, though this was not investigated in the project involved here. An equation describing the relationship between the strength and the temperature is shown as eq. (5.1):

$$f_{t,90,T} = f_{t,90,20}\left(1.188 - 0.0092T\right) \tag{5.1}$$

in which $f_{t,90,T}$ is the tangential tensile strength at a given temperature in [°C] at 18% MC, and $f_{t,90,20}$ is the tangential tensile strength at 20 °C. The strength at 20 °C shown in Figure 5.21 is set to $f_{t,90,20} =$ 2.4 MPa. The effect on MC of the tangential tensile strength was not evaluated in the present project, although according to Figure 5.19, also the tangential tensile strength appears to be dependent upon MC, whether this is in fact the case would be of interest to investigate further.

5.5.1 Simulation of crack propagation during disc drying

The tangential tensile strength dealt with in the previous section was used in the disc crack modelling of kiln drying carried out. A disc with crack zones as described in the section 3.3, fracture energy as presented in section 3.2.1 and with tangential tensile strength as described in the section 5.2 was simulated for climatic conditions of 20 °C and 30% RH. The fracture

energy was set to 240 J/m^2 and the tangential tensile strength to 2.3 MPa. The drying histories involved were created from experiments performed under these climatic conditions. The experimentally observed crack development of the discs (by Aramis) during the drying process was compared with the simulated results, as shown in Figure 5.22.

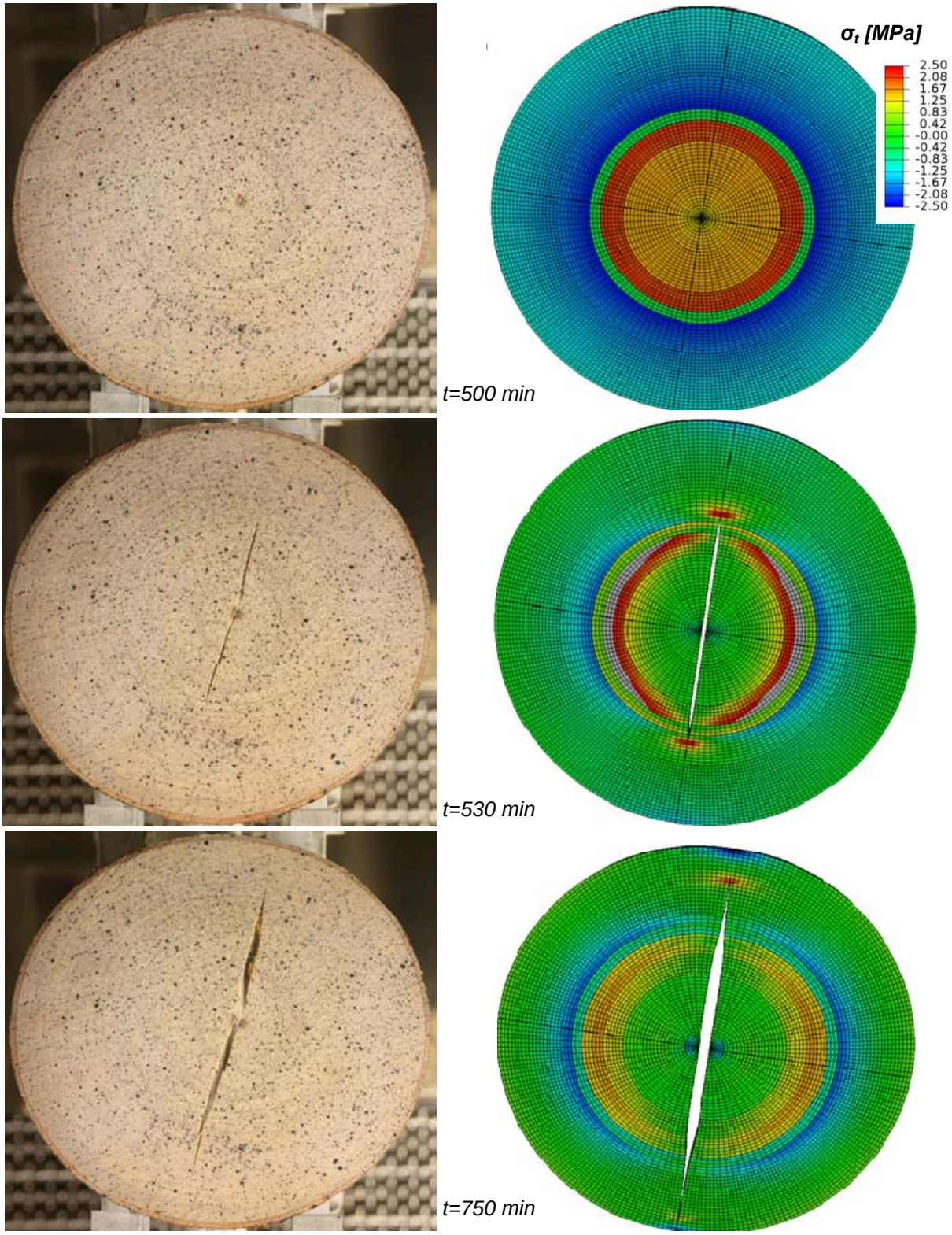

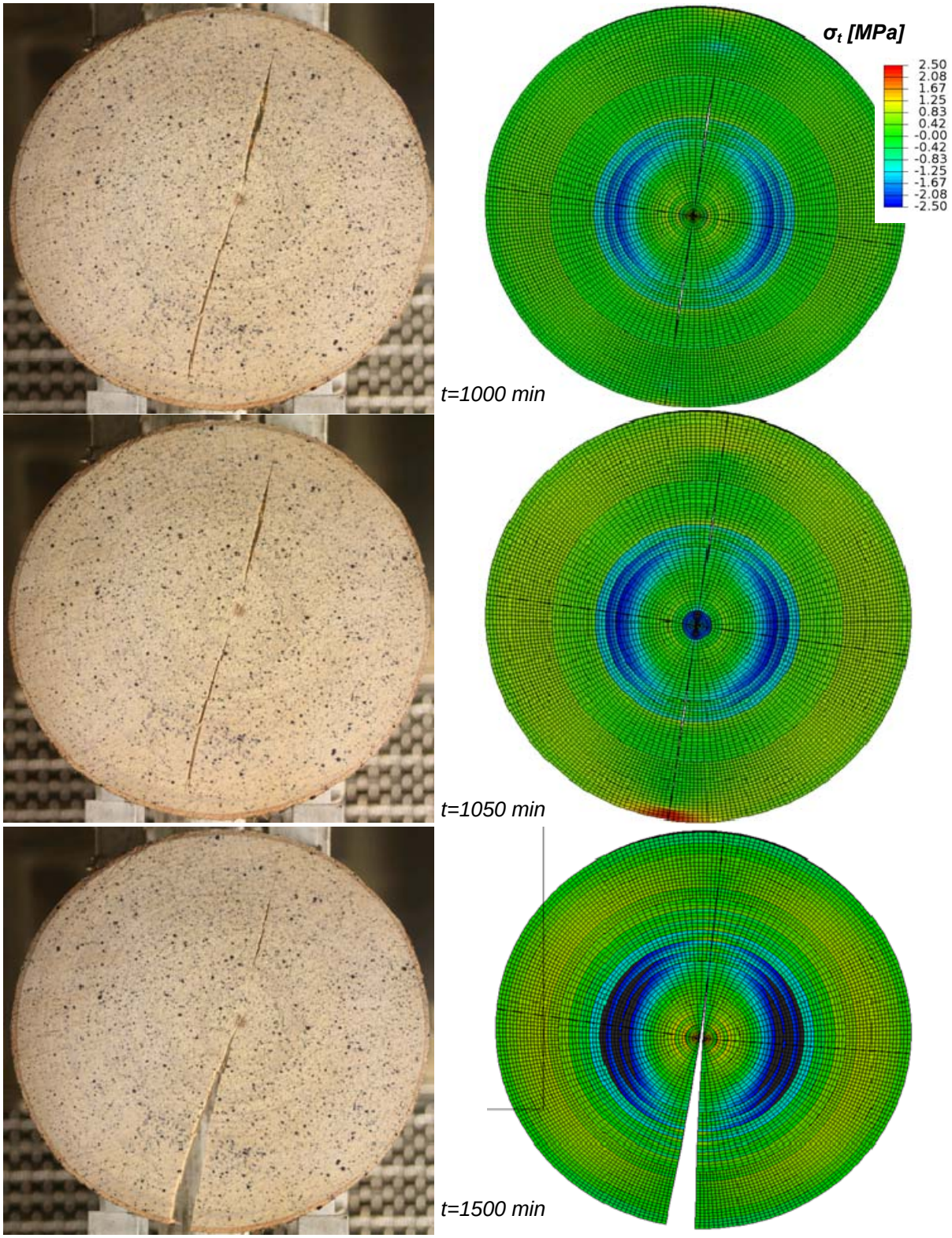

Figure 5.22: *Crack and stress development in a log disc during drying condition* 20 *°C and* 30*% RH, comparisons between results of the experiments and of the simulations after* 500, 530, 750, 1000, 1050 *and* 1500 *min. being shown.*

As shown in Figure 5.22, the MC after 500 min of drying was approximately 18% in the heartwood area, resulting in tangential tensile stresses in this area that were quite large. After 530 min of drying, the MC in the heartwood area was approximately 16% and a radial crack through this area had developed fully. After 750 min of drying, the MC in the heartwood area was close to EMC (MC=8-9%), whereas the sapwood area still is above the FSP. After 1000 min. the MC in the sapwood area was approximately 20%, which led to the crack closing because of shrinkage of the sapwood. The MC in the sapwood area decreased to 17%, the crack in the pith area was closing, and compressive stresses arose due to the contact involved. At the end of drying, which came after 1500 min, a full crack had developed. Note the high compressive stresses in the transition zone and the tangential tensile stresses in the sapwood area that had build up primarily because of the initial variation in MC over the cross section.

The results shown in Figure 5.22 indicate clearly that the correlation between the experimental results and results of the simulations states was rather high.

5.6 Water flux experiments

Large variations in MC often occur within wood cross sections when the wood is in a green condition. The stresses related to drying and the risk of cracking can be reduced if the RH-level in the surroundings is kept as high as possible until the whole cross section has dried down to an EMC level close to the FSP. Knowing how the temperature and the RH affect the water flux in wood is very useful in planning the drying schedules for timber board. It is especially important in the case of cross sections having high green MC gradients.

Water flux tests in the tangential and the radial direction were performed in the climate chamber at three constant temperatures (20, 60 and 90 °C) and at three humidity levels (70, 80 and 90% RH). The major goal of the study was to explore how water flux is affected by the temperature, the RH and the size of the external surfaces the samples possess. The test specimens used for these water flux experiments are described in sections 4.2.4 and 4.2.5.

5.6.1 Water flux above FSP

The water flux experiments were carried out in the climate chamber on both types of specimens at the same time, which were dried in the tangential and the radial direction simultaneously; this eliminating the risk of climate differences being found between the two highly similar experiments. Specimens with one and the same drying direction were grouped and were placed on a stand for this specific direction only. The weight of the specimens was logged every 5th minute. The climate around the specimens was kept constant during each test. Figure 5.23 shows the moisture history for both the radially and the tangentially dried specimens. The specimens were very similar and the drying conditions were identical for each of the two drying directions. The results also clearly show that the flow direction has almost no effect on the moisture histories of the samples.

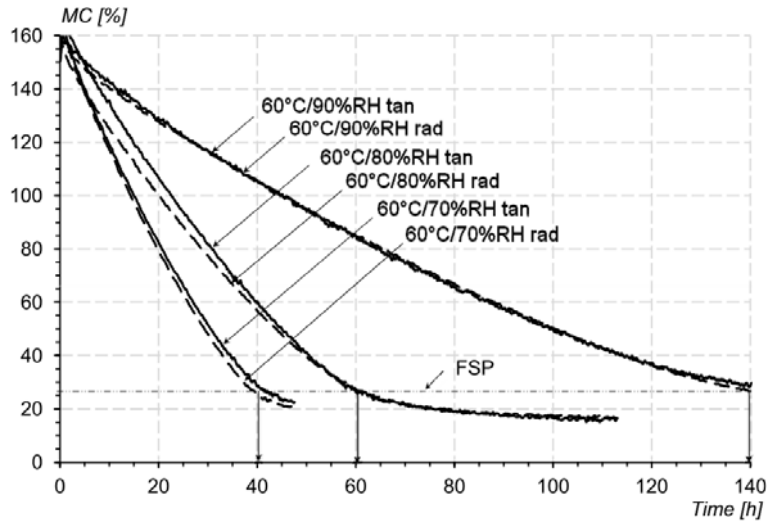

Figure 5.23: *The moisture history of samples having a radial and a tangential moisture flow at* 60 *°C and at an RH of* 70*,* 80 *and* 90*%.*

The same phenomenon was observed at 20 and at 90 °C. Figure 5.24 shows the moisture histories at 90 °C, the history from each humidity level being the average of results for the tangential and the radial drying direction.

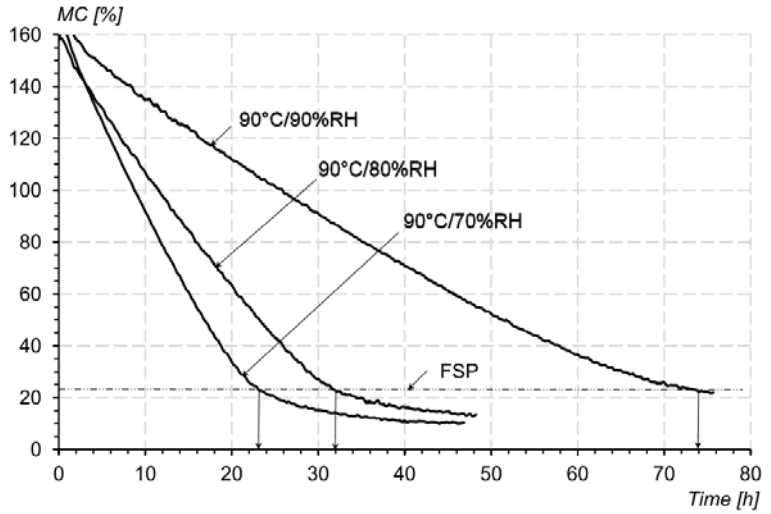

Figure 5.24: *Moisture history for samples dried at* 90 *°C and* 70*,* 80 *and* 90*% RH.*

The water flux above FSP was calculated as the loss of mass (water) from the green condition to FSP, divided by the area from which the water evaporates and the length of time involved. The average water flux for each climatic condition up to the time when FSP was reached was calculated, the results being presented in Paper IV [31]. The water flux for the nine experiments conducted is shown in Figure 5.25.

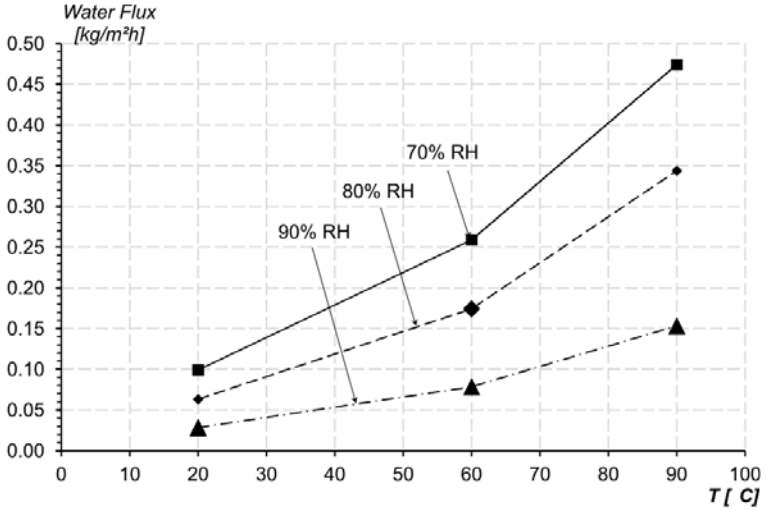

Figure 5.25: *Water flux above the FSP level under constant temperature and humidity conditions.*

As shown in Figure 5.25, the water flux increases as the temperature rises, just as the flux increases as the RH decreases. Under constant RH conditions, the drying time was reduced to approximately a 33% level when the temperature was increased from 20 °C to 60 °C and to a 20% level when the temperature was increased from 20 °C to 90 °C. In addition, the time could be reduced by a factor of two when the temperature was increased from 60 °C to 90 °C. The drying time could also be reduced to one-third when the humidity was changed from 90% RH to 70% RH and by 50% when the humidity was changed from 90% RH to 80% RH.

The results for water flux above the level of FSP were compared with water flux results above the FSP level for Pine that are presented in [59] and for 42 mm thick western hemlock boards presented in [6]. The water flux was of the same magnitude in all three experiments, despite the results applying three different species. All the species were softwoods.

5.7 **Drying of timber boards**

Simulations of stress development during the kiln drying of timber boards were performed to investigate how initial variation in MC values over the cross section affects the stress and the strain development during the drying process. The emphasis here was on the development of tangential stress development, since the strength in this direction is less than the strength in the radial direction; see e.g. [19] and [7]. The geometries and moisture histories of the timber boards are presented in Paper IV [31]. The kiln drying conditions were 60 °C and 80% RH. This climate provides an FSP of approximately 28% MC and an EMC of approx. 13% MC. The shrinkage coefficients employed for the simulations are $\alpha_{r\_heart} = 0.10$ and $\alpha_{t\_heart} = 0.20$ for the heartwood and $\alpha_{r\_sap} = 0.15$ and $\alpha_{t\_sap} = 0.30$ for the sapwood. The coefficients in the transition zones were interpolated between the heart and sapwood values. The drying-related stresses vary significantly during the drying process and the stresses are not necessarily largest at the end of the processes. Figure 5.26, Figure 5.27 and Figure 5.28 show the

tangential stress distribution at four specific times (15, 55, 110 and 165 hours) for each of the boards: board I, Board II and board III.

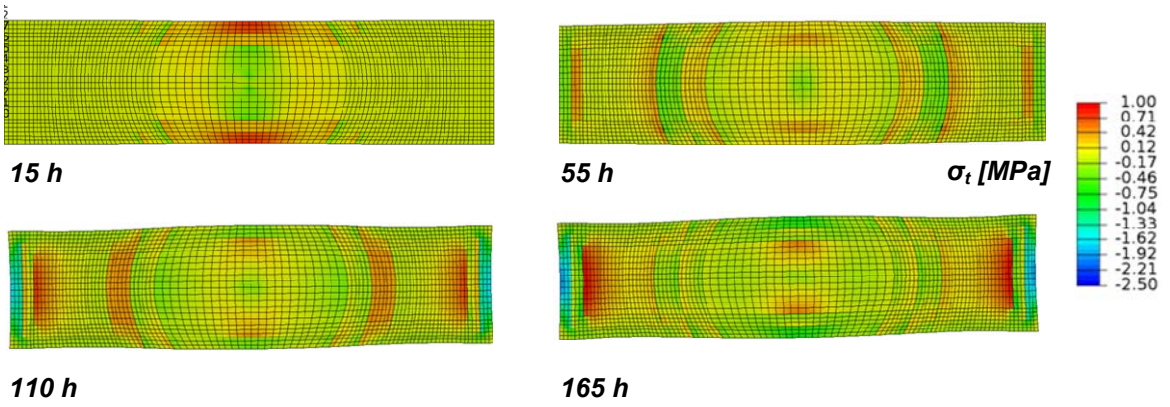

Figure 5.26: *Timber board I: Simulated tangential stress distribution after* 15, 55, 110 *and* 165 *h of drying at* 60°C *and* 80% *RH.*

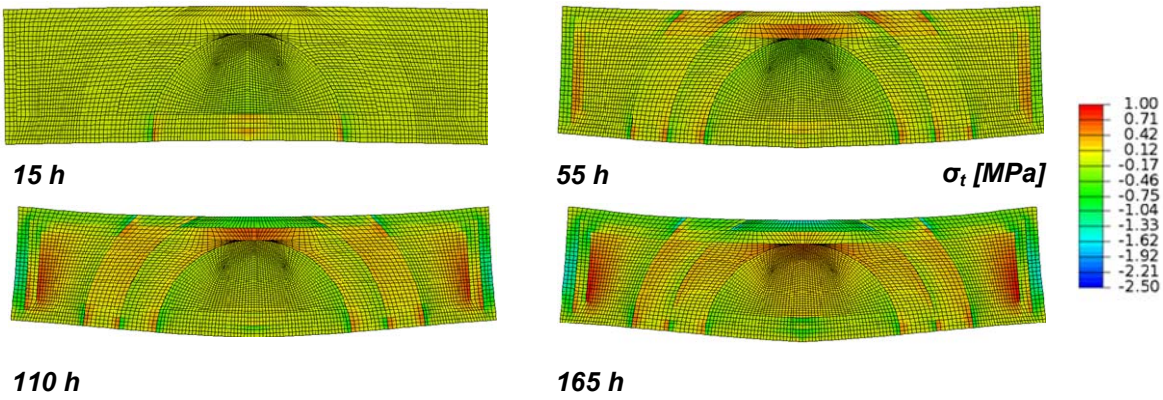

Figure 5.27: *The timber board II: Simulated tangential stress distribution after* 15, 55, 110 *and* 165 *h of drying at* 60°C *and* 80% *RH.*

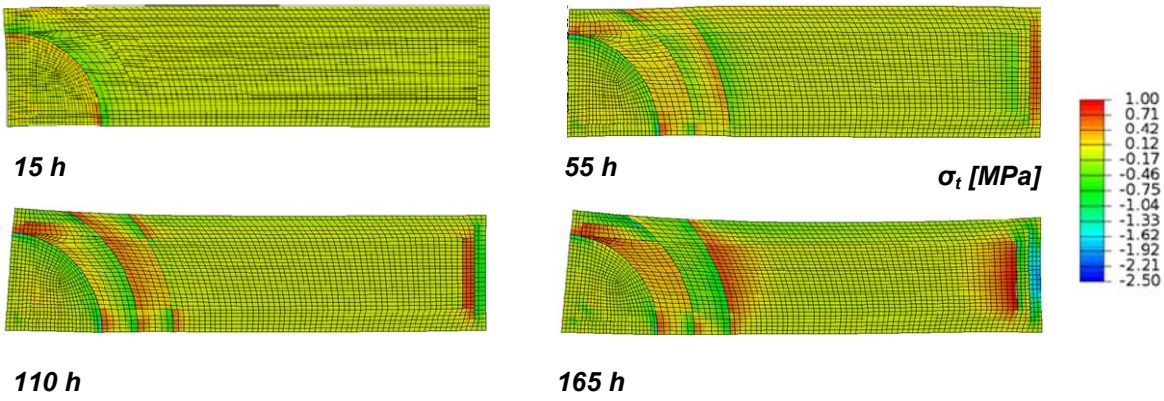

Figure 5.28: *Timber board III: Simulated tangential stress distribution after* 15, 55, 110 *and* 165 *h of drying at* 60°C *and* 80% *RH.*

The three figures above all show a stress development that changes as drying progresses, especially in the areas close to the transition zones, but the development for the three timber boards is different. These differences in behaviour between the boards that were studied arose primarily on the basis of how the heartwood dried, such as whether board III, in which the pith is located in the corner of the sample dries much faster than the heartwood of the two other boards. A good indicator of the drying speed is the ratio of the surface areas to the volumes involved. Larger ratios indicate faster drying of the volumes in question. The ratio of the sub-volumes to the surfaces involved is presented in Table 1 in Paper IV [31], together with detailed descriptions there of the tangential stresses in question, together with the tangential strains for each of the three simulated timber boards after 165 hours of drying.

Two parametric studies were carried out to study the effect of the shrinkage coefficient and whether the displaced moisture histories had any effect on stress development in the boards during drying. In the one study the shrinkage coefficients (such as for the sapwood) were designed to be identical for all the four sub-volumes, at the same time as the actual moisture histories and those in the original simulations were identical. The other study involved simulations based on moisture histories that were equilibrium for each of the sub-volumes, the drying starting simultaneously in each case from the FSP level. The shrinkage coefficients were graduated from the heartwood to the sapwood as in the original simulations. In the studies the tangential stress histories of a point centrally located in the transition zone closest to the heartwood, as shown for board I in Figure 5.29, for Board II in Figure 5.30 and for board III in Figure 5.31. The three curves represent the simulations Sim I, Sim II and Sim III.

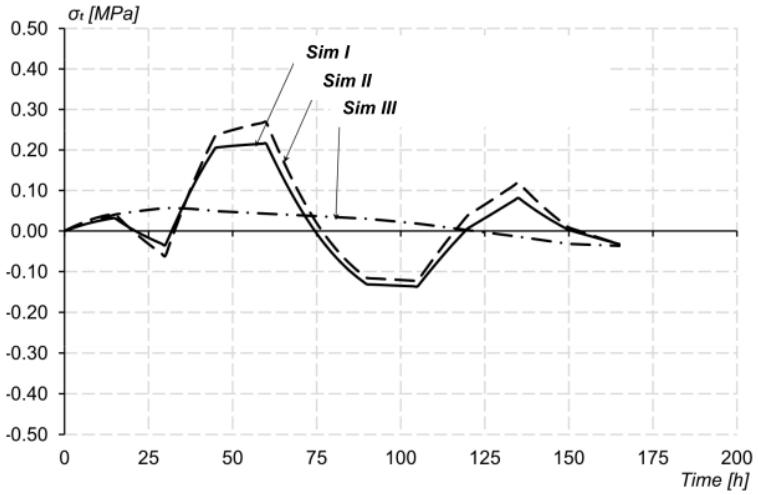

Figure 5.29: *Timber Board I: The simulated tangential stress history at a centrally located point in the transition wood close to the heartwood, Paper IV* [31].

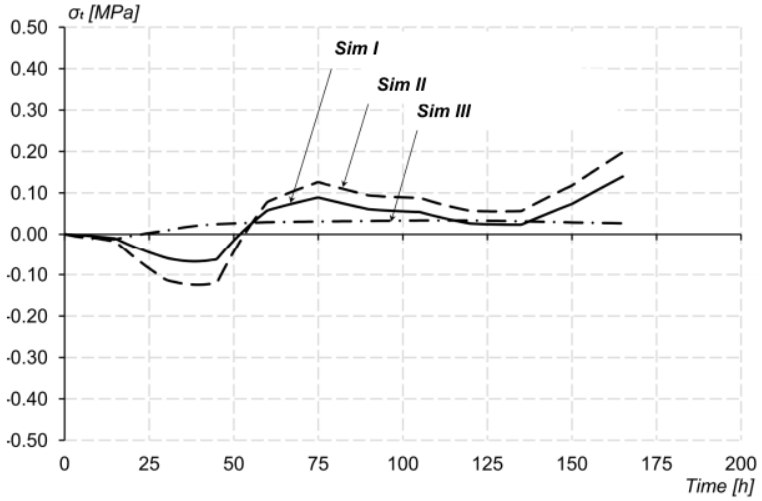

Figure 5.30: *Timber board II: The simulated tangential stress history at a centrally located point in the transition wood close to the heartwood, Paper IV* [31].

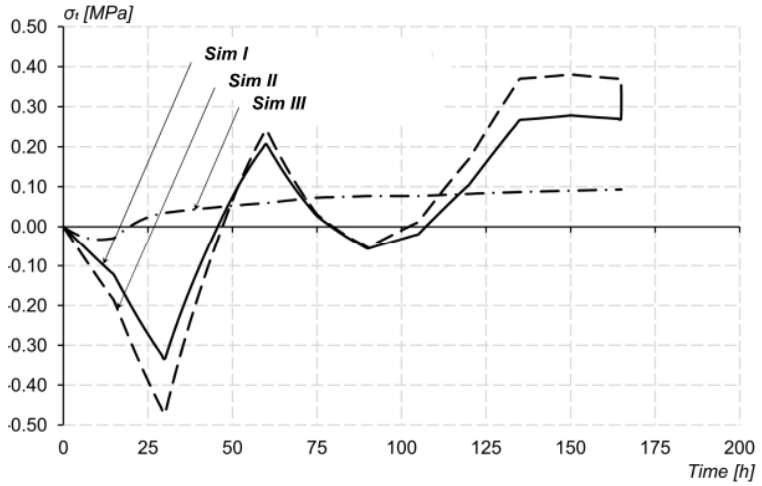

Figure 5.31: *Timber board III: The simulated tangential stress history at a centrally located point in transition wood close to the heartwood, Paper IV* [31].

The figures above show clearly how large variations in the green MC and changes in the shrinkage coefficients affect the stress development. One can also note that the sawn pattern has a strong effect on the stress development, the sawn pattern being most critical for board III, whereas for board II the sawn pattern has only a limited effect.

Chapter 6

6. Conclusions

The work reported on in the thesis can contribute to a better understanding of moisture- and temperature-related stresses and fracture in solid wood, when the inhomogeneity and the climatic dependency of the material parameters involved, as well as variations over the cross section of the wood in the initial (green) moisture content during the drying process are taken into account. Wood is a strongly orthotropic material, displaying large variations from tree to tree and from heartwood to sapwood. There are certain commonalities that can useful to take account of when wood is dried from a green condition to a state below FSP.

The investigations carried out here made use of wood samples involving strong contrasts in terms of material properties and MC between certain of the elements of which they were composed, such as heartwood and sapwood, which were included in all of the experiments and modelling investigations. The present project deals primarily with tangential stresses in wood and radially oriented cracks in it formed through the presence of a high degree of tangential tensile stress. The project is based in part on the results of earlier studies showing that it is tangential strains and stresses that are particularly critical for the occurrence of fracture in the radial direction.

The shrinkage parameters of the heartwood have been found to have an effect only about 50% as great as those of the sapwood. This contributes to significant stress generation in the transition zone between the heartwood and the sapwood, whatever effects other factors may have.

The results of experiments concerning crack development and results of simulations regarding this were found to agree rather closely with one another, use being made in both cases of measures of tangential tensile strength. The model employed here was verified by results of the experiments. It was also found that the tangential tensile strength decreased markedly with an increase in temperature, the dependency of the temperature and the tensile strength being almost linear. When the temperature of the wood material increased, the elastic moduli were reduced in size and the mechano-sorption parameters became larger. A reduction of this sort in the level of both properties resulted in a decrease of stresses when the temperature increased. As indicated earlier, an increase in temperature also led to a reduction in the strength of the wood, although in the disc experiments involving exposure of the wood to changes in the climatic conditions it was found that the reduction in strength was clearly less than the changes in the stiffness properties that occurred. In the experiments the RH could be reduced appreciably by a rise in temperature, without this being coupled with the emergence of cracks. Investigations of drying speed, also referred to as studies of water flux,

the drying above FSP being of particular interest, showed there to usually be an increase in drying rate with an elevation in temperature, when RH remained constant, the flux increasing as RH was reduced. Despite the cell structure of softwood providing the radially directed sides of the cell with far more pits than directed cells are provided with, the water flux was found to be quite similar in both directions. This may well be caused by the ray cells in the tangential direction contributing to the water flux. No linear relationship between the drying time, RH and the temperature was found however. At a constant RH, the drying time was reduced to one third of the original level when the temperature was increased from 20 °C to 60 °C, and it was reduced to one fifth of the original level when the temperature was increased from 20 °C to 90 °C. In addition, the time required for drying could be cut in factor two when the temperature was increased from 60 °C to 90 °C. The drying time could also be reduced to one-third when it was changed from 90% RH to 70% RH and by 50 % when the humidity was changed from 90% RH to 80% RH.

Moisture gradients that extend occurring from the surface to the depth during the drying of wood are well known and have been rather thoroughly investigated. It is far more seldom that investigations take account of the green moisture gradient over a wood cross section due to differences between the heartwood and the sapwood in the initial MC. When wood dries from a green condition down to a level below the FSP and a difference over the cross section in the initial MC is present, this leads to the different subparts of the cross section differing in the time at which they dry to a level below the FSP, this resulting in the risk of a moisture gradient producing unexpected constrains that lead to a buildup of stresses. This could be shown in simulations of rectangular cross sections having a variable initial MC. If there are large differences over a cross-section in the initial moisture level, the damaging moisture gradient just referred to can be reduced if the humidity of the surroundings is kept as high as possible during the initial drying, until the parts with the highest MC levels have been dried down close to the FSP level, a relatively high MC level in the parts with the lowest initial moisture level thus being maintained. This was demonstrated in the experiments involving the discs. After that, the drying stresses tend only to be affected by the moisture gradient from the surface to the depth. This is a familiar problem, one already accounted for in the drying process.

It was found that stress, crack development and the drying time became less at higher temperatures, making high-temperature drying appear more optimal, yet this fails to take account of economic considerations, since both energy and water consumption can rise dramatically at elevated temperatures. The costs of the increases use of energy might well exceed the costs of the material loss involved in using lower temperatures. In taking account of all of this, one might finally end up with a temperature somewhere in between the two extremes, a temperature at which the energy costs, the time requires for drying, and the amount of material which is damaged are acceptable.

Chapter 7

7. Future work

During the work carried out, various matters have appeared to be in particular need of further research if one is to obtain an adequate understanding of the strains and stresses and the crack behaviours that occur during the kiln-drying of softwood.

7.1 Tangential tensile strength

Much is yet to be investigated concerning the tangential tensile strength of Norway spruce, especially as regards its temperature and moisture dependence. Further experimental studies are needed to extend knowledge of dependency of the strength on factors of temperature and moisture. This is of interest not only for the wood drying industry, but also for those segments of the timber construction industry producing timber and glulam structures exposed to outdoor seasoning. It is likewise of interest for the design of constructions subjected to particular high or low temperature, such as structures exposed to heat due to a fire or outdoor construction in very cold climates. In the present work it was only the tangential tensile strength of small cross sections of logs, or segments of these, that were studied, the scale effects at dealing with much larger objects was not investigated. Matters of this sort are clearly in need of further investigations.

7.2 Fracture energy

The fracture energy results of the various investigations of Norway spruce that have been carried out provide a very scattered picture. The fracture energy level can vary, for example, anywhere from 140 to 440 J/m^2 for one and the same MC and temperature level. Further investigations of the effects of the temperature level on the fracture energy are needed. One reason for the widely varying results for measured fracture energies obtained could be the large numbers of test methods that have been employed. The methods seem to be too many and too different in their construction. Some of them are ones designed originally for concrete and metals and then adapted to use with wood, even though they may not be as satisfactory for the testing of wood. Also, the three point bending test for determining the tangential fracture energy of wood, for example, is a method that is rather complex to use, because of the experimental specimen needing to be composed of three wood pieces that are glued

together. Quite generally speaking, the results of the one method are often difficult to compare with results of another. This may be the reason for the broad scatter found in the fracture energy results.

A new standard for fracture energy tests of wood is needed, one in which varying temperature and MC values are dealt with more adequately in evaluating crack developments during kiln-drying.

7.3 **Modelling work**

In the present work, the conception of the moisture flow in the wood material was very much simplified. The MC field history created was based on the water flux results presented above. Further modelling work is needed to better simulate the transient moisture flow during the drying process as a whole from the green to the dry condition, considering taking the marked changes in drying speed from above FSP down to below this and further down to EMC into account.

In order to achieve a more adequate 3D stress model, a visco elastic model of strongly orthotropic creep behaviour needs to be developed. This latter model needs to be able to simulate accurately how the moisture level and the temperature affect the visco elastic behaviour of wood.

The crack model needs to be developed further to take adequate account of the moisture- and temperature- dependent stiffness of the wood and its strength and fracture-energy parameters. Another matter to investigate is whether there is any size effect that should be taken account of in connection with the crack parameters.

Bibliography

[1] ABAQUS. *Theory manual v6.8.* Simulia, 2008.

[2] Aramis v6 User Manual. GOM mbH, GOM Optical Measuring Techniques. (www.gom.com), 2007.

[3] L.D. Armstrong and R.S.T. Kingston. The effect of moisture content changes on the deformation of wood under stress. Australian Journal of Applied Science 13: 257-276, 1962.

[4] R.D. Ball, I.G. Simpson and S. Pang. Measurement, modelling and prediction of equilibrium moisture content in *Pinus radiata* heartwood and sapwood. Holz als Roh- und Werkstoff 59:457-462, 2001.

[5] R. Baronas, F. Ivanauskas, I. Juodeikienė and A. Kajalavicius. Modelling of Moisture Movement in Wood during Outdoor Storage. In Nonlinear Analysis: Modelling and Control 6,2:3-14, 2001.

[6] A.H. Berberovic´ and M. R. Milota. Simulation of drying Using a Kiln Model. In Drying Technology. 26:1097-1102, 2008.

[7] J. Bodig and B.A. Jayne. Mechanics of wood and wood composites. Van Nostrand Reinhold Company, New York, 1982.

[8] P. Bonneau and J.-R. Puiggali. Influence of heartwood-sapwood proportions on the drying kinetics of a board. In Wood Science and Technology. 28:67-85, 1993.

[9] M. Campean. Timber Drying Methods-Passing Through History Into The Future. *11th International IUFRO Wood Drying Conference*, 2010.

[10] B. Clair, G. Jaouen, J. Beauchêne and M. Fournier. Mapping Radial, Tangential and Longitudinal Shrinkages and Relation to Tension Wood in Discs of the Tropical Tree *Symphonia globulifera*. In Holzforschung. 57:665-671, 2003.

[11] A. Cloutier and Y. Fortin. Wood drying modelling based on the water potential concept: Hysteresis effects. Drying technology, 12(8):1793-1814, 1994.

[12] J.L. Coureau, S. Morel and P.J. Gustafsson. Influence of the fracture softening behaviour of wood on load-COD curve and R-curve. Materials and Structures, 40:97-106, 2006.

[13] O. Dahlblom, H. Petersson and S. Ormarsson. Characterization of shrinkage, European project FAIR CT 96-1915, Improved Spruce Timber Utilization, Final report Sub-task AB1.5; 1999.

[14] N. Dourado, S. Morel, M.F.S.F. de Moura, G. Valentin and J. Morais. Comparison of fracture properties of two wood species through cohesive crack simulations. Composites: Part A 39:415-427, 2008.

[15] N. Dourado. R-curve behaviour and size effect of a quasibrittle material: Wood. PhD thesis. N° d'ordre: 3734. L'Université Bordeaux I, France, 2008.

[16] M. Ekevad, N. Lundgren and J. Flodin. Drying shrinkage of sawn timber of Norway spruce (Picea abies): Industrial measurements and finite element simulations. Wood Material Science and Engineering. 6:41-48, 2011.

[17] S. Felix, P. Morlier. Modelling of Stresses and Strains in a Piece of Wood Under Drying. In Holzforschung. 46:369-377, 1992.

[18] S. Fortino, F. Mirianon and T. Toratti. A 3D moisture-stress FEM analysis for time dependent problems in timber structures. Mech Time-Depend Mater. 13:333-356, 2009.

[19] P.J. Gustafsson. Timber Engineering. John Wiley & Sons Ltd. Pages 103-130, 2003. ISBN 0-470-84469-8.

[20] A.J. Hailwood and S. Horrobin. Absorption of water by polymers: analysis in terms of a simple model. Transactions of Faraday Society. 42B:84-92 and 94-102, 1946.

[21] Hyper physics. Department of Physics and Astronomy, Georgia State University, 2012.

[22] W. Kang and N.-H. Lee. Mathematical modelling to predict drying deformation and stress due to differential shrinkage within a tree disk. Wood Science and Technology. 36:463-476, 2002.

[23] W. Kang and N.-H. Lee. Relationskip between radial variations in shrinkage and drying defects of tree disks. J Wood Sci. 50:209-216, 2004.

[24] Kowalski SJ, Smoczkiewicz-Wojciechowska A (2007) Stresses in dried wood. Modelling and experimental identification. Transp Porous Med. 66:145-158.

[25] K. Krabbenhøft. Chapter 4 and 5, Moisture Transport in Wood. A Study of Physical-Mathematical Models and their Numerical Implementation. Ph.D. Thesis. ISBN nr. 87-7877-225-7. Denmark, 2003.

[26] F. Larsen, S. Ormarsson and J.F. Olesen. *Proceedings of the 11th International IUFRO Wood Drying Conference, 2010*. 137-144, Luleå University of Technology, Skellefteå, Sweden.

[27] F. Larsen, S. Ormarsson and J.F. Olesen. *Proceedings of the 11th World Conference on Timber Engineering, 2010*. 449-451, Riva del Garda, Italy.

[28] F. Larsen, S. Ormarsson and J.F. Olesen. Moisture-driven fracture in solid wood. In Wood Material Science and Engineering. 6(1-2):49-57, 2011.

[29] F. Larsen and S. Ormarsson. Numerical and experimental study of moisture-induced stress and strain field developments in timber logs. Wood Science and Technology, 2012.

[30] F. Larsen and S. Ormarsson. Numerical and experimental study of temperature and moisture related fracture behaviour in timber logs. Submitted in Holzforschung, 2012.

[31] F. Larsen and S. Ormarsson. Influence of initial (green state) moisture gradients on stresses in timber boards during drying. Submitted in Wood Science and Technology, 2012.

[32] C. Lazarescu, S. Avramidis. Drying Related Strain Development in Restrained Wood. Drying Technology 26(5):544-551, 2008.

[33] H. Lindström. Intra-Tree Models of Juvenile Wood in Norway Spruce as an Input to Simulation Software. Silva Fennica 36(2):521-534, 2002.

[34] H. Mounji, M. El Kouali, J. Bouzon and J.M. Vergnaud. Modelling of the drying process of wood in 3-dimensions. Drying Technology 9(5):1295-1314, 1991.

[35] S. Ormarsson, O. Dahlblom and H. Petersson. A numerical study of the shape stability of sawn timber subjected to moisture variation part 1: Theory. Wood Science and Technology 32:325-334, 1998.

[36] S. Ormarsson, O. Dahlblom and H. Petersson. A numerical study of the shape stability of sawn timber subjected to moisture variation part 2: Simulation of drying board. In Wood Science and Technology. 33:407-423, 1999.

[37] S. Ormarsson. Numerical Analysis of Moisture-Related Distortions in Sawn Timber. PhD thesis. ISBN 91-7197-834-8. Göteborg, Sweden, 1999.

[38] A. Reiterer and G. Sinn. Fracture Behaviour of Modified Spruce Wood: A Study Using Linear and Non Linear Fracture Mechanics. In Holzforshung 56:191-198, 2002.

[39] S. Rosner, B. Karlsson, J. Konnerth and C. Hansmann. Shrinkage processes in standard-size Norway spruce wood specimens with different vulnerability to cavitation. Tree Physiology 29:1419-1431, 2009.

[40] J.-G. Salin. Modelling of the behaviour of free water in sapwood during drying. In Wood Material Science & Engineering. 1:4-11, 2006.

[41] J.-G. Salin. Drying of Liquid Water in Wood as Influenced by the Capillary Fiber Network. Drying Technology, 26(5):569-567, 2008.

[42] J.-G. Salin. Problems and solutions in wood drying modelling: History and future. In Wood Material Science & Engineering. 5:123-134, 2010.

[43] J.F. Siau. Transport Processes in Wood: Springer Series in Wood Science, 1984. ISBN 0387125744.

[44] J.F. Siau. Wood: Influence of moisture on physical properties: Department of Wood Science and Forest Products Virginia Polytechnic Institute and State University, 1995. ISBN no: 0-9622181-0-3.

[45] W.T. Simpson. Predicting equilibrium moisture content of wood by mathematical models. Wood and Fiber Science 5:41-49, 1973.

[46] I. Smith, E. Landis and M. Gong. Fracture and Fatique in Wood, Wiley, 2003. ISBN 0-471-48708.

[47] I. Smith, S Vasic. Fracture behaviour of softwood. In Mechanics of Materials 35:803-815, 2003.

[48] M. Sreekanth, A.K. Kolar. Transient Thermal Behavior and Stress Development within a Cylindrical Wooden Disk during Drying in a Fluidized Bed Dryer. Drying Technology 27:344-358, 2009.

[49] S.E. Stanzl-Tschegg, E.K. Tschegg and A. Teischinger. Fracture energy of spruce wood after different drying procedures. In Wood and Fiber Science, 26(4):467-478, 1994.

[50] S.E. Stanzl-Tschegg, D.M. Tan and E.K. Tschegg. New splitting method for wood fracture characterization. In Wood Science and Technology 29:31-50, 1995.

[51] S. Svensson. Strain and Shrinkage Force in Wood under Kiln Drying Conditions. Holzforschung 49:363-368, 1995.

[52] S. Svensson. Internal stress in wood caused by climate variations. Report TVBK-1013. Lund University, 1997.

[53] http://www.swedishwood.com April 2012

[54] T. Thomassen. Trætørring, Praktisk vejledning. Træ 45. Træbranchens Oplysningsråd, 2000. ISBN:87 90856 10-4. In danish.

[55] B. Time. Studies on hygroscopic moisture transport in Norway spruce (Picea abies). Part 2: Modelling of transient moisture transport and hysteresis in wood. Holz als Roh- und Werkstoff 60:405-410, 2002.

[56] G.H. Valentin, L. Boström, P.J. Gustafsson, A. Ranta-Maunus and S. Gowda. Application of fracture mechanics to timber structures RILEM state-of-the-art report, Statens tekniska forskningscentral, Technical Research Centre of Finland, Research Notes 1262, ESPOO 1991.

[57] S. Vasic and I. Smith. Bridging crack model for fracture of spruce. Engineering Fracture Mechanics 69:745-760, 2002.

[58] S. Vasic and S. Stranzl-Tschegg. Experimental and numerical investigation of wood fracture mechanisms at different humidity levels. Holzforschung 61:367-374, 2007.

[59] P. Wiberg, S.M.B. Sehlstedt-Persson and T.J. More'n. Heat and Mass Transfer During Sapwood Drying Above the Fibre Saturation Point. Drying Technology 18(8):1647-1664, 2000.

[60] A.G. Yiotis, A.K. Stubos, A.G. Boudouvis, I.N. Tsimpanogiannis and C.Y. Yortsos. Modeling of Drying Processes in Pore Networks. Mathematics in industry 8:293-297, 2004.

List of Figures

List of Tables

Appendix A: Mode I test methods

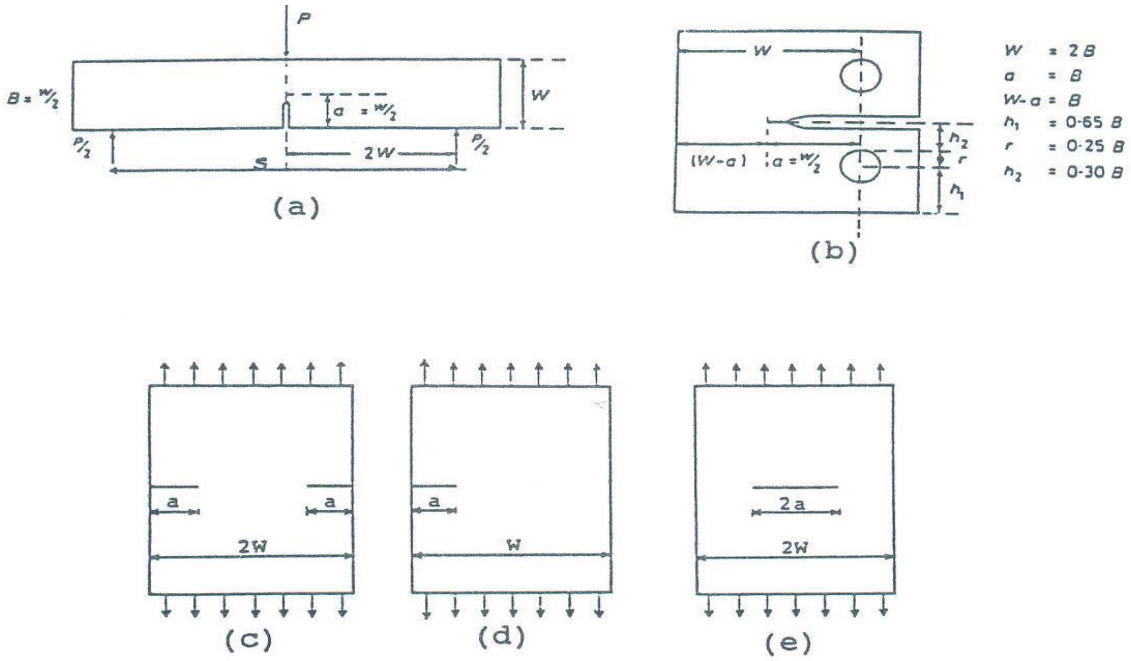

Figure 19. Different types of specimens.
(a) Three-point bending (TPB)
(b) Compact tension (CT)
(c) Double-edge notched (DEN)
(d) Single-edge notched (SEN)
(e) Center notched (CN).

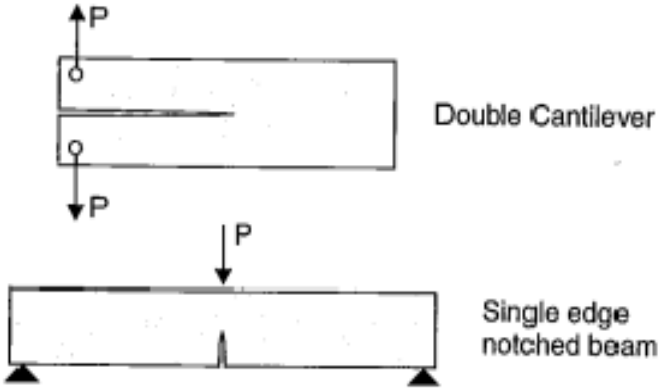

Appendix B: Tangential tensile strength

Tangential tensile strength tests performed by Jesper and Ejnar Videbæk

Tangential tensile strength

Specimen no.	Dato:	t [m]	b [m]	F [N]	$f_{t,90}$ [MPa]	$f_{t,90}$ [MPa]
Experiment 1 (20gr, 85RH, 18%MC):						
1	03/04/2012	0.01491	0.01944	739.71114	2.552045	
4	03/04/2012	0.01492	0.01935	709.76014	2.458452	
6	11/04/2012	0.01484	0.01989	663.50794	2.247902	
8	16/04/2012	0.0148	0.01986	691.20034	2.351597	
9	16/04/2012	0.01481	0.02009	608.90874	2.046526	
					Meanvalue	2.331305
					Stand var.	0.195806

Specimen no.	Dato:	t [m]	b [m]	F [N]	$f_{t,90}$ [MPa]
Experiment 2 (60gr, 91RH, 18%MC):					
13	16/04/2012	0.0149	0.01948	331.59194	1.142428
14	16/04/2012	0.01471	0.0196	454.83294	1.57755
15	16/04/2012	0.01474	0.0194	397.48414	1.390019
16	16/04/2012	0.01465	0.01945	491.55974	1.725119
17	19/04/2012	0.01435	0.0183	198.03994	0.754136
19	19/04/2012	0.01465	0.0195	363.89974	1.273824
20	19/04/2012	0.01415	0.02	417.02594	1.47359
				Meanvalue		1.333809
				Stand var.		0.319238

Specimen no.	Dato:	t [m]	b [m]	F [N]	$f_{t,90}$ [MPa]
Experiment 3 (90gr, 96RH, 18%MC):					
22	24/04/2012	0.01433	0.02014	345.89477	1.198501
26	24/04/2012	0.01455	0.02077	192.01537	0.635384
25	25/04/2012	0.01441	0.02007	190.44417	0.658501
28	25/04/2012	0.01453	0.02045	251.13177	0.845167
				Meanvalue		0.834388
				Stand var.		0.260277

Appendix C: Climate chamber data

Performance range for climatic testing

Temperature range	+10 °C to +95 °C
Temperature deviation in time in centre of working space	±0.1 K to ±0.3 K
Temperature homogeneity in space relative to the set value	±0.5 K to ±1.0 K
Humidity range	10 % to 95 % r. h.
Dew point range	+4°C to +94°C when using plain floor element
Humidity deviation in time in centre of working space	±1 % r. h. to ±3 % r. h.
Heat compensation	500 W at 25 °C to 90 °C humidity up to max. 90 % r. h. is maintained
Climatic calibration values are measured at	+23 °C / 50 % r. h. and +95 °C / 50 % r. h.

Humidity diagram

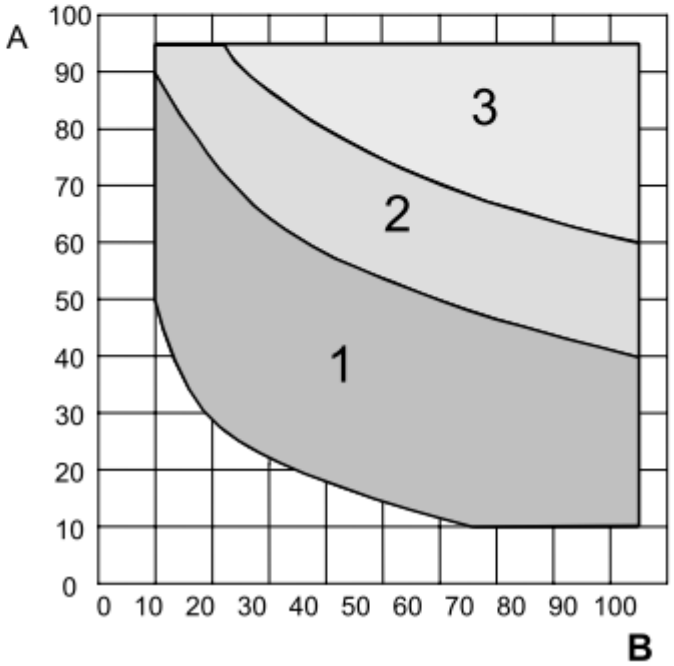

Legend

A test space temperature in °C
B relative humidity in % r. h.

1 range in combination with horizontal vibration
1+2 range in combination with vertical vibration
1+2+3 range with plane floor element

Definition of linear temperature rate of change

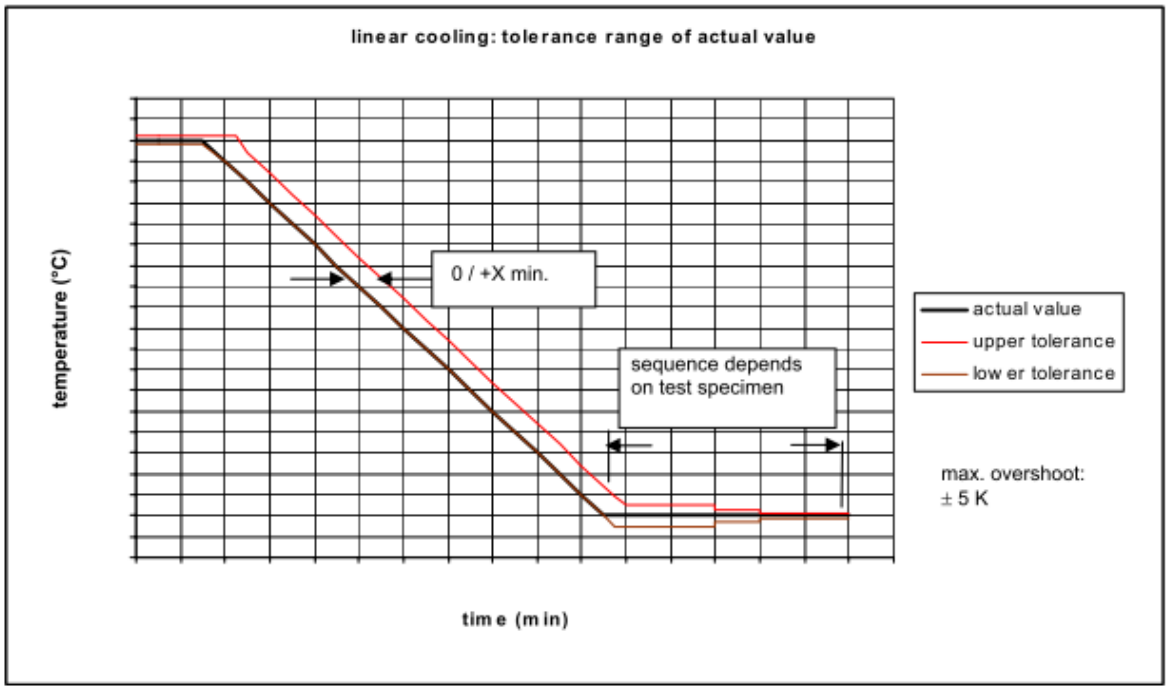

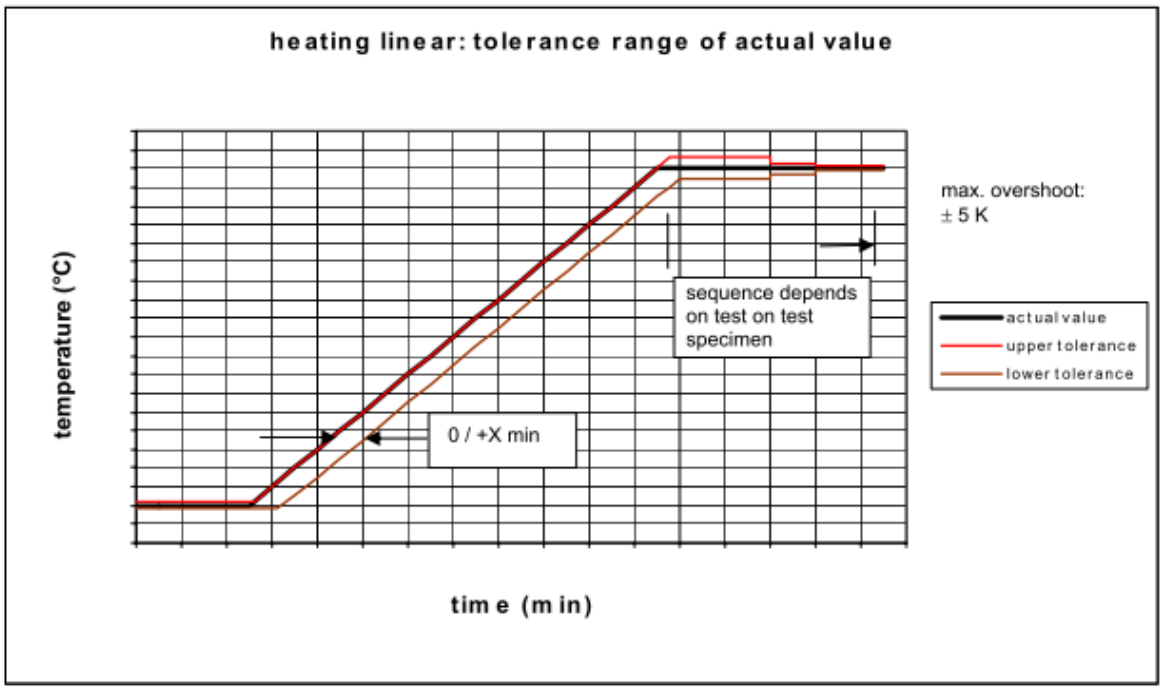

Definition: temporal fluctuation while cooling resp. heating phase depends on the temperature rate of change:
at Δt 5 K/min: X = 1,2 min
at Δt 10 K/min: X = 1,4 min
at Δt 15 K/min: X = 1,6 min
at Δt 20 K/min: X = 1,8 min

Appendix D: Critical stress and ass. MC

The following figures App D, Figure 0.1 and App D, Figure 0.1 show the maximum tangential stresses and the MC at the state of maximum stresses.

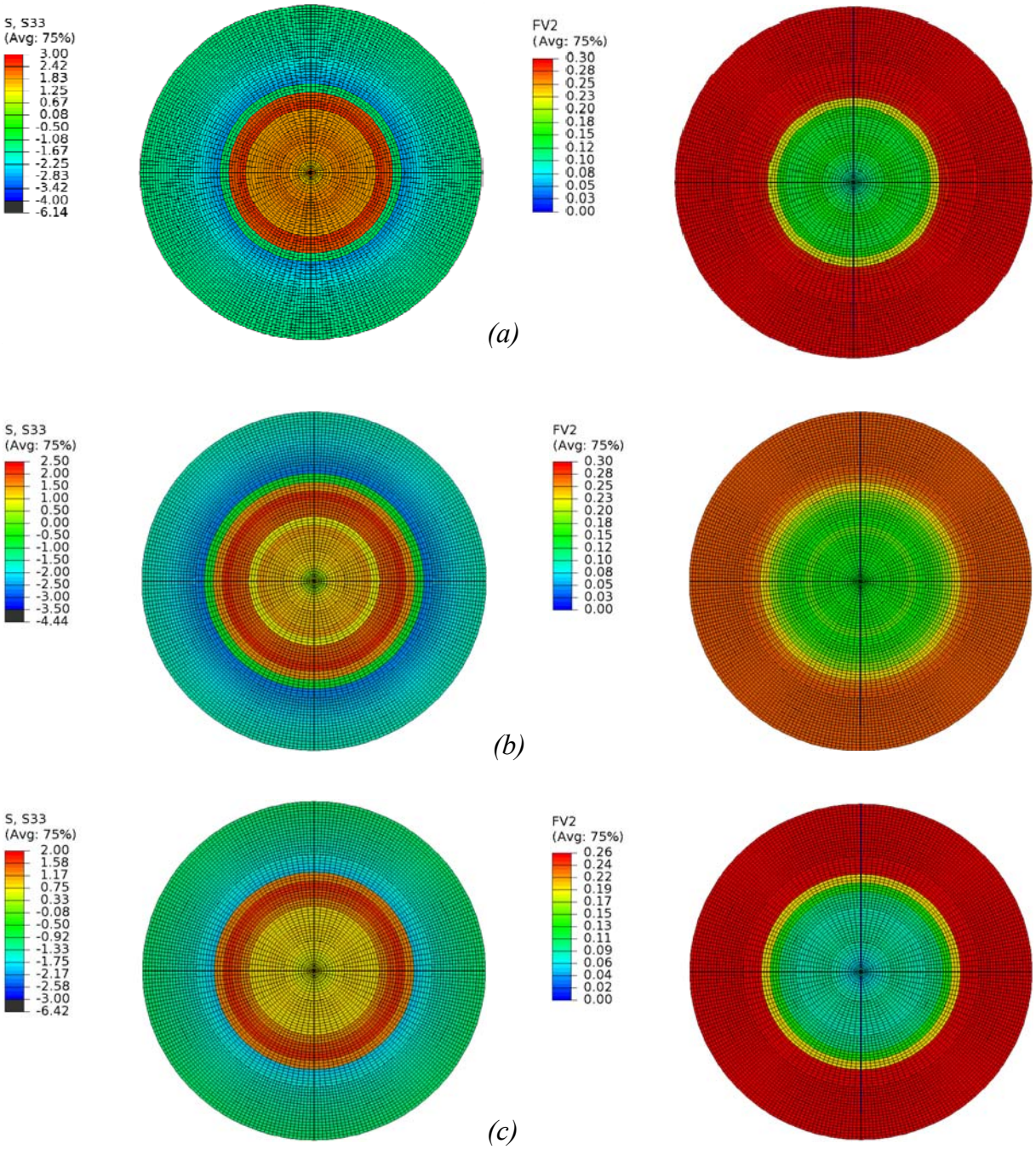

App D, Figure 0.1: *Maximal simulated tangential stress without crack development: S33=σ_t and FV2=MC, (a);*20 *°C and* 50*% RH, (b);* 20 *°C and* 60*% RH, (c);* 60 *°C and* 40*% RH.*

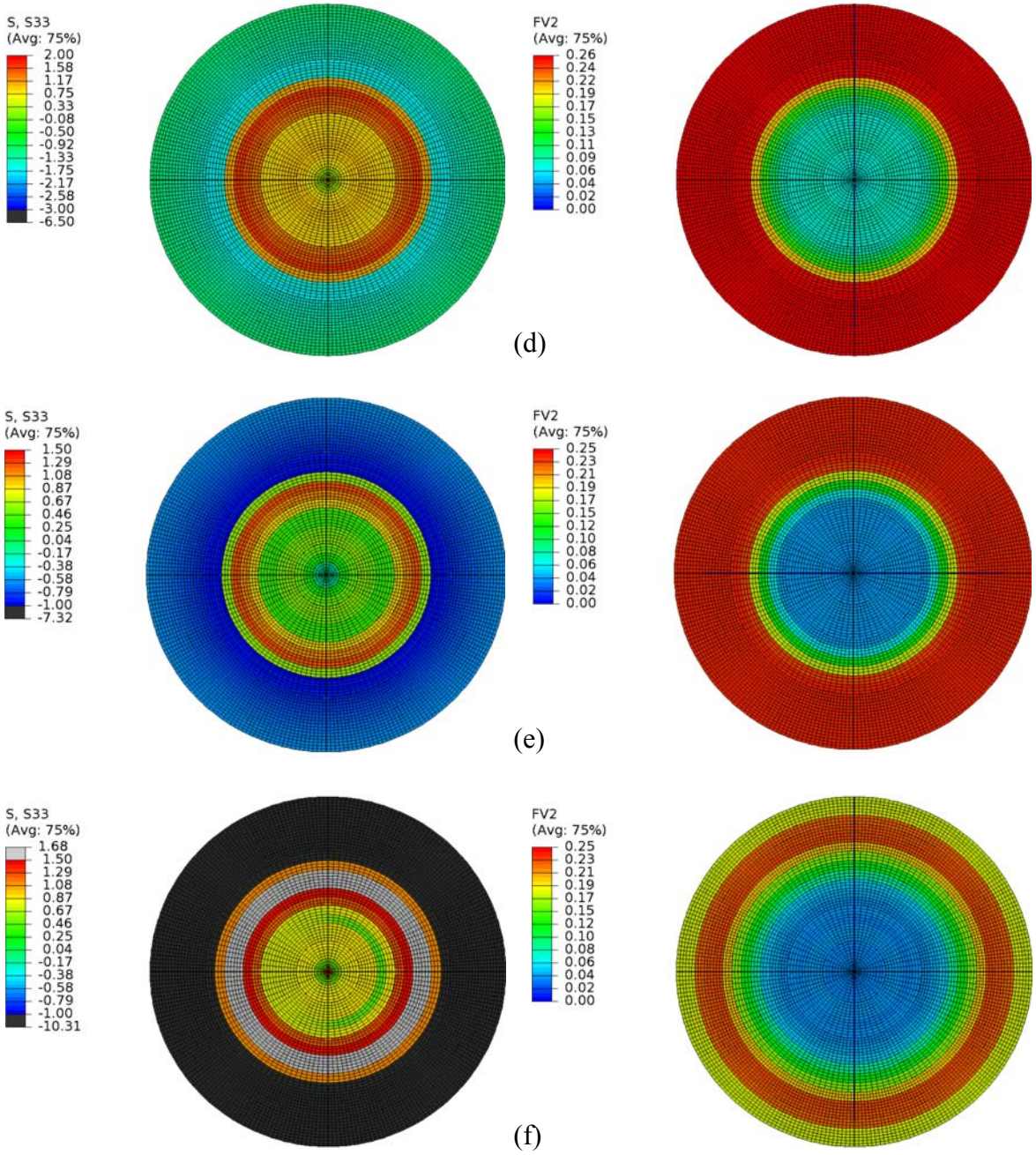

App D, Figure 0.2: *Maximal simulated stress without crack development: S33= σ_t and FV2=MC, (d);* 60 *°C and* 50*% RH, (e);* 80 *°C and* 30*% RH, (f);* 90 *°C and* 30*% RH.*

Part II Appended papers

Paper I

”Moisture-driven fracture in solid wood”

F. Larsen, S. Ormarsson & J.F. Olesen

Published in Wood Science and Technology, 2011

Wood Material Science and Engineering, 2011; 6: 49–57

Taylor & Francis
Taylor & Francis Group

ORIGINAL ARTICLE

Moisture-driven fracture in solid wood

FINN LARSEN, SIGURDUR ORMARSSON & JOHN FORBES OLESEN

Department of Civil Engineering, Technical University of Denmark, Brovej, DK-2800 Kgs. Lyngby, Denmark

Abstract
Moisture-induced fractures in solid timber create considerable problems for both building industries and sawmills. Cracks caused by kiln-drying of solid timber are extremely difficult to predict. This paper reports on experiments concerned with methods of reducing cracks in wood and with the cracking behaviour of Norway spruce discs. The spruce was dried from green moisture content down to equilibrium moisture content at 23°C and 64% relative humidity. Moisture-related strains and crack development were measured using a digital image correlation system, Aramis. The moisture gradient in the longitudinal direction had a major influence on crack behaviour and was quite pronounced in discs more than 30 mm thick, but much more limited in discs only 15 mm thick. Although the thicker discs often cracked very early in the drying process, many of these cracks became invisible later on in the drying process, suggesting that sealing the ends of timber logs while in the green moisture state could considerably reduce the development of end-cracks. The initial moisture content and the shrinkage properties of the wood varied markedly from pith to bark. The importance of taking material inhomogeneities into account when modelling crack propagation in solid wood is emphasized.

Keywords: *Aramis, cracks, drying, moisture, wood.*

Introduction

Wood is a strongly orthotropic, non-homogeneous material that often contains many microscopic defects. These can initiate cracks that propagate during the drying process. Stresses and cracks that develop in drying are created primarily by moisture gradients and internal constraints caused by orthotropic shrinkage.

The moisture content (MC) of green wood varies within the cross-section of a timber log. The MC of heartwood, for example, is considerably lower than that of sapwood. Heartwood and sapwood differ from each other during drying in the time required for the fibre saturation point (FSP) to be reached; this also suggests that shrinkage starts at different times within different parts of the cross-section. A complex state of strains and stresses develops as a result. Experiments on moisture loss above the FSP, conducted by Wiberg *et al.* (2000), showed a marked difference in the rate of drying (evaporation) from a state above, to a state below, the FSP. Krabbenhøft (2003) has modelled and studied numerically and experimentally the moisture transport in wood both above and below the FSP. He found the drying of wood above the FSP to be strongly dependent on evaporation from the surface of the wood, and drying below the FSP to be strongly dependent on moisture transport inside the wood. Drying above the FSP was also found to be faster than drying below the FSP.

Mechanosorptive strains in wood can develop as a result of drying in areas in which strong tensile or compressive stresses build up. Numerous experiments have been conducted in efforts to identify mechanosorption caused by changes in the ambient climate. Studies of the mechanosorptive behaviour of wood material under constant loading and controlled climatic conditions have been carried out by Lazarescu and Avramidis (2008) and Svensson (1995), who were able to identify and determine the magnitude of elastic strains. The difference between the shrinkage coefficients in the radial and tangential directions was found to affect strongly the internal stress generation that occurred during the drying process (Dahlblom *et al.*, 1999).

Correspondence: F. Larsen, Department of Civil Engineering, Technical University of Denmark, Brovej, DK-2800 Kgs. Lyngby, Denmark. E-mail: finla@byg.dtu.dk

(Received 15 February 2010; accepted 11 October 2010)

ISSN 1748-0272 print/ISSN 1748-0280 online
DOI: 10.1080/17480272.2010.532234

The moisture-related crack pattern in wood is often quite complex, owing to the annual ring structure and the different MC levels found within the heartwood and the sapwood. Six different orientations regarding the crack directions involved can be distinguished: TL, RL, LR, TR, RT and LT, where L = longitudinal, R = radial and T = tangential. Three different fracture modes (modes I, II and III) can occur in connection with each of the six cracking orientations. For a more detailed account of different fracture modes, see Valentin *et al.* (1991). For mode I, the directions TL and TR, which relate to the cross-sectional behaviour of a timber log, are the most relevant for moisture-related crack propagation. One hypothesis to be investigated in this study is that the crack behaviour is strongly affected by the moisture gradient in the fibre direction.

The drying of wood usually occurs five to 10 times more quickly in the longitudinal direction than in any other direction. To examine this in detail, tests were conducted on thin slices (discs) of a timber log, enabling a large number of experiments to be carried out within a short period. The boundary conditions were simplified by using thin discs for calibration of a combined moisture, distortion and fracture model. Experiments were also carried out to clarify differences in drying time and in the drying rate pertaining to a particular evaporation direction. In practical terms, the R and T directions are the major transport directions, owing to the preponderance of lengthwise surfaces compared with cross-sectional areas.

The experimental results were used for calibration and verification of a numerical crack model. This model is a further development of a three-dimensional (3D) distortion model presented in Ormarsson *et al.* (1998, 1999).

Materials and methods

Test specimens

Wood specimens were taken from a 20-year-old Norway spruce tree from the North Zealand region in Denmark. The tree was felled in the morning of 20 January 2009. A timber log, 1.5 m long and 200 mm in diameter (Figure 1), was removed from the tree and cross-cut into four parts, which were marked sequentially from 1 to 4 (top to bottom), before being placed in a freezer. Specimens cut from part 1 were numbered 1.x, and specimens from other parts 2.x, and so on. Specimens from parts 1–3 were generally cut into discs 30 mm thick or thicker, whereas part 4 was generally cut into discs 15 mm thick.

Experiments were conducted to analyse wood cracking behaviour using the discs which were dried from a green condition down to an MC of approximately 12%.

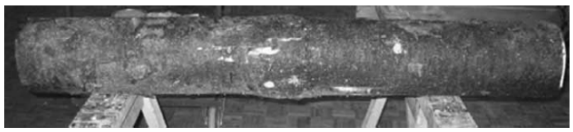

Figure 1. The timber log used for the experiments.

Experimental set-up

The experimental set-up involved several components, which provided results for strain and weight during drying. Figure 2 shows the equipment that was used for strain and weight measurement during changes in MC.

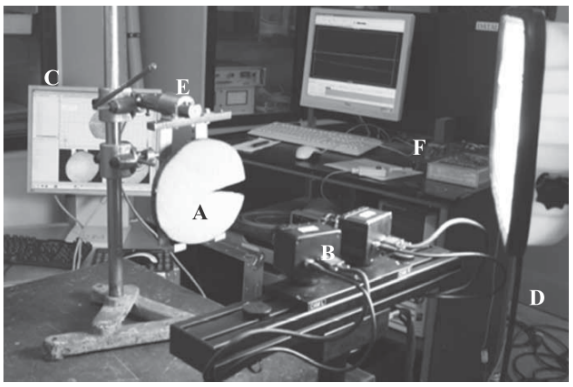

Figure 2. Experimental set-up: (A) wood disc specimen (15 mm thick) placed on a stand; (B) two digital cameras for the Aramis system, held in place by a camera support mounted on a tripod; (C) Aramis computer; (D) spotlight for illuminating the specimen; (E) load cell mounted on a stand; and (F) load cell logger.

Online weight registration

The weight of each test specimen was recorded during experimentation. The weight history was used to calculate and describe the MC history. A load cell that had a maximum capacity of 10 kg ($\pm$ 1 g) was connected to a data logger with weights being recorded at the same intervals (15 min) as for the Aramis software recording. This facilitated comparison of the two data sets.

Temperature and relative humidity

The temperature and the relative humidity (RH) were measured by a hygrometer throughout the experiments. Both the temperature and the RH were kept constant at between 23 and 24°C, and 62 and 64%. These climatic conditions resulted in an equilibrium moisture content (EMC) of 12% for each of the test specimens.

Spatial variation in the moisture content of green wood

To study spatial variations in MC within the cross-section of the timber in a green condition, a 50 mm thick disc was cut into small sticks, each 13 × 13 mm in cross-section. After initial determination of the MC of each of the sticks, the sticks were dried at 103°C until their weight had come into equilibrium (MC = 0%). The weight of the sticks was determined with a precision of ±0.01 g and weighed between 2.70 and 3.30 g after drying.

Strain measurements

The strains that developed in each disc were measured by Aramis, a non-contact optical 3D deformation measuring system (Aramis, 2007). The system recognizes the surface structure of specimens in terms of digital images where coordinates are assigned to image pixels. Initial reference conditions are obtained from image measurements of initially undeformed specimens. Further images are recorded both during and after deformation of the specimen. Aramis then determines the deformation of a specimen from one image to another by means of various square image details (facets) which are typically 15 × 15 pixel facets with a 2 pixel area of overlap. The changes in position of the different squares define the deformations that occur. Using two cameras enables 3D displacements and strains to be determined. Aramis takes pictures (representing stages) at specific time steps, and displacements on the surface of the specimen are measured and the strains calculated. Since each facet needs to be unique and easy to recognize, it is important that the surface has an arbitrary pattern involving many object characteristics and striking contrasts. This is usually achieved, if the original surface structure is not sufficient, by employing a stochastic colour spray pattern. Displacements and deformations that develop on the surface of the specimen during the experimental process can then be both visualized and calculated by use of the Aramis software.

Normally, preparation of the specimens is very simple. The surface is first painted white and is then sprayed to produce an arbitrary pattern of black dots, but this procedure is not an optimal one for wood since applying the paint would seal the surface and thus impede the moisture transport. However, preliminary tests also indicated that unless marked in some way, wood was too homogeneous in appearance. Another consideration was that wood changes colour during drying, sometimes to the extent that the Aramis equipment no longer recognizes the surface facets owing to changes in colour. Further, preliminary experiments were carried out to investigate how wood surfaces could be kept as permeable as possible. The results led to the development of a procedure in which the use of white background paint was omitted, since the light colour of the wood itself served as a background. Black dots were then applied as sparingly as possible in an arbitrary pattern, where the size and intensity of the most appropriate dots depended on the size of the specimen. Several tests using the equipment were performed before each set of measurements since Aramis needed to be able to recognize the surface in its entirety and supplementary dots needed to be provided if recognition of the surface was not intact. An example of a usable pattern is presented in Figure 3, where moisture could evaporate from the surface almost unhindered.

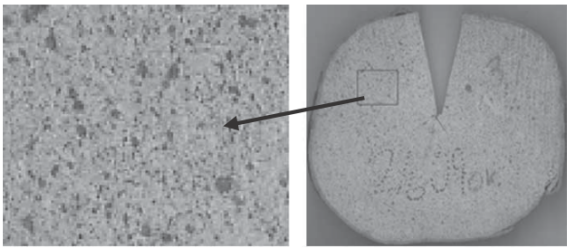

Figure 3. Arbitrarily applied pattern sprayed onto the surface of a specimen.

When strains due to moisture gradients in the wood appear Aramis carries out measurements on the surface of the specimen. Gradients in wood can develop owing to the rate of moisture transport from the interior to the surface of the wood being slower than the rate of water evaporation from the surface. If evaporation occurs through a surface and a moisture gradient develops, there can be a difference between the strains that are measured at the surface and those that occur within the material.

Since each Aramis stage (picture) consists of 2–3 MB of data, it is important to reduce the number of stages to an acceptable level. At the same time, there needs to be a sufficient number of stages to represent experimental strain history adequately. Pictures were taken at 15 min interval for all the experiments, since this was considered to be an adequate time-step. The use of impermeable white paint is an option if evaporation through the surface is unwanted. For example, Conclad is a two-component material which has an extremely evaporation-resistant surface and is able to stick to wood, even when the MC values are very high. Conclad was used in the experiments to coat selected surfaces of the specimens for which the effect of the direction of evaporation on the loss in moisture was to be examined.

Results and discussion

Moisture content of green wood

The MC in green wood was found to vary markedly within the cross-section of the timber log. The MC was low within the heartwood, which was generally around the FSP, but was as high as 200% in the sapwood. The first Aramis investigations of crack propagation were expected to differ drastically between the heartwood and sapwood. The experimental results shown in Figure 4 indicated that the transition between the heartwood and the sapwood was not distinct.

The MC varied almost linearly from 20 mm (MC = 50%) to 50 mm (MC = 200%). Close to the pith the MC was slightly higher than the FSP (MC = 40–45%), whereas in the sapwood the MC remained constant at about 200%. The transition zone from low MC to high occurred in the space of about three to four growth rings.

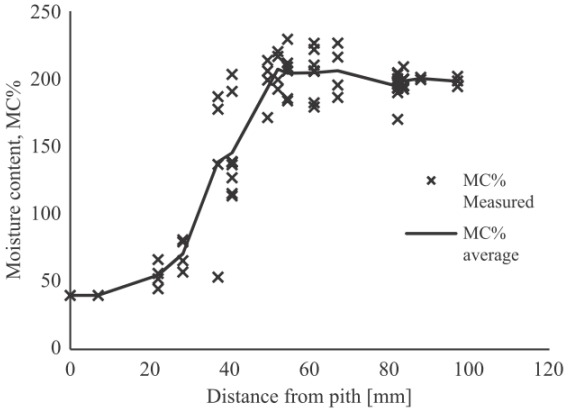

Figure 4. Variation in the initial (green) moisture content (MC) between the pith and the bark (specimen 4.8).

Drying history of test specimens

Figure 4 clearly shows how the initial MC varied markedly over the cross-section of a log. The shrinkage of the wood material started at different times in different areas of the cross-section. Online weight measurements were used to record the average moisture changes that occurred within the entire cross-section as a whole, and within the heartwood and the sapwood separately. A 40 mm heartwood radius segment was cut from the discs, as shown in Figure 9, for samples 4.10, 4.4, 4.7 and 4.12.

The average MC history was calculated from results for the heartwood, the sapwood and the discs in their entirety (heartwood and sapwood). The heartwood and sapwood history was compared with the history of a complete disc (4.10) containing both heartwood and sapwood (Figure 5). Figure 5 shows that above FSP (MC ~30%) the MC rate was high and fairly constant until FSP was reached. The rate changed non-linearly from slightly below FSP until EMC was reached. The combined curve (for the heartwood and sapwood) was an average curve for all the heartwood and sapwood samples. The difference between this curve and the curve for sample 4.10 was less than the variation found between the individual samples that were used to calculate the average curve.

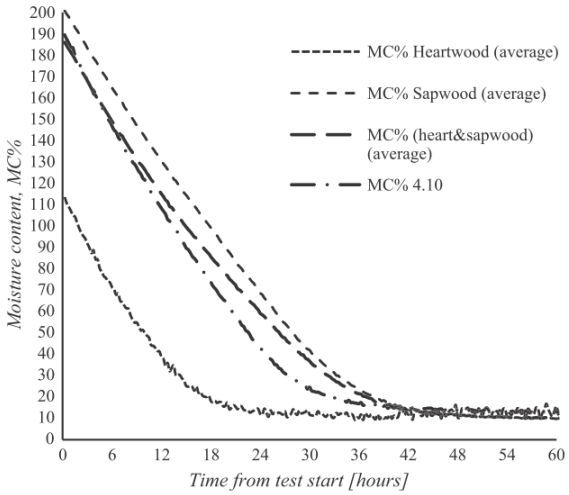

Figure 5. Moisture content (MC) history of the 15 mm thick disc.

The same trend of moisture loss was obtained for both the heartwood and the sapwood parts of the samples, excluding any difference between initial MCs. Knowledge of the initial MC value and the MC during drying enabled an MC history for a whole cross-section to be generated (Figure 6).

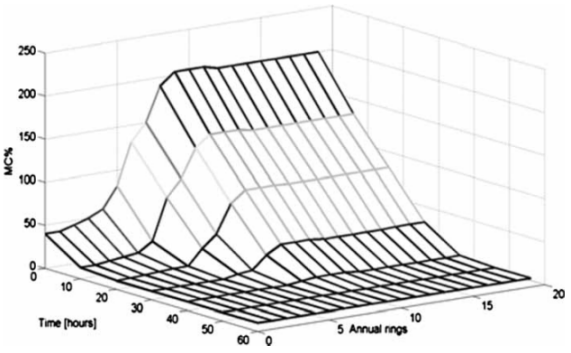

Figure 6. Average moisture content (MC) history for discs 15 mm thick.

Dependence of the course of drying on direction of evaporation

As already indicated, moisture transport in wood is much faster in the longitudinal (fibre) direction than in the radial and tangential directions. Figure 5 shows the progress of moisture transport for the longitudinal direction alone. The effects that the direction of evaporation had on the drying rate were investigated for two wood samples that were similar in character regarding sample thickness and size of the evaporation surfaces. The wood specimen 4.5-1 shown in Figures 7 and 8 was dried in the fibre direction, whereas specimen 4.5-2 was dried in combined radial and tangential directions. Both specimens had a geometry of $50 \times 150 \times 50$ mm, and both samples were coated with Conclad on the smaller 50×50 mm surfaces and on the two surfaces opposite to each other. The surfaces were sealed at points at which moisture release was to be prevented, which left two surfaces open. Since earlier investigations had shown that moisture gradients in the longitudinal direction were smaller for 15 mm thick discs, data from a disc of this sort (4.10) were also included for comparison.

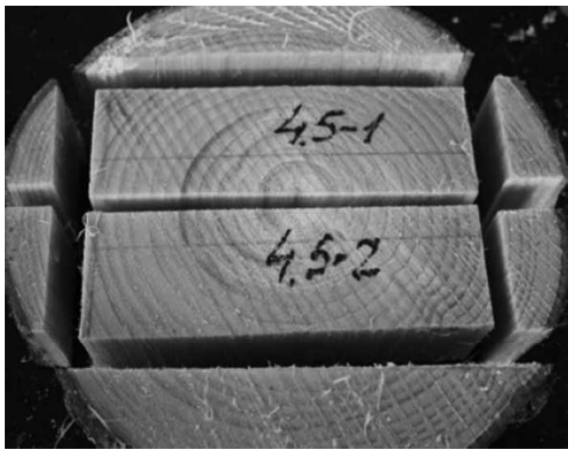

Figure 7. Sawn pattern of specimens 4.5-1 and 4.5-2.

Figure 8 shows the effects of the MC gradient (piece thickness) on the rate of moisture loss. Evaporation from specimen 4.10 was considerably faster than that from specimen 4.5-1. Above the FSP, the evaporation rate for both specimens was constant. The rate of moisture release decreased thereafter until the EMC state was reached. Evaporation during this phase was also faster for the thinner specimen 4.10 than for sample 4.5-1, which was thicker.

Comparison of the longitudinally dried specimen 4.5-1 and the transversally dried specimen 4.5-2 showed the rate of moisture loss from green down to an MC = 60–70% to be almost the same. The rate of moisture loss in 4.5-2 changed gradually from this state until FSP was reached, and this was followed by a linear decrease in MC until EMC was reached.

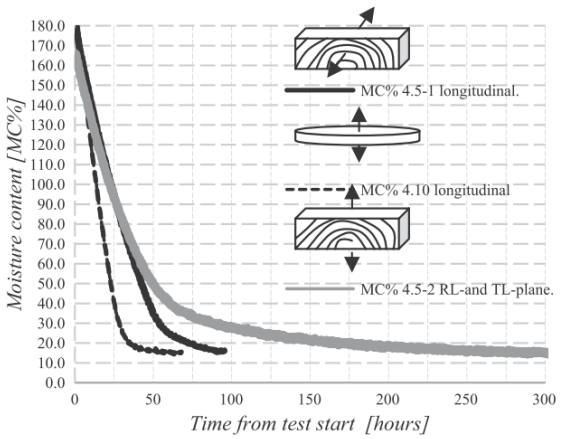

Figure 8. Effects of the direction of evaporation and the specimen thickness on moisture loss. MC = moisture content.

Shrinkage coefficient

Since free shrinkage is the main factor causing distortion of the wood, good shrinkage data are needed for simulating moisture-related deformation. The experimental study presented here dealt with the estimation of the radial and the tangential shrinkage coefficients (α_r and α_t) for heartwood and sapwood, respectively. Examples of specimens used for estimating the shrinkage coefficient are shown in Figure 9. All the specimens used for estimation of the shrinkage coefficients were slit from the pith to the periphery, allowing the shrinkage to develop quite freely within samples that consisted solely of heartwood or sapwood (Figure 9c–e).

Tangential and radial dimensions were measured at different MC levels. The initial dimensions was determined for green wood (MC > FSP), which determined the geometry at the FSP and under oven-dry condition (MC = 0%).

The dimensions and MC were also determined when EMC was reached. The initial length in the radial direction at stage (1) is denoted as l_{r1}, whereas the initial length in the tangential direction (along the bark) is denoted as the perimeter length l_{t1}, the inner perimeter as $4.4_{sapwood}$ and the outer perimeter as $4.4_{heartwood}$. The corresponding total weight of the specimens is denoted as m_{tot1}. The total weight is $m_{water1} + m_0$, where m_0 = dry weight of the wood at MC = 0%. The new lengths (l_{r2} and l_{t2}) and the weight (m_{tot2}) at stage 2 were determined following the loss in moisture.

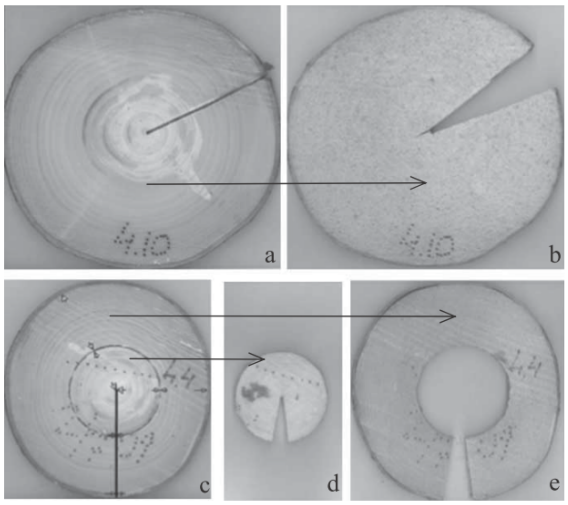

Figure 9. Samples 4.10 and 4.4 used for estimating the shrinkage coefficients: (a) 4.10, wet condition; (b) 4.10, dry condition; (c) 4.4, wet condition; (d) $4.4_{heartwood}$, dry condition for heartwood; (e) $4.4_{sapwood}$, dry condition for sapwood.

These data enable both the change in moisture and the shrinkage coefficients to be estimated as noted in eqs (1)–(3):

$$\Delta w = \frac{m_{tot2} - m_{tot1}}{m_0} \tag{1}$$

$$\alpha_t = \frac{(l_{t2} - l_{t1})/l_{t1}}{\Delta w} \tag{2}$$

$$\alpha_r = \frac{(l_{r2} - l_{r1})/l_{r1}}{\Delta w} \tag{3}$$

The tangential shrinkage coefficients for all of the samples were quite similar, but there was a rather large variation in the radial coefficient. The shrinkage coefficients and the FSP obtained for specimens 3.1, 4.10 and 4.4 are shown in Table I.

Table I. Shrinkage coefficients and fibre saturation point (FSP).

Sample no.	$\alpha_{t,\ inner}$	$\alpha_{t,\ outer}$	α_r	FSP (MC%)
3.1		0.29	0.14	30.0
4.10		0.31	0.15	31.8
$4.4_{heartwood}$		0.28	0.09	30.4
$4.4_{sapwood}$	0.31	0.29	0.16	31.1

Note: α_t = tangential shrinkage coefficient; α_r = radial shrinkage coefficient; MC = moisture content.

Heartwood ($\alpha_r \sim 0.1$) was also found to have a smaller radial shrinkage coefficient than sapwood ($\alpha_r \sim 0.16$).

Strain results

The Aramis system was used to register progressive surface strain generation during drying from green down to EMC. Three and two examples of strain fields involving major strains are shown for specimen 3.1 and 2.7, respectively, in Figures 10–14. The examples are from different times during the drying process. The specimens were 30 mm thick and specimen 3.1 had a 5 mm wide slit that extended from the pith to the bark, while specimen 2.7 had no slit. Figure 10 shows a major strain plot after 37 h of drying.

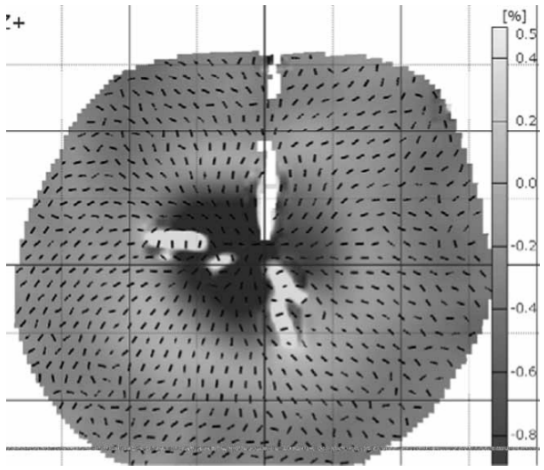

Figure 10. Distribution of major strains within specimen 3.1 after 37 h of drying ($MC_{heartwood} \sim 12$–20%, $MC_{sapwood} \sim 60$–70%). MC = moisture content.

Figure 6 indicates the heartwood was below, but the sapwood was above the FSP. Major strains are the largest principal strains, whereas minor strains are the smallest principal strains. The small lines in Figures 10–14 indicate the strain direction. If major and minor strains are both negative then minor strains are numerically largest. Major negative strains were found for samples 3.1 and 2.7 in almost the entire cross-section and were mainly oriented in the radial direction, which shows that minor strains are mainly tangential, except for the fracture zones where major strains were positive and tangentially oriented.

Subtracting the shrinkage strains from the total strains indicated that positive strains were present in large areas in both tangential and radial directions. Figure 10 shows furthermore that the slit is partly (almost completely) closed in the sapwood area, which is due to shrinkage deformation of the heartwood. Figure 11 shows a clear crack pattern in the radial direction, extending across the entire sapwood area. This crack pattern is similar to the crack patterns observed at the ends of the logs, which indicates the moisture gradients in the longitudinal

direction to have a pronounced effect on the crack pattern. Note also in Figure 11 that when the slit had started to open the heartwood cracks were mainly closed, showing major negative strains in the radial direction of heartwood.

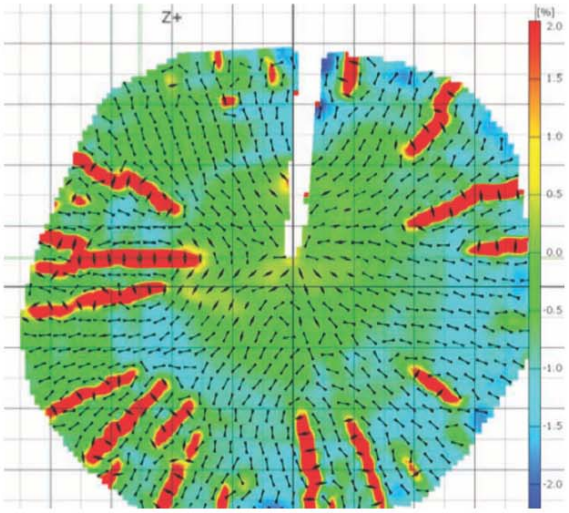

Figure 11. Distribution of major strains within specimen 3.1 after 55 h of drying ($MC_{heartwood}$ ~12–15%, $MC_{sapwood}$ ~25–35%). MC = moisture content.

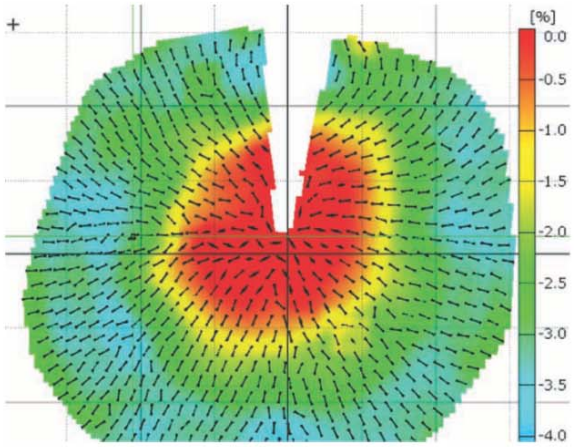

Figure 12. Distribution of major strains within specimen 3.1 after 75 h of drying ($MC_{heartwood}$ = $MC_{sapwood}$ = equilibrium moisture content). MC = moisture content.

Figure 12 shows the major strain field after drying of the entire cross-section down to an EMC of 12%. Each of the cracks observed in Figures 10 and 11 are closed and not observable from the Aramis results. The slit is large and there are relatively large negative (radially oriented) major strains within the entire cross-sectional area. Plots of the major strains for specimen 2.7 without a slit are shown in Figures 13 and 14. The plots apply to the same drying stage as in Figures 10 and 11.

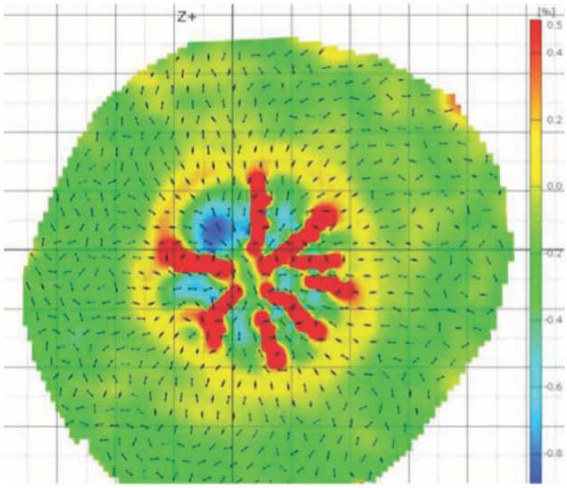

Figure 13. Distribution of major strains within specimen 2.7 after 37 h of drying ($MC_{heartwood}$ ~12–20%, $MC_{sapwood}$ ~60–70%). MC = moisture content.

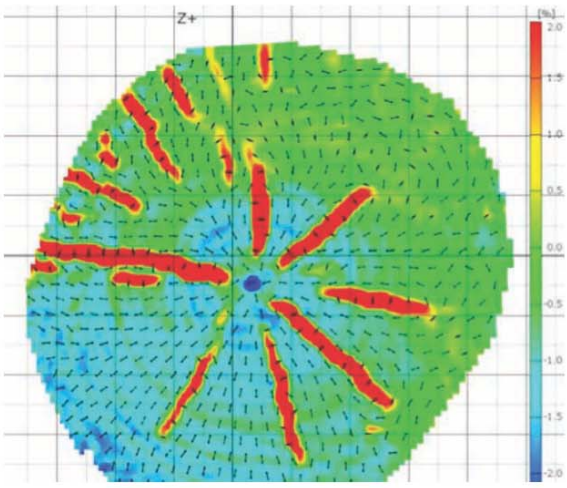

Figure 14. Distribution of major strains within specimen 2.7 after 55 h of drying ($MC_{heartwood}$ ~12–15%, $MC_{sapwood}$ ~25–35%). MC = moisture content.

The crack patterns, which consist mainly of radial cracks, are similar to the patterns observed for the specimens with a slit, except that the heartwood cracks were also present after 55 h of drying.

The results presented in Figures 10–14 supports the hypothesis that the moisture gradients in both the longitudinal and the radial directions had a pronounced effect on the crack pattern, the effect of the slit becoming limited owing to the moisture gradient being the main driving force for crack propagation.

To reduce the effect of the longitudinal moisture gradient on the crack pattern in 15 mm thick specimens, 4.10 and 4.6 were also studied. Figures 15 and 16 shows major strain plots after approximately 25 h of drying, in discs both with and without a slit.

The drying of a 15 mm thick disc for 25 h produces a degree of drying corresponding that found in a 30 mm thick disc after 37 h of drying. The moisture gradient in the fibre direction in these thinner discs was markedly reduced compared with the thicker discs and led to a large radial variation in the major strains presented within the transition zone without any fracturing of the specimens.

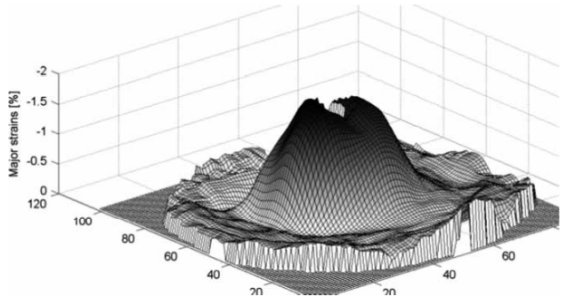

Figure 15. Distribution of major strains within specimen 4.10 (with a slit) after 25 h of drying ($MC_{heartwood}$ ~12%, $MC_{sapwood}$ ~60–70%). MC = moisture content.

The development of strains in different discs, all at the same early drying state, shows the same tendency as can be observed when comparing Figures 10, 13, 15 and 16.

The strains in the sapwood areas are approximately zero, especially when the MC in the sapwood is above the FSP, whereas the shrinkage-related strains in the heartwood areas, which are mainly negative strains, are considerably larger. The major strains vary in a rather smooth fashion across the heartwood area in the case of the 15 mm thick discs (Figures 15 and 16), whereas in the 30 mm thick discs the propagation of cracks (in zones with positive strains) occurs in more varying fashion. In the longitudinal direction, the propagation of cracks was found to be related to the moisture gradient.

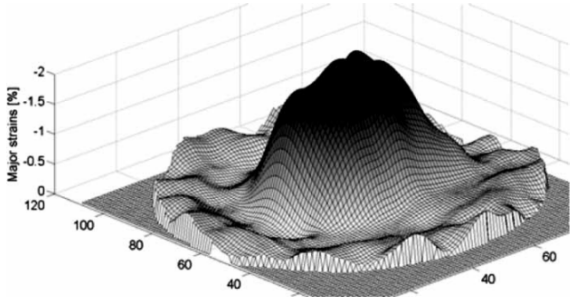

Figure 16. Distribution of major strains within specimen 4.6 (without a slit) after 25 h of drying ($MC_{heartwood}$ ~12%, $MC_{sapwood}$ ~60–70%). MC = moisture content.

Conclusions

The experimental results presented contribute to the knowledge of how roundwood samples behave during drying. The MC difference between the heartwood and the sapwood, specimen thickness, boundary conditions (slits or no slits) and shrinkage variations strongly affect the strain and fracture behaviour that occurs during drying. The longitudinal MC gradient had a pronounced effect on the crack pattern in the roundwood disc specimens 30 mm thick or thicker. Cracks that developed at an early stage in the drying process were found to disappear visually at the end of the drying process. It would therefore appear that the sealing of the ends of logs under green moisture conditions would markedly reduce the risk of cracks at the ends of logs during the drying of solid timber products.

It has been verified that the radial shrinkage properties are different in the heartwood area compared with the sapwood area.

The results indicate that moisture-related fracture modelling should take the degree of inhomogeneity of the material into consideration, along with the MC gradient in the longitudinal direction and variations in MC development, both in heartwood and in sapwood zones.

Future work

The use of Aramis measurements opens up new possibilities for calibrating and validating distortion and crack models. The results obtained can be used to compare how moisture-induced displacement and strain fields develop during the drying process as a whole. Aramis measurements also make it possible to compare in detail how strains and cracks develop in small regions of a specimen. The aim here was to develop and explore the use of numerical models that simulate distortion and fracturing in solid wood under ambient climatic conditions corresponding to those found in typical kiln-drying. New models can be calibrated by experimental verification when moisture-related strains and fracture propagation during kiln-drying are measured using Aramis. In addition, drying schemes were sought that were as effective as possible for the elimination of cracks in drying.

Acknowledgements

The authors thank the Danish Forest and Nature Agency for funding this research.

References

Aramis (2007). *Aramis v6 user manual*. GOM mbH, GOM optical measuring techniques. http://www.gom.com

Dahlblom, O., Petersson, H. & Ormarsson, S. (1999). Characterization of shrinkage. European project FAIR CT 96-1915, *Improved spruce timber utilization* (Final Rep. sub-task AB1.5). Division of Structural Mechanics, Lund Institute of Technology, Lund University, Sweden.

Krabbenhøft, K. (2003). *Moisture transport in wood. A study of physical–mathematical models and their numerical implementation*. PhD thesis (Chapters 4 and 5), Technical University of Denmark, Copenhagen.

Lazarescu, C. & Avramidis, S. (2008). Drying related strain development in restrained wood. *Drying Technology*, *26*, 544–551.

Ormarsson, S., Dahlblom, O. & Petersson, H. (1998). A numerical study of the shape stability of sawn timber subjected to moisture variation. Part 1: Theory. *Wood Science and Technology*, *32*, 325–334.

Ormarsson, S., Dahlblom, O. & Petersson, H. (1999). A numerical study of the shape stability of sawn timber subjected to moisture variation. Part 2: Simulation of drying board. *Wood Science and Technology*, *33*, 407–423.

Svensson, S. (1995). Strain and shrinkage force in wood under kiln drying conditions. *Holzforschung*, *49*, 63–368.

Valentin, G. H., Boström, L. , Gustafsson, P. J., Ranta-Maunus, A. & Gowda, S. (1991). *Application of fracture mechanics to timber structures.* RILEM state-of-the-art report (Res. Notes 1262), Technical Research Centre of Finland, Espoo, Finland.

Wiberg, P., Sehlstedt-Persson, S. M. B. & More'n, T. J. (2000). Heat and Mass transfer during sapwood drying above the fibre saturation point. *Drying Technology*, *18*, 1647–1664.

Paper II

”Numerical and experimental study of moisture-induced stress and strain field developments in timber logs”

F. Larsen & S. Ormarsson

Accepted for publishing in Wood Science and Technology, 2012

Numerical and experimental study of moisture-induced stress and strain field developments in timber logs

Finn Larsen[1#] and Sigurdur Ormarsson[1,*]

[1]Department of Civil Engineering, Technical University of Denmark, Brovej, DK-2800 Kgs. Lyngby, Denmark,

[#]E-mail: finla@byg.dtu.dk

*Corresponding author.
E-mail: sor@byg.dtu.dk

Abstract:
When solid wood dries from a green condition to a moisture content used for further processing, moisture-induced fracture and stresses can occur. The drying stresses arise because of internal deformation constraints that are strongly affected by the cross sectional moisture gradient differential shrinkage and the inhomogeneity of the material. To obtain a better understanding of how stresses develop during climatic variations, the field histories of stresses (and strains) in cross-sections in their entirety need to be studied. The present paper reports on experiments and numerical simulations concerned with analysing the development of strains and stresses during the drying of 15 mm thick discs of Norway spruce timber log. The samples were dried at 23 °C and relative humidity (RH) of 64% from a green condition to equilibrium moisture content (EMC). The moisture gradient in the longitudinal direction was minimised by use of thin discs simplifying the moisture history of the samples studied. The strain field history was measured throughout the drying process by use of a digital image correlation (DIC) system. Numerical simulations of the samples agreed rather well with the experimental strain results obtained. The stress results also indicated where in the cross section and when fractures could be expected to occur during drying. More optimal drying schemes showed markedly reduced stress generation.

Keywords:
Drying, modelling, moisture, wood, digital image correlation system, FEM

Introduction:
Solid wood is a hygroscopic, orthotropic and nonhomogeneous material, the stiffness properties of which are strongly affected by the moisture content (MC). The MC within a timber log in a green condition varies over the cross section, since the heartwood has a considerably lower initial MC than the sapwood. Solid timber needs to be dried from a green condition down to moisture content below that of the fiber saturation point (FSP) before it can be used as a construction material. When a solid piece of timber contains both heartwood and sapwood, considerable stresses can develop during drying because of the large moisture gradients that arise. The heartwood part starts to shrink at an early stage since it reaches FSP much earlier than the sapwood part does. The drying history is likewise complex through drying occurring faster above than below the FSP. Experiments by Wiberg et al. (2000) and by Krabbenhøft (2003) on moisture loss above and below the FSP showed the rate of drying (evaporation) to be higher above the FSP than below it. It was found that above the FSP the drying of wood is strongly dependent upon evaporation from the surface of the wood, and drying below the FSP was strongly dependent upon moisture transport inside the wood. Further numerical investigations of drying above the FSP have been carried out by Salin (2006) (2010),

who evaluated the occurrence of damage zones produced by sawing and by other actions affecting the wood surface as a function of for the drying speed.
Mechano-sorptive strains that develop during the combined occurrence of moisture change and stress generation can reduce the occurrence of stresses related to drying. Numerous experiments have been conducted in efforts to identify mechano-sorption strains caused by changes in the ambient climate. Studies of the mechano-sorptive behaviour of wood material under constant loading and controlled climatic conditions have been carried out by Armstrong et al. (1962), Lazarescu et al. (2008) and Svensson (1995), who were able to identify and determine the magnitude of elastic, mechano-sorptive and visco elastic strains. How mechano-sorption parameters affect the distortion of solid timber has been investigated numerically by Ormarsson (1999) and by Fortino et al. (2009), for example. Differences between shrinkage coefficients in the radial and the tangential directions have been studied experimentally and been found to strongly affect the stress generation that occurs during the drying process (Dahlblom et al., 1999).

Moisture related stress and strain fields in nonhomogeneous cross sections are extremely difficult to predict. Several numerical investigations taking different approaches to this have been conducted: Felix et al. (1992) modelled stress and strain development in thin quadratic cross sections (discs). Clair et al. (2003) used discs taken from logs to investigate shrinkages properties, primarily in the radial and the tangential directions. Bonneau et al. (1993) constructed a 2-zone model for analysing the drying of wood containing both heart and sapwood, Kang et al. (2002) developed a mathematical model for studying strains and stress development (within a cross section) based on differences between MC in heartwood and in sapwood. The numerical results presented showed stress variations of interest within the cross sections. Kang et al. (2004) conducted an experimental investigation later of radial shrinkage in solid wood discs. Kowalski et al. (2007) made use of an acoustic emission method in experiments aimed at monitoring the state of stresses in dried wood discs. The experiments were so performed that evaporation could only occur from the bark of a cylindrical wood disc. Sreekanth et al. (2009) performed drying experiments at 130 °C in a specially constructed setting involving use of discs 30 mm in diameter, for studying crack propagation due to tangential stresses. The experimental findings were used to verify a model developed for predicting fracture behaviour.

The experiments reported on in the present paper were conducted to examine strain field development during the drying of thin discs taken from a timber log. Since the drying of wood occurs much faster in the longitudinal direction than in any other directions, using thin discs enables the experimental time to be reduced appreciably and the moisture gradient in the longitudinal direction to be reduced to an absolute minimum. The degree of deformation constraint can also be varied by using discs with and without a slit from pith to bark, these having open and closed annual rings respectively. The drying direction for kiln dried timber is predominant radial and tangential which is different from the direction in these experiments. The thin discs are used because they provide simple and well defined moisture histories which facilitate calibration of the simulation model. The mechano-sorptive behaviour caused by moisture gradients (or internal constraint) during drying is universal regardless the drying direction. The calibrated model is therefore useful in general and can easily be used for simulation of stresses and fracture of kiln dried timber boards, especially when drying of boards with large moisture gradients in green condition are simulated. Note, large gradient can occur in wooden discs because they consist of both heartwood and sapwood with marked difference in green moisture content. The degree of variation in the transversal strain fields within the cross sections of the wood was measured during the drying process by means of a DIC system, Aramis (2007). The experimental samples were also simulated

by use of a 3D distortion model developed by Ormarsson et al. (1998, 1999), the moisture content history and the shrinkage properties of the samples being obtained in the experimental study.

Materials and methods

The research method employed is a combined experimental and numerical one. Strain fields in thin disc specimens obtained from a solid timber log were measured during drying by use of the DIC system, simulations of the drying stresses and strains being performed by use of a finite element model.

Strain field measurements

Test specimens

The test specimens were selected from a timber log (1.5 m long and 200 mm in diameter) 20-year old Norway spruce tree growing in the North Zealand section of Denmark and felled in January, 2009. After the log was removed from the tree, it was cross cut into 4 sections before being placed in a freezer for conservation purposes. The disc-shaped specimens to be studied were later cut from the respective sections of the log in a frozen condition so as to avoid moisture loss during preparation of the specimens. The specimens were carefully selected (see Figure 1) from areas free insofar as possible of defects and with the aim of obtaining samples as homogeneous (in tangential direction) as possible so as to keep the effects of variations in the material properties at a minimum. Even such carefully selected specimens varied to some extent, the colour variations shown in Figure 2 indicating there to be certain variations both in moisture content and in material properties.

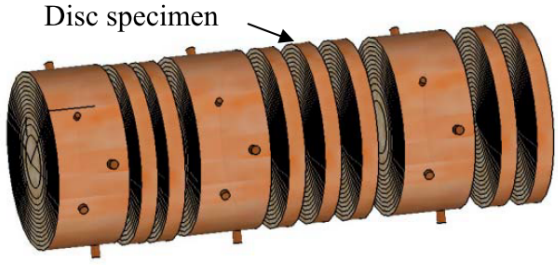

Figure 1: ***Principle of selecting test specimens.***

To reduce internal constraints within the disc specimens during the drying process that followed, a 1.5 mm wide slit was sawn from the bark to the pith; see Figure 2 (a).

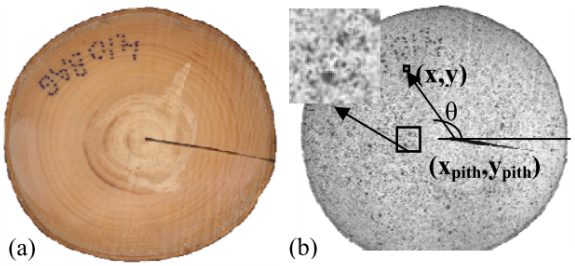

Figure 2: (a) ***Disc specimen with a slit (b) sprayed specimen with random pattern used for Aramis measurements.***

Experimental setup

To study drying deformations of the specimen by use of the DIC system, the disc was placed on a stand containing a digital weight cell together with fan ventilation around the disc (see Figure 3).

An arbitrary pattern of dots, as shown in Figure 2(b), was sprayed on the surface for use in obtaining strain measurements. The entire strain field history of the disc specimen was measured by the DIC system, at the same time as the weight of the test specimen, together with the temperature and RH of the surrounding air, were recorded by a logger at 15 minutes intervals.
Both the temperature and the RH were kept (nearly) constant throughout the experiments, their being set to values of 23 °C and 63% RH. According to the Hailwood-Horrobin equation adapted for wood by Simpson (1973) and described in Baronas et al. (2001) and in Ball et al. (2001), the EMC of the samples could be expected to reach about 12%. For a more detailed account of the experimental setup, see Larsen et al. (2011). The dry weight of the specimens was determined by oven drying of them at 103 °C.

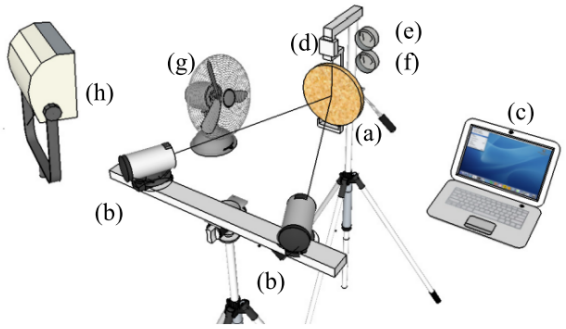

Figure 3: ***Experimental setup: (a) Disc specimen, (b) Digital cameras, (c) Computer for data logging, (d) Weight cell, (e) Relative humidity gauge, (f) Temperature gauge, (g) Fan ventilation, (h) Cold light.***

Data recording
The strain field across the surface of the disc was measured by the DIC system. The system recognized the surface pattern of the specimen on the basis of digital images, coordinates being assigned to the pixels of the images. Initial images obtained in the undeformed stage served as the reference state, the image stages thereafter being recorded during the deformation phase of the specimen with use of fixed intervals. The DIC system computes displacements and strains occurring from one image to another by means of movements of small square facets that are typically 15x15 pixels in size with a 2x15 pixel area of overlap with each neighbouring facet. The normal strains (ε_x and ε_y) and shear strains ($\gamma_{xy}=2\varepsilon_{xy}$) are found for each of the facets. The principal strains, termed major and minor strains (ε_1 and ε_2), which are based on the two types of strains just referred to, are calculated by use of Eq. (1). Note that the minor strains can be numerically the largest if these are negative or if both the major and the minor strains are negative. The angle between the x-axis and the first principal axis (1-axis) is also calculated by use of the DIC system on the basis of Eq. (2).

$$\varepsilon_{1,2} = \frac{\varepsilon_x + \varepsilon_y}{2} \pm \sqrt{\left(\frac{\varepsilon_x + \varepsilon_y}{2}\right)^2 + {\varepsilon_{xy}}^2} \qquad (1)$$

$$\phi = 0.5 \tan\left(\frac{2 \cdot \varepsilon_{xy}}{\varepsilon_x - \varepsilon_y}\right)^{-1} \qquad (2)$$

Further processing of the experimental data
To compare the strains measured by use of DIC system with simulated strains, those strains referring to the (x,y) coordinate system were transformed to the coordinate system (r,t) of the wood material. The disc specimens studied had almost circular annual rings and the pith was located close

to the centre of the discs. Each facet in the undeformed state has (x,y) coordinates in the DIC system. The values for all other facets were estimated on the basis of the coordinates for the facets covering the pith and the radial and tangential directions, making use of the angle between the x-axis and the radius, the latter extending from the pith to the facet; see Fig. 2(b).
The strain transformation from the (x,y) coordinate system to the (r,t) coordinate system is given in matrix form as

$$\bar{\boldsymbol{\varepsilon}} = \boldsymbol{G}\boldsymbol{\varepsilon} \tag{3}$$

Or

$$\begin{bmatrix} \varepsilon_r \\ \varepsilon_t \\ \gamma_{rt} \end{bmatrix} = \begin{bmatrix} \cos^2\theta & \sin^2\theta & \sin\theta\cos\theta \\ \sin^2\theta & \cos^2\theta & -\sin\theta\cos\theta \\ -2\sin\theta\cos\theta & 2\sin\theta\cos\theta & \cos^2\theta - \sin^2\theta \end{bmatrix} \begin{bmatrix} \varepsilon_x \\ \varepsilon_y \\ \gamma_{xy} \end{bmatrix} \tag{4}$$

where $\bar{\boldsymbol{\varepsilon}}$ represents the transformed strains in the directions (r,t) of the wood material, $\boldsymbol{G}$ is the transformation matrix and $\boldsymbol{\varepsilon}$ contains the measured strains in the global coordinate system (x,y).

Modelling

Simulation of the disc specimens that were studied was performed by the finite element (FE) software Abaqus (2008), a 3D stress analysis being carried out using 8-node linear brick elements of type C3D8. The type of specimen studied was a circular 15 mm thick disc divided into 20 geometrical parts, its consisting of a small pith area and 19 annual rings. These parts were connected by a so-called tie-constraint that allowed the disc to function as an inhomogeneous continuum. Each part of it has its own set of material parameters and its own moisture and temperature histories. The simulation model involved the use of special routines for wood distortion developed by Ormarsson (1999). The model takes account of elastic deformation, moisture-induced shrinkage and mechano-sorptive deformation. Visco-elastic deformations are not taken account of, since according to investigations conducted by Svensson (1997), drying-related visco-elastic strains represent only a very small part of the total strains. The references employed concerned a local coordinate system including the *l* (longitudinal), *r* (radial) and *t* (tangential) directions, the pith serving as the centre. The experimentally observed changes in moisture content beneath the FSP functioned as a driver for the deformations. The initial variations in MC (under the green conditions, t = 0) as well as the development of the MC-curve over time were obtained along the radius (r) of the discs. Figure 4 shows the result of the measured moisture history for the disc specimen used to provide input data for the model. In the model, the moisture content field over the cross-section is assumed to be axisymmetrically distributed around the pith.

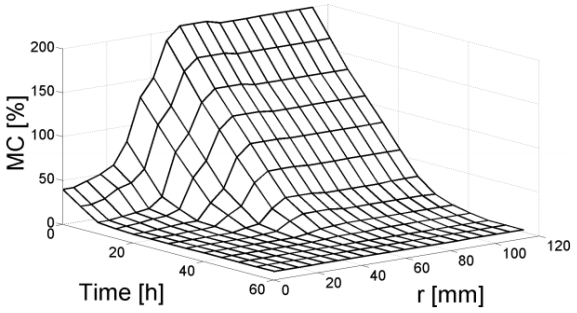

Figure 4: ***MC history used as input for simulation of the disc specimen.***

Results and discussions

The development of the strain field over the cross-section of the disc specimen was measured during drying, the results being used to verify the simulation model. The strain results at various times (obtained from the DIC system and FE-software) were compared, although here the results for just one time level (25 h of drying) will be presented.

Experimental verification of the simulation model

Material parameters

Table 1 shows the material parameters used in the simulation model. Both the parameters and the indices refer to notations described in Ormarsson (1999). The stiffness, mechano-sorptive, shrinkage and temperature parameters used are representative parameters for Norway spruce trees.

Table 1. Material parameters used in the simulations

$E_{l0}=9700MPa$	$E_{r0}=400MPa$	$E_{t0}=220MPa$
$E_{lT}=0.013°C^{-1}$	$E_{rT}=0.013°C^{-1}$	$E_{tT}=0.013°C^{-1}$
$E_{lw}=21000MPa$	$E_{rw}=2200MPa$	$E_{tw}=1300MPa$
$v_{lr}=0.35$	$v_{lt}=0.60$	$v_{rt}=0.55$
$G_{lr0}=400MPa$	$G_{lt0}=250MPa$	$G_{rt0}=25MPa$
$G_{lrT}=0.013°C^{-1}$	$G_{ltT}=0.013°C^{-1}$	$G_{rtT}=0.013°C^{-1}$
$G_{lrw}=1163MPa$	$G_{ltw}=122MPa$	$G_{rtw}=72MPa$
$m_{l0}=0.0001MPa^{-1}$	$m_{r0}=0.15MPa^{-1}$	$m_{t0}=0.2MPa^{-1}$
$m_{lT}=-0.01°C^{-1}$	$m_{rT}=-0.01°C^{-1}$	$m_{tT}=-0.01°C^{-1}$
$m_{lrT}=-0.01°C^{-1}$	$m_{ltT}=-0.01°C^{-1}$	$m_{rtT}=-0.01°C^{-1}$
$m_{lrw}=0.008MPa^{-1}$	$m_{ltw}=0.008MPa^{-1}$	$m_{rtw}=-0.8MPa^{-1}$
$\mu_{lr}=0.0$	$\mu_{lt}=0.0$	$\mu_{rt}=1.0$
$\alpha_l=0.0071$	$\alpha_{r\ heart}=0.10$	$\alpha_{t\ heart}=0.20$
$\alpha_{slope}=-0.038$	$\alpha_{r\ sap}=0.17$	$\alpha_{t\ sap}=0.35$
$T_0=20°C$	$w_{f0}=0.30$	$w_{fT}=0.0033$
$T=23°C$	$w_{init}\geq 0.30$	$E_{l0\ slope}=0.0$

A typical expression for the modulus of elasticity and its rate of change as functions of MC and of temperature are given by

$$E_i = E_{i0}(1 + E_{iT}(T_0 - T)) + E_{iw}(w_{f0}(1 + w_{fT}(T_0 - T)) - w_a) \quad (5)$$

$$\dot{E}_i = E_{iw}(-w_{f0}w_{fT}\dot{T} - \dot{w}_a) - E_{i0}E_{iT}\dot{T} \quad (6)$$

where the index i represents the material directions (l,r,t), E_{i0} is the basic elastic modulus and G_{i0} is the basic shear modulus, both of them at the reference temperature $T_0=20$ °C, E_{iT}, E_{iw}, G_{iT} and G_{iw} representing the effects of the temperature and of the moisture level on the reference modulus. The additional parameters contained in the table are Poisson's ratios v_{ij}; the mechano sorption behaviour m_{i0}, m_{iT}, m_{iw}; the coefficients μ_{ij} describing the coupling between the mechano-sorption effect in the different directions; the shrinkage coefficients α_i; the coefficients w_{f0}, w_{fT} representing the fibre saturation point; the reference temperature T_0; and the initial temperature T. The difference between the radial shrinkage coefficients for heartwood and for sapwood was obtained in an experimental study presented in Larsen et al. (2011). A similar difference has been confirmed by Rosner et al. (2009) and by Larsen et al. (2011), for example. The tangential shrinkage coefficient (α_t) was assumed to be twice as large as the radial coefficient (α_r) both for heartwood and for sapwood. Note that both of the indices i and j represent the material directions (l,r,t).

Experimental results

For the disc specimens studied, development of the strain field was measured during the drying process by use of the DIC system, the slit opening next to the bark being measured at regular time intervals as well. The correlation between the experimental and simulated results was assessed for the strain state attained after 25 hours drying. Figures 2 (b), 5 and 6 show the deformation state that resulted after 25 hours of drying, and Figure 4 shows the conditions present when the heartwood reached EMC of 12%, the sapwood at that point still lying significantly above the FSP. Note that the slit shown in Figure 2 (b), which originally was 1.5 mm wide, had closed in the sapwood area and become wider than 1.5 mm in the heartwood area. This occurred because of the tangential shrinkage of the heartwood material striving to open the slit, at the same time as the opening of it was suppressed by the sapwood, which had not yet started to shrink, while the radial shrinkage in the heartwood area dragged the sapwood towards the pith, resulting in the closing of the slit in the sapwood area.

Strain plots from the DIC system show that minor strains, which all were negative and the numerically largest strains represented the limiting values. In most areas, the directions of the strains were nearly tangential, this corresponding closely to the direction of the largest shrinkage coefficient. In the heartwood area, close to the free edges of the slit in particular, much larger strains occurred than in the remainder of the cross section. The minor plots from the DIC system was almost identical with the transformed strain plot shown in Figure 5(a).

Verification of the simulation model

The global strains (ε_x, ε_y and ε_{xy}) that were measured by the DIC system were transformed into tangential and radial directions so as to be comparable to the simulated strains. Figure 5 shows the transformed tangential strains and the simulated strains at the same point in time. The simulated strain field in Figure 5(b) shows tendencies similar to those of the transformed one shown in Figure 5(a), except for certain uneven strain variations. The path r used to compare experimental and numerical strains in terms of their variation is shown in Figures 5 (a and b), the results obtained being shown in Figure 5 (c).

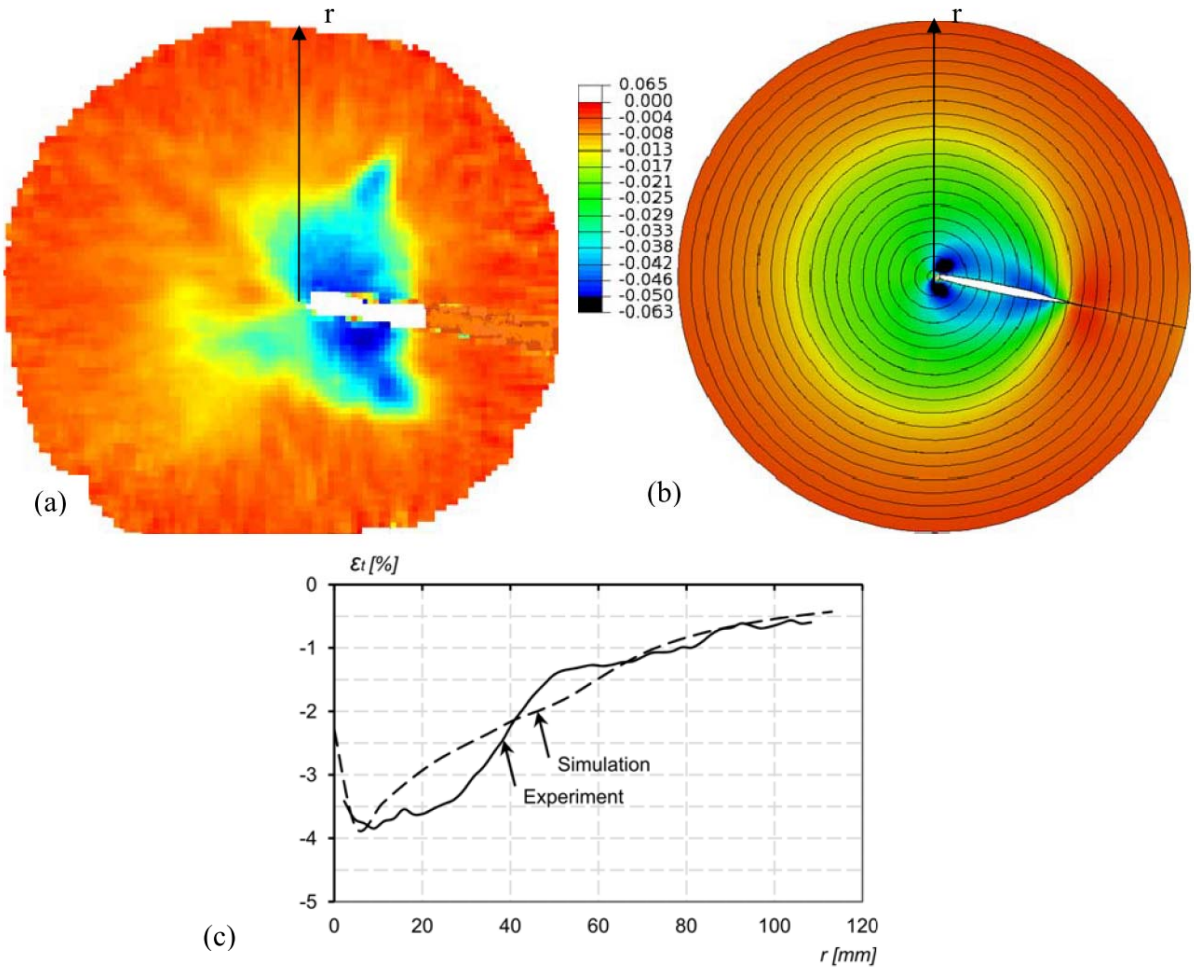

Figure 5: ***Tangential strain distribution after 25 hours drying. (a) Measured strain (b) Simulated strain (c) Strain variation along the path r.***

The variations in strains along path r show an acceptable degree of correspondence between the experimental and the simulated result. The measured slit opening after 25 hours of drying and at the final EMC stage corresponded rather closely in size to that of the simulated opening shown in Figure 6. After the model was verified experimentally it was used to investigate strain, stress and the development of distortion of the disc specimen during the drying process as a whole.

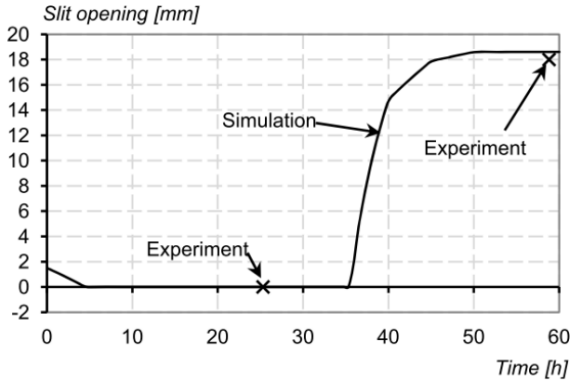

Figure 6: ***Variation in the slit opening during drying.***

Simulation results

Strain development

To study in a more detailed way the moisture-related behaviour of the disc specimens, simulation results obtained along the path r were used to investigate how strains and stresses develop during drying. The tangential strains and stresses were studied because of the cracks propagating primarily from pith to bark due to tangential stresses exceeding the tensile strength of the material.

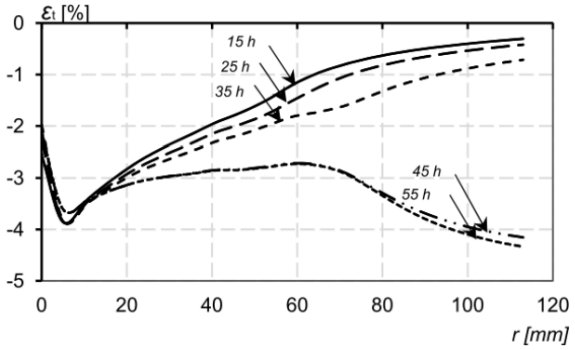

Figure 7: ***Variation in the (total) tangential strain development along r at different times during drying.***

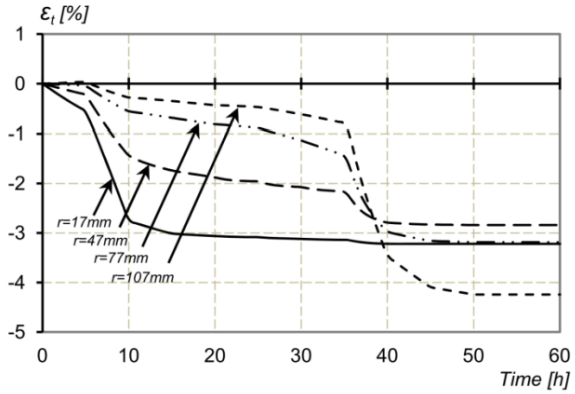

Figure 8: ***History plots for tangential strain located at different distances from the pith.***

The simulation results presented in Figure 7 indicate that strain development in one part of the disc (e.g. in the sapwood) is affected by the moisture history and the shrinkage behaviour in other parts

and vice versa. For example, the central part (from the pith outward to a radius of 20 mm) showed material properties and a moisture history that in the case of free shrinking would have been identical throughout, although under the conditions present the surrounding material partly hindered shrinking, this generating stresses and mechano-sorption strains that led to a reduction in the total value of the tangential strains. The same phenomenon could be noted in the sapwood area. By comparison, the strain of free tangential shrinking was about 5 % after 45 hours of drying. The marked curves in Figure 7, which represent 45 and 55 hours of drying, respectively, show marked mechano-sorptive strain behaviour. The sapwood closest to the bark was least affected by this mechano-sorptive behaviour. Figure 8 shows historical plots of the tangential strain at different positions along the path. Note the elastic strains in the sapwood area (r=77 and r=107 mm) during the first 35 hours of drying before the sapwood area starts to shrink, and how the strains are largest close to the heartwood.

Stress development

The mechano-sorption effects make the stress development difficult to predict. Figure 9 presents plots of the tangential stress along the path *r* at different drying times, Figure 10 shows historical plots of the tangential stress at fixed locations along the same path. Figure 9 indicates there to be large variations in stress for all the drying times that were studied. The largest stress gradients occur close to the pith and within the transition zone between the heartwood and sapwood. The largest tensile stresses occur close to the pith at the end of the drying process. This is caused mainly by a local stress concentration that builds up in front of the tip of the slit when the slit starts to open. The tensile stresses within the transition zone are found to be very close in size to the tensile strength of the material. The sapwood begins shrinking after about 35 hours of drying, as clearly evident in Figures 8 and 10. Shortly after this, the slit starts to open (see Figure 6), which changes the stress distribution markedly within cross section as a whole. The most pronounced changes occur in the transition zone between the heartwood and the sapwood (see curves r=47 mm and r=77 mm in Figure 10). The stress generation in this zone is strongly affected by the early shrinking of the heartwood and the simultaneous resistance of the sapwood, followed by shrinking of the sapwood and constraint caused by the heartwood when it has reached EMC. The largest compressive stresses occur in the middle zone at the end of the drying process, whereas the large tensile stresses in this zone occur much earlier in the drying process.

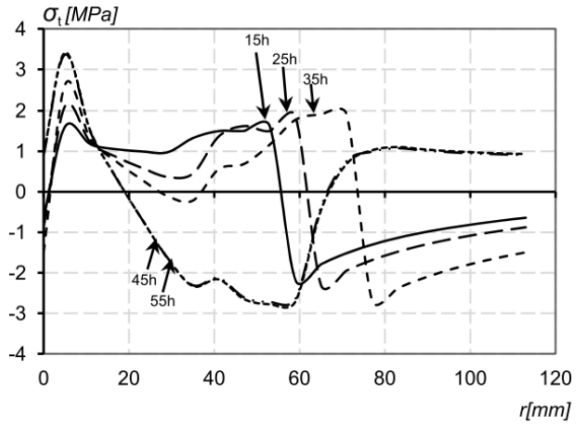

Figure 9: ***Variation in the tangential stress along r at different drying times.***

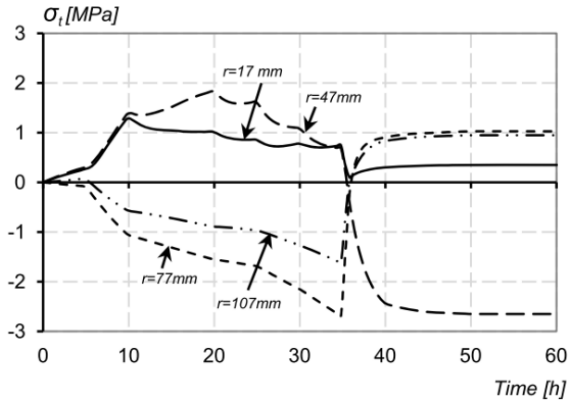

Figure 10: ***History plots for tangential stress located at different distances from the pith.***

Effects of the drying schedules on the development of stress

Further numerical investigations were performed to examine how different drying conditions affect the development of strains and of stresses. Instead of using constant climatic conditions as in the experimental study (63% RH and 23 °C applying there), two variable drying schedules were employed. The first schedule began with a relative humidity of 95% RH and a temperature of 23 °C, changes occurring then until the entire cross section had reached EMC. From this stage onward then, the moisture history based in the experimental results was followed down to where EMC=12%. In terms of the Hailwood-Horrobin equation, EMC=23% when conditions of 95% RH and 23 °C are reached. The moisture history used as input for simulation of the disc specimens is presented in Figure 11.

The second drying schedule began with climate conditions of 95% RH and 60 °C, changes that occurred then leading, just as for the first schedule, to conditions of EMC=12%. Under these initial climate conditions, the equilibrium moisture content became EMC=20%. During this simulation, the temperature was held at 60 °C. These two schedules aimed at removing the free water from the sapwood, before the disc specimen as a whole was dried to a lower moisture content, resulting in there being virtually no MC gradient below the FSP. Each of the three drying schedules lasted for 60 hours and ended at EMC=12%. For each of the schedules beginning at 95% RH, the course of MC from 40 to 60 hours was the same.

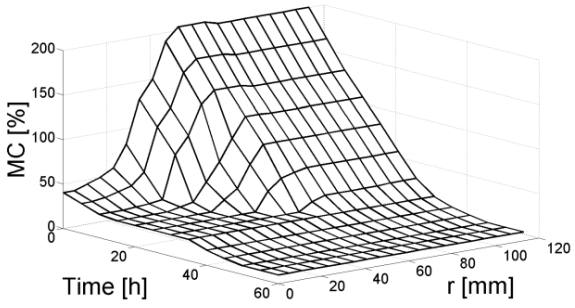

Figure 11: ***Moisture content history for the disc specimen, when the starting climate condition was 23 °C, 95 % RH and the ending condition was 23 °C, 63% RH.***

Variations in stress along path *r*, as shown in Figure 9, can be compared with those caused by each of the two modified moisture histories. Figure 12 shows the variations in tangential stresses caused by the three drying schedules after 15 and 45 hours of drying.

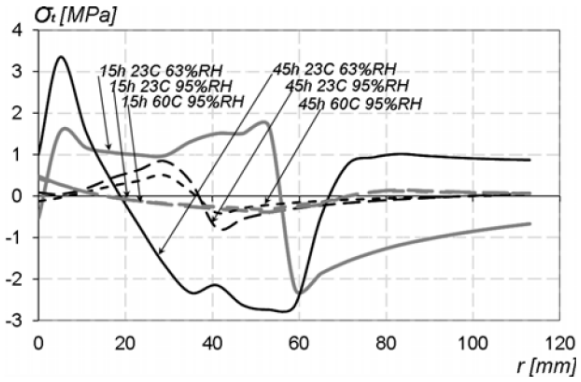

Figure 12: ***Influence of drying schemes on variation of tangential stress along the path r after 15 and 45 hours drying.***

Figure 12 shows substantial reductions in the stresses occurring under the conditions that the modified drying schedules involved. The stress reduction in the diagram for 15 hours of drying was most evident for the schedule with the highest temperature, although at 95% RH the EMC was lower at this temperature. These results indicate the clear effect of temperature on the elasticity and mechano-sorptive properties of the discs. Table 2 shows how the elastic moduli and mechano-sorption parameters change from 23 °C to 60 °C. Both the reduction in the elasticity modulus and the increase in the mechano-sorption parameters lead to an increase in mechano-sorptive strain and a reduction in constraints at 60 °C, this resulting in a lower stress level there.

Table 2. Stiffness and mechano-sorption parameters for different temperatures at EMC with 95% RH

Temp.	*Parameters*
23°C	E_t=286MPa
23°C	E_r=510MPa
23°C	m_t=0.21 MPa^{-1}
23°C	m_r=0.16 MPa^{-1}
60°C	E_t=184MPa
60°C	E_r=325MPa
60°C	m_t=0.28 MPa^{-1}
60°C	m_r=0.21 MPa^{-1}

At the end of the drying process there was almost no discernable difference between the stress values for the two modified drying schedules, despite their obviously differing in the level of variation in stresses earlier in the drying process.

Conclusions

The results for the experimental strain field (as recorded by DIC system Aramis) for the disc specimen that was studied was used to verify the simulation model. The materiel parameters used in earlier model investigations of Norway spruce were found to be appropriate here. The model was used to simulate the distribution of moisture-related strains and stresses within the disc specimens, making use of moisture histories based on different drying schedules that were similar to schedules in practical use in kiln drying. The results of the simulations clearly emphasize the decided effect that drying schedules have on stress development during the drying process.

Drying schedules beginning at 95% RH (slow drying at the start) showed more marked stress reductions than found under climate conditions of 63% RH. The modified drying schedules employed showed the final stress level to not be affected by the temperature level. Differences between the material properties of the heartwood and the sapwood were found to have only a limited effect on the stress development as compared with the much larger effects that variations in MC had.

Future work

Further numerical results are to be verified by experiments to be conducted in a new climate chamber at DTU.byg, where strain developments are to be measured by use of Aramis under ambient climate conditions that correspond to those of typical kiln-drying. A major aim of this work will be to enable drying schedules to be optimised more effectively through reducing the stresses that occur during drying, this in turn serving to reduce the risk of crack propagations. Another aim of the experiments that are planned will be to clarify the time consumption within different drying schedules so as to be able to better optimise the drying process through taking both time relations and stress developments in the wood into account.

Acknowledgement

Funding:

The Danish Forest and Nature Agency, Haraldsgade 51, 2100 København Ø.

Reference

Abaqus. Theory manual v6.8 (2008). Simulia

Aramis v6 User Manual. (2007)GOM mbH, GOM Optical Measuring Techniques. (www.gom.com)

Armstrong LD, Kingston RST (1962) The effect of moisture content changes on the deformation of wood under stress. Australian Journal of Applied Science 13: 257-276

Ball RD, Simpson IG, Pang S (2001) Measurement, modelling and prediction of equilibrium moisture content in *Pinus radiata* heartwood and sapwood. Holz als Roh- und Werkstoff 59:457-462

Baronas R, Ivanauskas F, Juodeikienė I, Kajalavicius A (2001) Modelling of Moisture Movement in Wood during Outdoor Storage. In Nonlinear Analysis: Modelling and Control 6,2:3-14

Bonneau P, Puiggali J-R (1993) Influence of heartwood-sapwood proportions on the drying kinetics of a board. Wood Science and Technology 28:67-85

Clair B, Jaouen G, Beauchêne J, Fournier M (2003) Mapping Radial, Tangential and Longitudinal Shrinkages and Relation to Tension Wood in Discs of the Tropical Tree *Symphonia globulifera*. Holzforschung 57:665-671

Dahlblom O, Petersson H and Ormarsson S (1999) Characterization of shrinkage, European project FAIR CT 96-1915, Improved Spruce Timber Utilization, Final report Sub-task AB1.5; 1999

Felix S, Morlier P (1992) Modelling of Stresses and Strains in a Piece of Wood Under Drying. Holzforschung 46:369-377

Fortino S, Mirianon F and Toratti T (2009) A 3D moisture-stress FEM analysis for time dependent problems in timber structures. Mech Time-Depend Mater 13:333-356

Kang W, Lee N-H (2002) Mathematical modelling to predict drying deformation and stress due to differential shrinkage within a tree disk. Wood Science and Technology 36:463-476

Kang W, Lee N-H (2004) Relationskip between radial variations in shrinkage and drying defects of tree disks. J Wood Sci. 50:209-216

Kowalski SJ, Smoczkiewicz-Wojciechowska A (2007) Stresses in dried wood. Modelling and experimental identification. Transp Porous Med. 66:145-158

Krabbenhøft K (2003) Chapter 4 and 5, Moisture Transport in Wood. A Study of Physical-Mathematical Models and their Numerical Implementation. Ph.D. Thesis. ISBN nr. 87-7877-225-7. Denmark

Larsen F, Ormarsson S, Olesen JF (2010) *Proceedings of the 11th International IUFRO Wood Drying Conference, 2010:*137-144, Luleå University of Technology, Skellefteå, Sweden.

Larsen F, Ormarsson S, Olesen JF (2010) *Proceedings of the 11th World Conference on Timber Engineering, 2010:*449-451, Riva del Garda, Italy.

Larsen F, Ormarsson S, Olesen JF (2011) Moisture-driven fracture in solid wood. Wood Material Science and Engineering. Vol. 6,1-2:49-57

Lazarescu C, Avramidis S (2008) Drying Related Strain Development in Restrained Wood. Drying Technology 26(5):544-551

Ormarsson S, Dahlblom O, Petersson H (1998) A numerical study of the shape stability of sawn timber subjected to moisture variation part 1: Theory. Wood Science and Technology 32:325-334

Ormarsson S, Dahlblom O, Petersson H (1999) A numerical study of the shape stability of sawn timber subjected to moisture variation part 2: Simulation of drying board. Wood Science and Technology 33:407-423

Ormarsson S (1999) Numerical Analysis of Moisture-Related Distortions in Sawn Timber. PhD thesis. ISBN 91-7197-834-8. Göteborg, Sweden

Rosner S, Karlsson B, Konnerth J, Hansmann C (2009) Shrinkage processes in standard-size Norway spruce wood specimens with different vulnerability to cavitation. Tree Physiology 29:1419-1431

Salin J-G (2006) Modelling of the behaviour of free water in sapwood during drying. Wood Material Science & Engineering 1:4-11

Salin J-G (2010) Problems and solutions in wood drying modelling: History and future. Wood Material Science & Engineering 5:123-134

Simpson WT (1973) Predicting equilibrium moisture content of wood by mathematical models. Wood and Fiber Science 5:41-49

Sreekanth M, Kolar AK (2009) Transient Thermal Behavior and Stress Development within a Cylindrical Wooden Disk during Drying in a Fluidized Bed Dryer. Drying Technology 27:344-358

Svensson S (1995) Strain and Shrinkage Force in Wood under Kiln Drying Conditions. Holzforschung 49:363-368

Svensson S (1997) Internal stress in wood caused by climate variations. Report TVBK-1013. Lund University

Wiberg P, Sehlstedt-Persson SMB, More'n TJ (2000) Heat and Mass Transfer During Sapwood Drying Above the Fibre Saturation Point. Drying Technology 18,8:1647-1664

Paper III

”A numerical and experimental study of temperature and moisture related fracture behaviour in timber logs”

F. Larsen & S. Ormarsson

Submitted in Holzforschung, 2012

A numerical and experimental study of temperature and moisture related fracture behaviour in timber logs

Finn Larsen[1#] and Sigurdur Ormarsson[1,*]

[1]Department of Civil Engineering, Technical University of Denmark, Brovej, DK-2800 Kgs. Lyngby, Denmark,

[#] Corresponding author.
E-mail: finla@byg.dtu.dk

*E-mail: sor@byg.dtu.dk

Abstract:

After timber logs have been sawed into solid boards, and before they have been processed further, they need to be dried from a green condition to a moisture level below the FSP. Timber is normally dried by kiln-drying, during which moisture-induced stresses and fractures can occur. The drying stresses arise through internal constraints that are strongly affected by differences in green moisture content between the heartwood and the sapwood, the moisture gradient being caused by the forced drying, the differential shrinkage taking place and the inhomogeneity of the material. Cracks occur primarily in the radial direction, due to tangential stresses that exceed the strength of the material. The present paper reports on experiments, numerical simulations and studies concerned with determining the fracture behaviour of Norway spruce log discs under various climatic conditions. The moisture gradient in the longitudinal direction was minimised by use of thin specimens, simplifying the description of the moisture flow in the samples studied. The specimens designed for tensile testing were acclimatised to a moisture content of 18%, their tangential tensile strength at 20, 60 and 90 °C being measured. These tensile strength values were used in disc simulations as limit state values for crack initiation. The disc results of the simulations were compared with those of experiments involving the same temperature levels as those for the tensile strength tests. The comparison showed rather close agreement between results of the simulations and experiments.

Keywords:

Tangential tensile strength, cracks, drying, modelling, moisture, wood, FEM

Introduction:

Solid timber needs to be dried from a green condition down to a moisture content (MC) below that of the fiber saturation point (FSP) before it is used as a construction material. When a solid piece of timber board contains both heartwood and sapwood, considerable stresses can develop during drying due to the increases in the internal constraints that arise. These stresses can easily exceed the tensile strength of the boards, cracks in it thus developing. In the course of time, comprehensive

efforts have been made to reveal the secrets of cracks in materials of nearly all kinds. Crack development is generally categorized in terms of three major fracture modes. A mode I fracture is a crack caused by tensile stresses perpendicular to the direction of the crack. A mode II crack is one caused by shear stress acting parallel to the direction of the crack. A mode III crack, finally, comes about through shear stress acting in the crack plane as well, perpendicular to the direction of the crack. In addition to these three basic modes, combined modes, termed Mixed Modes, can occur. For isotropic material, the three basic modes are quite sufficient for describing what occurs, but for strongly orthotropic materials such as wood further crack modes are needed in order to describe the orthotropic crack behaviour that takes place. Smith et al. (2003) and Valentin et al. (1991) pointed out, in connection with each of the three basic crack modes, the six possible crack orientations that are possible in relation to the material axis within the wood. Crack propagation in the TL and TR directions is of major interest in the present study, earlier investigations having shown these to be the direction most critical for the development of moisture-related fractures.

Ever since the late 1960s, efforts have been made experimentally to determine the fracture properties of wood so as to verify and supplement fracture theories for wood that here been employed. Up till now, no standard testing methods have been prescribed for investigations of this sort. That which makes wood crack tests particularly complex is the fact that wood fracture properties depend both on temperature and on MC, making it highly important, when results are presented, that information regarding climatic conditions be included as well. A Linear Elastic Fracture Mechanic (LEFM) was the first theoretical approach used in efforts to understand wood fracture, but it failed to account for all of the physical phenomena associated with wood fracture. The fictitious crack model, also termed the cohesive crack model, was found to be a better approach.

The basic description of the cohesive crack model is that, for Mode I fractures, a fracture process zone of a finite width can be described by a fictitious (line) crack that transmit the normal stress σ, the size of which is a function of the separation w (width of the opening) involved. By definition, when w=0, the normal stress σ which is transmitted corresponds to the tensile strength of the material, whereas when w=w_c the normal stress is nil, this defining the state of a complete fracture of a cohesive crack. The area under the softening stress-separation curve in its entirety represents the fracture energy G_F [J/m^2] required to completely separate the crack faces at a given point. The relationship between the stress reduction and the opening width involved is termed the crack softening behaviour. The softening behaviour obtained in experiments is normally not linear. Instead polynomial functions can be fitted to some degree to the experimental curves obtained, see e.g. Coureau et al. (2006).

Many investigations of crack development and of the softening curves related to these have been undertaken in the attempt to describe behaviour in an easy, yet sufficient way. Stanzl-Tschegg et al. (1995) presented a splitting method to use for studying fracturing of wood. The results led to new ways of describing the crack softening behaviour of wood. Microscopic observations of crack development indicated that the cracking process could be divided in two phases; first, development of a micro-cracking zone and then the change to a fibre-bridging zone. The crack-softening behaviour was approximated on the basis of the linear behaviour in each of these two zones. Stanzl-Tschegg et al. (1994) presented prior to this the bilinear crack softening model employed here, in which the stress-softening zone (that appeared after a peak-point (w_0, f_t) had been reached) was defined by two descending lines. The energy associated with the first span, involving the line extending from the peak-point to the break-point (w_b, f_b), is termed the cohesive micro-cracking energy $G_{f\mu}$. For the second span, represented by the line extending from the break-point on to (w_c, *0*), the energy involved is termed the cohesive fibre-bridging energy G_{fb}. The total encompassed by

the bilinear crack softening model corresponds to the cohesive fracture energy $G_F=G_{f\mu}+G_{fb}$. This same basic model was also described by Vasic and Smith (2002).

The fracture properties of wood can vary markedly within individual species. Many of these reported results do not differ whether the property is in the radial or the tangential directions, despite these two directions differ markedly in term of tensile strength, indicating there to be differences as well in terms of fracture energy and the way fractures propagate. Dourado at al. (2008) measured the fracture energy in the tangential direction and the related tangential tensile strength under climatic conditions of 20 °C and 65% RH (EMC~12%) for 12 specimens. The results were obtained using a three point bending test setup. Vasic and Stranzl-Tschegg (2007) obtained fracture energies in both the radial and the tangential directions at four different levels of moisture content, presumably at 20 °C for each of 4 different species, although the tensile strength of these different wood species was not presented, the results being obtained using a wedge-splitting technique. Smith et al. (2003) reported fracture energies for spruce, but without information concerning direction, temperature or humidity. Smith and Vasic (2003) determined experimentally the relative distributions of the total fracture energy and the bridging fracture energy under conditions in which the bridging fracture energy represented only about 10% of the total energy, testing being performed using small end-tapered double-cantilever-beam specimens. Valentin et al. (1991) presented a summary of the state of the art in this area based on test results obtained using different test types and different wood species in Mode I. These were found to be large variations of the fracture properties obtained. Gustafsson (2003) presented tangential tensile strength results for birch, pine and spruce, the effects of temperature, moisture and density on the strength of the wood being shown, in addition to this was the degree of dependence of the fracture energy on the wood density involved presented, the latter under constant climatic conditions of 12% MC and presumably at 20 °C. Reiterer and Sinn (2002) obtained the fracture energy at 20 °C and 12% MC for 15 test samples of spruce, although the crack direction and the tensile strength were not reported. The results were obtained using a wedge-splitting technique. Their load displacement curve showed the micro-crack part of the total fracture energy to be considerably larger than that for the fibre-bridging part. Vasic and Stranzl-Tschegg (2007) showed the fracture energy in the tangential direction to be considerably greater than that in the radial direction. The tensile strength values of Norway spruce that Dourado et al. (2008), Dourado (2008), and Gustafsson (2003) obtained differed a great deal in size.

The experimental results reported in the present paper aimed at to determining the tangential tensile strength of Norway spruce and how it is affected by the temperature. Experiments of two different types were performed: One of these involved uniaxial tensile strength testing within a climate chamber at three different temperature levels (20, 60 and 90 °C), the humidity level being set so as to obtain a moisture content of 18% MC (according to Simpson (1973)). The other type of experiment involved kiln-drying tests of wood discs at different temperature levels and different humidity's. Whether the discs cracked and the crack development if they did crack were studied during the drying process. The experimental disc samples were then simulated by use of a 3D distortion model developed by Ormarsson et al. (1998 and 1999), the moisture histories and the shrinkage properties of the samples being obtained by experimental study. At the experimentally observed crack location, the maximum tangential stress values (that should represent approximately the tangential strength of the material) and the associated moisture content were found for different climatic states on the basis of disc simulations. These two different approaches to determining the tangential tensile strength were then compared, showed their agreeing rather well and indicating there to be a marked reduction in strength as the temperature increases.

Materials and methods

The research method employed was a combined experimental and numerical method in which the crack development as measured was used to validate simulated results**.**

Test specimens

The test specimens were selected from 20-year old Norway spruce trees from North Zealand in Denmark. The trees were felled in the winter months of the years 2009-2012, logs having a diameter of 200-250 mm being removed from the trees. The specimens were selected from areas free of defects. The pieces of logs obtained were conserved in a freezer at approximately -10 °C. The specimens were shaped in a frozen condition so as to reduce the risk of the evaporation of moisture.

Specimens for tensile strength tests

The specimens were initially cut in a green condition, each to a size of approximately 18x50x140 mm. The specimens were then acclimatized in a climate chamber to 18% MC at 20 °C and 85% RH before the final shaping was carried out. The climatic conditions were set in accordance with equivalent moisture content (EMC) calculations as given in Simpson (1973). The final dimensions of the samples were 15x40x125 mm, there being a curved narrowing zone in the middle of each as shown in Figure 1. The narrowest area, at the centre of each sample, where failure was expected to occur, was approximately 15x20 mm in size. The exact geometry of each specimen was measured before the test measurements began, each specimens being conserved in a freezer until the tests were carried out.

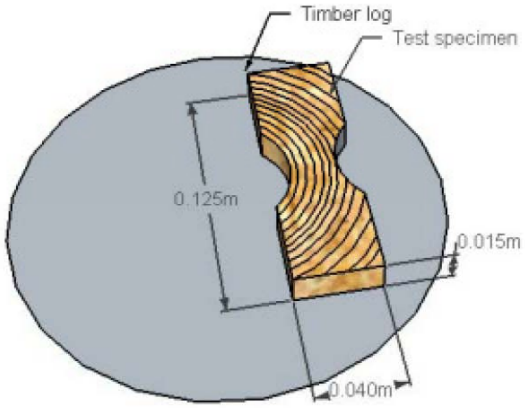

Figure 1: ***Geometry and the annual ring pattern of the specimen used for tangential tensile strength tests.***

Disc specimens for kiln drying tests

Discs 15 mm thick were sawn out from the log under frozen conditions. The thickness employed was based on preliminary test results, the moisture gradient in the longitudinal direction being disregarded; see Larsen et al. (2010 and 2011). The samples were sawn gently by hand so as to reduce the risk of damages occurring. Each sawn disc was examined for defects, each disc with some defect being discarded.

Experimental setup

Tensile strength tests

The tangential tensile strength tests were performed in the setup as shown in Figure 2. The setup consisted of a test frame, a rod between the frame and the clamp holder for the specimen,, a rod between the lower clamp holder and the loading device (the load bucket), a deformation device and the test specimen attached to the two clamp holders. The loading on the specimen was carried out slowly by filling the load bucket with small metal chips until the specimen finally broke. The loading was increased linearly over a period of approximately five minutes.

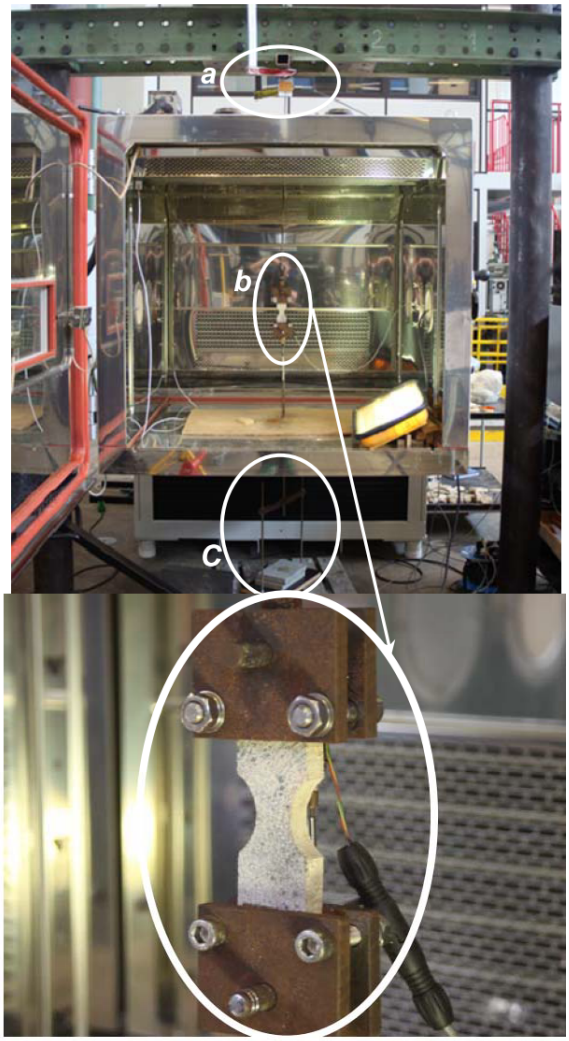

Figure 2: ***The setup for tensile strength test within the climate chamber: a. load cell, b. the specimen together with the clamps, c. the loading device.***

The tests were conducted in the climate chamber under three well-defined sets of climatic conditions; 20 °C and 86% RH, 60 °C and 91% RH, and 90 °C and 96% RH. The test frame was placed outside the chamber, the upper rod going through a moisture-tight rubber bushing on the top of the chamber, the lower rod going through a small pipe that also goes through a bushing on the bottom side of the chamber, allowing the lower rod to move freely up and down within the pipe.

The load bucket was hanging beneath the chamber. This setup made it possible to acclimatize the specimen prior to testing and to perform the testing under different climatic conditions.

Disc drying setup

The log disc experiments were conducted in a setup that involved use of a climate chamber, a stand, a load cell for weight logging of the disc specimen, together with Aramis (2007), a digital image correlation system for measuring deformations of the disc specimens. The experimental setup is shown in Figure 3. The load cell was built into the stand, the stand being designed so as to enable there to be free ventilation around the test specimens: Each specimen only touched the stand at three individual points, its being placed at the height of the heated window, enabling the cameras (located outside of the chamber) to record the deformation of the disc during the drying process. The load cell was connected to a data logger outside the chamber. When the experiments were finished, the dry weight of each of the specimens was determined after oven drying of them at 103 °C.

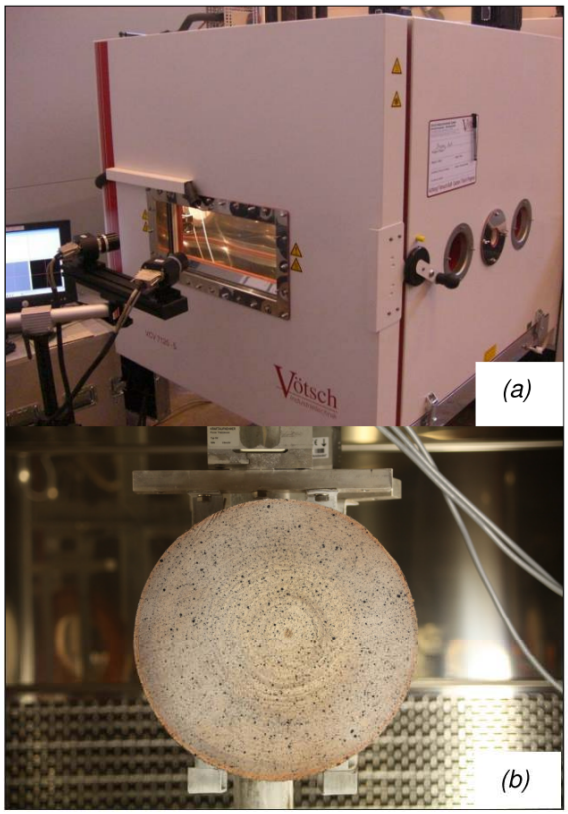

Figure 3: ***Experimental setup: (a) the climate chamber, its having specially designed window and well-controlled lighting, temperature, humidity and air circulation, as well as the Aramis cameras placed outside the chamber; (b) the specimen placed on a specially designed stand having a load cell located inside the chamber.***

Numerical simulations

A number of simulations of the disc specimens that were studied were performed by use of the FE software Abaqus (2008), special routines for wood distortion developed earlier by Ormarsson et al. (1998 and 1999) being included in it. The stress analysis carried out made use of using 8-node linear brick elements of type C3D8. The specimen studied was a circular 15 mm thick log disc containing 19 annual rings and a pith. The 19 annual rings were divided further into 8 parts, each with its own set of material parameters, as well as of moisture and temperature histories. Four of

these parts were assumed to represent crack zones having cohesive crack properties, each of the other parts being shaped in the form of a quarter of an annual ring. All the annual ring parts were connected by tie-constraints that allowed the disc to function as an inhomogeneous continuum. The disc diameter was 232 mm, which was approximately the same diameter as that of the test specimens.

Figure 4 shows the mesh of the disc sample that was studied, as well as the position of the crack zones. The possible crack zones were simulated with use of 0.2 mm thick cohesive hexahedral elements of type COH3D8. The crack zones were connected to the solid parts by so-called tie-constraints. The initial variations in MC (under the green conditions) as well as the development of the MC-curve over time were obtained along the radius (r) of the discs. Figure 5 and *Figure 6* show experimental results for the disc specimens used to generate the moisture history that was needed as input data for the model. In the model, the moisture content field over the cross-section is assumed (for the case in question) to be axisymmetrically distributed around the pith.

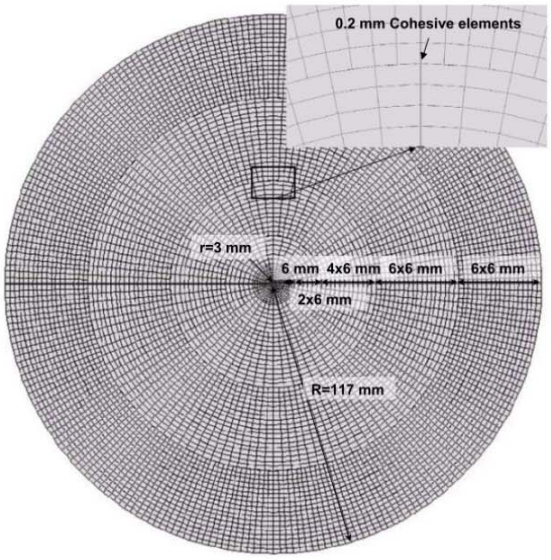

Figure 4: ***Dimensions, predefined crack pattern and element mesh of the disc sample that was studied.***

Moisture histories needed for the disc simulations

The drying history of the disc specimen in terms of weight vs. time was recorded during the drying process. The weight was an average value that took account of both the sapwood and the heartwood. It was used to calculate the average MC for the disc specimen; see Figure 5. The sapwood had a green MC value that was considerably higher than the average MC value. The drying history of the sapwood was calculated on the basis of the average curve of the MC history. In earlier investigations by Larsen et al. (2010a, 2010b) it was shown that the course of drying (reduction in MC) for the heartwood and sapwood sections could be considered to be virtually identical, but that the drying started at very different MC levels under green conditions. For example, as shown in Figure 7, a part with an initial MC of 190% needed 350 minutes to reach EMC, whereas a part with an initial MC of 75% needed 175 minutes to reach the same MC level. Figure 7 shows the average moisture history for the pith and for areas at five different distances from the pith.

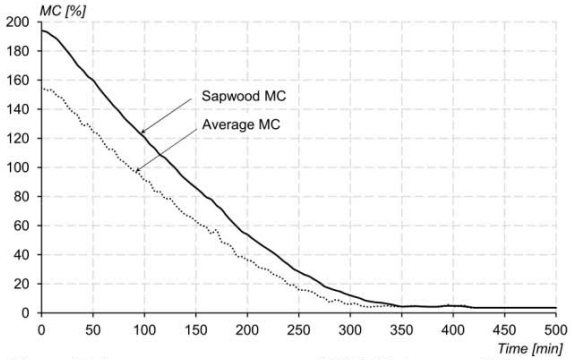

Figure 5: ***An average measured MC history and the corresponding calculated sapwood MC history at 90 °C and 30% RH.***

Initial variations in MC under green conditions, (beginning at t = 0) as well as curves over time for the MC history were obtained for several points along the radius (r) of the disc specimens on the basis of small ovendried sticks taken from the cross section of the disc.

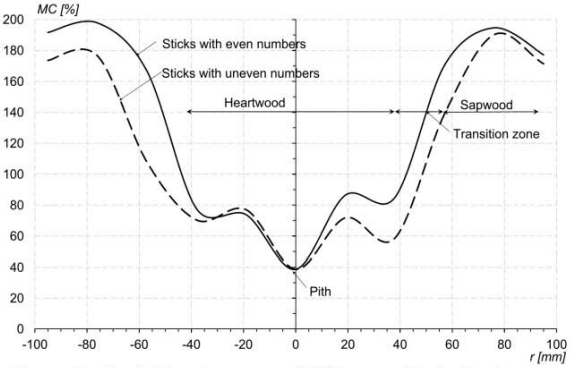

Figure 6: ***Variation in green MC from pith to bark.***

Figure 6 shows variations in the green MC from pith to the bark. The four MC paths are not identical, each curve applying to only a quarter of the disc. The existence of these different MC path curves, each under green conditions, results in the nineteen annual rings and the pith zone all having their own moisture histories, a total of seventy-seven different drying histories being generated in connection with each simulation.

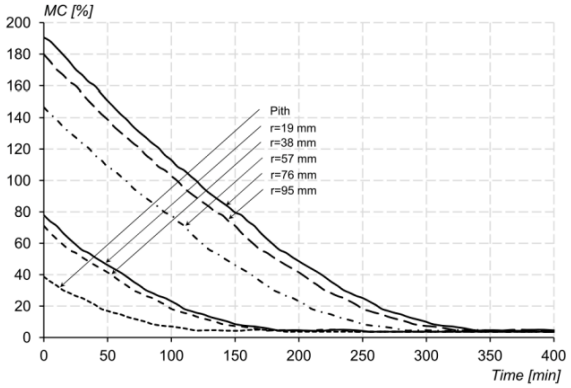

Figure 7: ***MC histories for the pith and at five different material points along the r at climatic conditions of 90 °C and 30% RH.***

Material parameters

The material parameters used for the solid wood material here are ones presented earlier in Larsen et al. (2012) and in Ormarsson (1999). The stiffness, mechano-sorptive, shrinkage and temperature parameters employed here are ones representative of Norway spruce trees. Radial shrinkage coefficients for heartwood and for sapwood obtained in experimental studies reported in Larsen et al. (2011) and Rosner et al. (2009) constitute supplements to the parameters given in Ormarsson (1999). The tangential shrinkage coefficient (α_t) employed in the present study was assumed to be twice as large as the radial coefficient (α_r), for the heartwood and the sapwood alike.

The fracture properties of the wood, including fracture energy, the softening curves and the tensile strength, are needed for the cohesive crack simulations carried out. The investigations of the fracture energy presented in the introduction are summarised in Figure 8:

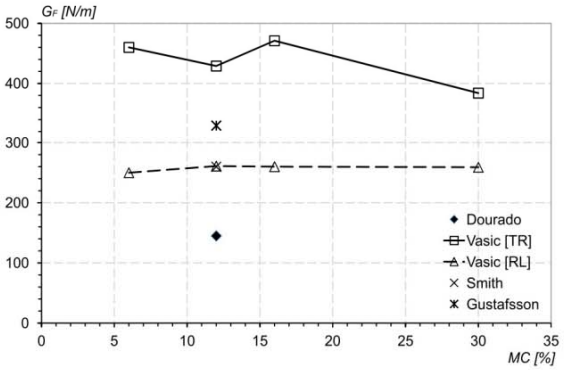

Figure 8: ***Summary of the fracture energy results obtained for spruce at 20 °C.***

Dourado at al. (2008) and Dourado (2008) reported the tangential tensile strength of Norway spruce to be 1.66 MPa, whereas Gustafsson (2003) found it, under similar conditions, to be 3.0 MPa. No such contradictory results for the fracture energy of the wood, for the ratio of its micro-crack to its fibre-bridging energy level, or for its tensile strength have been obtained, however. According to Smith and Vasic (2003) the micro-crack energy level appears to be appreciably higher than the fibre-bridging energy level, only limited results being obtained regarding temperature effects on the fracture properties. In the present simulations, the crack properties employed were based on an evaluation of the results presented above and on own experimental results. The fracture energy employed was G_F = 240 J/m^2, its being assumed to be independent of the temperature. Since according to Smith and Vasic (2003) the fibre-bridging part of the fracture energy is relatively small, the softening curve was designed as representing the evolution of linear damage. In the simulations presented here the following cohesive fracture relations were employed:

$$G_F = \frac{f_t \cdot \omega_c}{2} \qquad (1)$$

$$\sigma_{t,c} = f_t - \frac{f_t^2 \cdot \omega}{2G_F} \qquad (2)$$

where G_F is the fracture energy needed for cohesive crack generation, $\sigma_{t,c}$ is the tangential stress in the crack zone, f_t is the tangential tensile strength of the wood material, ω is the crack opening variable in the crack zone and ω_c is the limiting value for the crack opening at the ultimate fracture point. The cohesive expressions presented above represents a linear softening model for the crack

generation, instead of a bilinear model applying both to micro-cracking and to fibre-bridge cracking.
Figure 9 shows both linear and bilinear softening behaviours to represent identical fracture energies but differing tensile strengths. It can be noted that for the bilinear softening behaviour the fibre-bridging part is only 10% of the total fracture energy G_F.

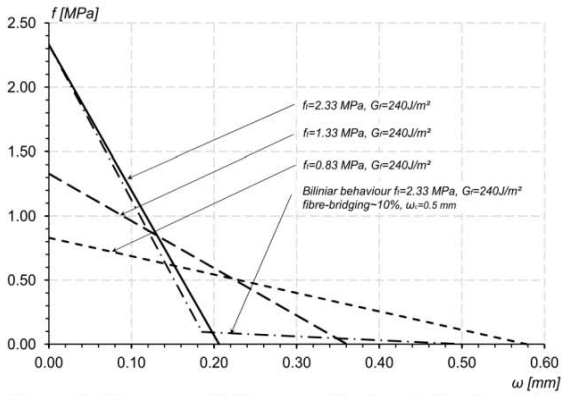

Figure 9: ***Linear and bilinear softening behaviours involving the same fracture energy but three different tensile strengths.***

Figure 9 shows the linear and the bilinear model to involve identical tensile strengths and to follow almost the same path because of the only small fibre-bridging part.

Results and discussions

The tangential tensile strength of the wood material was measured by means of the tensile strength test described above and by comparing the simulated stresses involved with the degree of crack initiation during disc drying produced experimentally. The aim here was to study how the tangential tensile strength of the wood is affected by the temperature level and to verify the model through comparing the simulated stress levels at the point of failure with the strength as determined by means of the tensile strength test. Crack simulations were performed on the discs then making use of the tensile strength as assessed here and of the fracture energy as described above, these being considered to be primary cohesive crack properties. The crack development was followed and compared with pictures generated by the Aramis equipment at selected points in time during the drying process.

Tangential tensile strength test

The tangential tensile strength is a parameter needed for crack modelling. Tests of tangential tensile strength were performed at three different temperatures - 20, 60 and 90 °C - under constant climatic conditions of 20 °C and 85% RH, 60 °C and 91% RH, and 90 °C and 96% RH respectively, coupled with 18% EMC in the wood. The specimens were acclimatized in the chamber for at least 12 hours, under the climatic conditions present there, before the test started. The results are summarised in table 1:

Table 1: Effects of temperature on the tangential tensile strength of Norway spruce at MC=18%.

Temperature	20 °C $f_{t,90}$ [MPa]	60 °C $f_{t,90}$ [MPa]	90 °C $f_{t,90}$ [MPa]
Test no. 1	2,55	1,14	1,20
Test no. 2	2,46	1,58	0,64
Test no. 3	2,25	1,39	0,66
Test no. 4	2,35	1,73	0,85
Test no. 5	2,05	0,75	
Test no. 6		1,27	
Test no. 7		1,47	
Average	2,33	1,33	0,83
Stand. dev.	0,20	0,32	0,26

The results presented in Table 1 show a marked decrease in the strength of the wood occurred with an increase in temperature, slight variations in the standard deviation taking place while this was under way.

Determination of the tangential tensile strength by drying of the disc specimens

Both numerical and experimental investigations of disc specimens were performed to study the effects of temperature on the tangential tensile strength of the wood. The disc specimens were selected from the same timber log as before so as to minimise the variation between samples. The discs were dried with use of different drying schedules (involving both different temperatures and different RH levels in the climate chamber). The Aramis system and the load cell were used to measure the strain and the changes in weight during the drying process. Aramis was also used to study whether and at what point in time the discs cracked. The experimental results, representing both cracked and uncracked samples are shown in Figure 10.

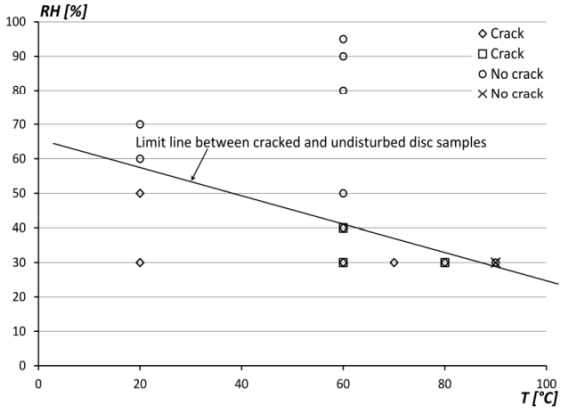

Figure 10: ***Illustrations of cracked and uncracked disc samples after various drying processes.***

The limit curve separating the cracked and uncracked samples is almost linear, the cracked samples being placed beneath the line and the uncracked samples above it. At low temperatures the discs crack at a higher level of humidity than they do at higher temperatures. An average moisture history was generated for each of the test samples, on the basis of the recorded weights of the samples. All of the disc samples close to the crack-limit line were simulated in Abaqus (2008) when exposed to

climatic conditions corresponding to those shown in Figure 10, MC histories being generated for all of the annual rings, as shown in Figure 7. The tensile strength limit was set at a level higher than that of the expected maximum tensile stresses in order to determine the areas in which the maximum stresses and the related MCs occurred. Table 2 shows the climatic conditions, the critical tangential tensile stresses in the transition zone where cracking begins, the MC values related to this and whether cracks are created or not during the drying process for those specimens that were closest to the crack-limit line shown in Figure 10.

Table 2: Simulated critical tangential tensile stresses in the transition zone under different climatic conditions.

Temperature [°C]	RH [%]	Critical tensile stress [MPa]	Moisture content [%]	Crack information Crack/No crack
20	50	2,50	23,0	Crack
20	60	2,11	19,0	No crack
60	40	1,69	20,0	Crack
60	50	1,68	14,5	No crack
80	30	1,26	18,5	Crack
90	30	1,65	9,0	No crack

Table 2 shows that a rise in temperature tends to reduce the critical tensile stress in the samples, even though the stress results in the table cannot be compared with one another directly because of their differing in the MC values associated with them. Taking as a point of departure results reported by F.E. Siimes (1967), Gustafsson (2003) found tangential tensile strength to be affected by both temperature and MC for each of three different wood species, (see Figure 11). His results indicated the strength of wood to decrease with an increase in temperature and in MC, except for a rise in spruce when the temperatures rise from 20 to 40 °C.

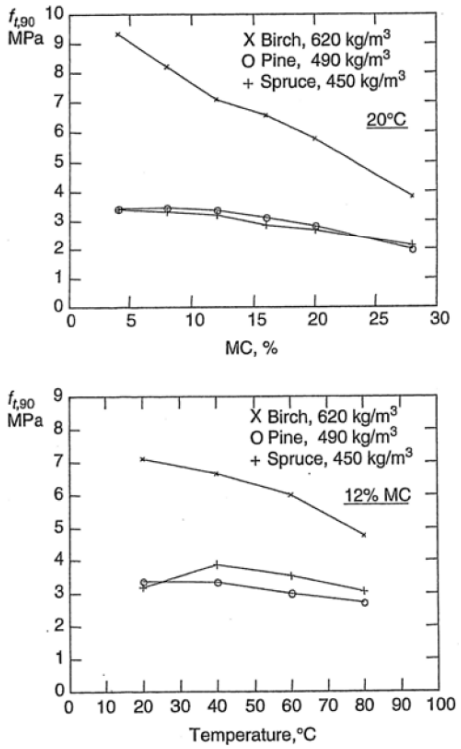

Figure 11: ***Dependence the tangential tensile strength on temperature and on MC, Gustafsson (2003).***

Figure 11 also shows how the strength of the wood is reduced when MC increases from 5% and upwards. Results of this sort can also be expected in connection with increases in MC involving other starting temperatures. The stresses shown in Table 2 have been adjusted in Table 3 to a MC of 18% on basis of the results shown in Figure 11. The values in question were evaluated further to determine the tensile stress values for each temperature at which cracks could develop. These stress values were somewhere in between the simulated stress values for cracked and for not cracked discs, taking the middle value between cracked and not cracked discs at 20 °C and so forth. The values, shown by the circular markers, are plotted directly in Figure 12. The crosses in Figure 12 are the tangential tensile strength results from table 1.

Table 3: Estimated tangential tensile stresses under conditions of 18% MC state.

Temperature [°C]	RH [%]	Critical tensile stress [MPa]	Moisture content [%]	Crack information Crack/no crack
20	50	3.03	18.0	Crack
20	60	2.19	18.0	No crack
60	40	2.05	18.0	Crack
60	50	1.42	18.0	No crack
80	30	1.30	18.0	Crack
90	30	1.01	18.0	No crack

The critical stress values obtained were compared with the results of the tests of axial tensile strength presented in Table 1. The results presented in Figure 12 indicate there to be a close correlation between the critical stresses and the measured strengths, even though the two trend lines are slightly displaced. An equation describing the relationship between tangential tensile strength and temperature is

$$f_{t,90,T} = f_{t,90,20}\left(1.188 - 0.0092T\right) \qquad (3)$$

where $f_{t,90,T}$ is the tangential tensile strength at a fixed temperature T in °C at 18% MC, and $f_{t,90,20}$ is the reference strength at T=20 °C. In Figure 12 the parameter $f_{t,90,20}$ is set to 2.4 MPa. The effect of MC on the strength was not evaluated in the present study, but according to Figure 11 the strength of the wood is highly dependent upon the MC level.

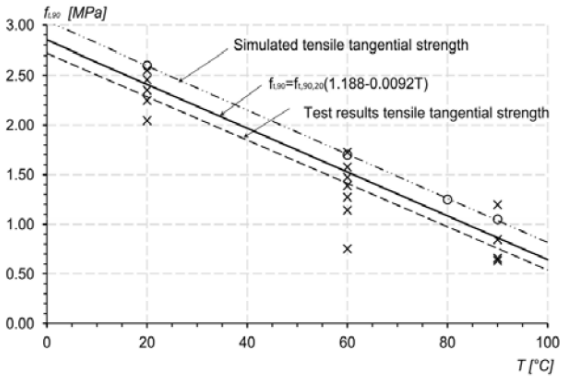

Figure 12: ***Effect of the temperature on the tangential tensile strength as estimated from tests and from disc simulations at 18% MC.***

Both simulated and experimentally obtained results show clearly that the temperature has a marked effect on the tangential tensile strength. Although this temperature-strength relationship could be thought to also occur in the radial and the longitudinal directions, this was not investigated here.

Comparison of experimentally observed and simulated crack development

The fracture model based on equations 1 and 2 was implemented in a disc model. The disc simulation presented in Figure 13 is for low temperature drying at 20 °C and 30% RH. Results of the simulation were compared with those of a disc drying experiment involving exposure to the same climatic conditions. Figure 13 shows both simulated and experimentally observed crack patterns at four different points in time during the drying process.

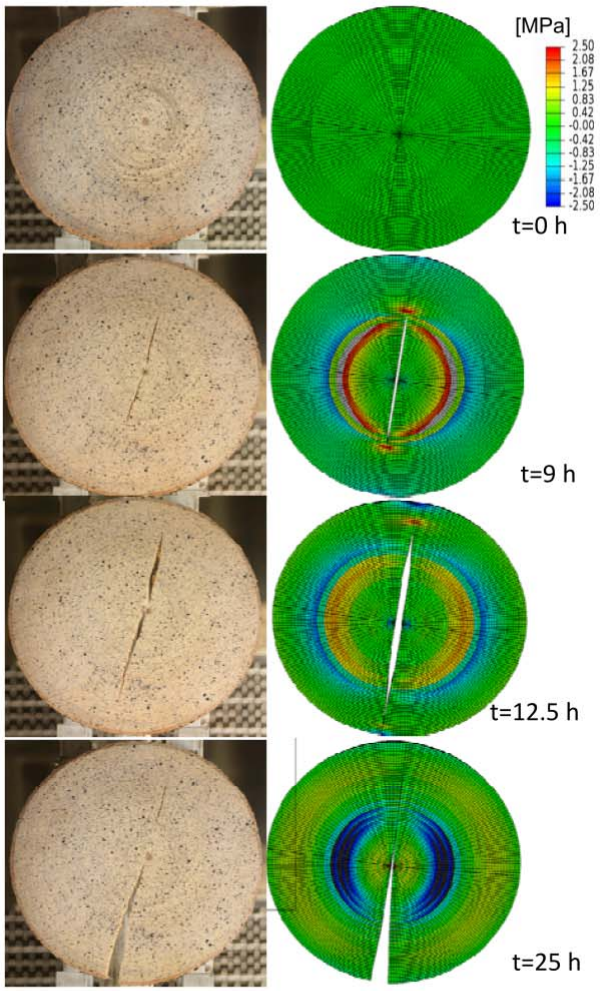

Figure 13: ***Both experimentally observed and simulated crack patterns, together with variations in tangential stress in a disc sample at different times during the drying process under climatic conditions of 20 °C and 30% RH.***

The comparisons provided in Figure 13 show there to be close agreement between the simulated crack development obtained and the experimental results. The stress situation after 9 hours of drying, when only the heartwood had dried just below FSP, reveals a crack in the heartwood that developed shortly before this state had been reached. The heartwood area was geometrically fixed by the surrounding sapwood, which led to a buildup of stress when the heartwood shrank. The crack generation that occurred released some of the tensile stress in the heartwood zone, whereas marked

tensile and compressive stresses accumulated in the transition zone. The stress situation after 12.5 hours of drying, when a large part of the transition zone had dried to a MC below FSP, shows the tensile stresses having been reduced and the zone of large tensile and compressive stresses having moved further out towards the sapwood. The final stress situation after 25 hours of drying shows marked compression stresses that had been built up in the outer zone of the heartwood area due to the shrinkage of the sapwood area.

Conclusions

The two differing approaches employed (the one based on use of tensile tests and the other on use of disc simulations) for determining the tangential tensile strength of Norway spruce were found to correlate closely with one another. It was also that when MC remained constant the strength of the wood markedly decreased in linear fashion in response to a rise in temperature. An equation applying to this relationship was found. The close agreement of the two methods could be seen as rather clear verification of the simulation model.

Through taking advantage of the present strength findings, together with the related crack formulation, the simulation model that was developed was able to simulate the entirely of the crack propagation that took place in the disc samples studied when they were exposed to different drying schedules. The examples shown in Figure 13 illustrate rather well the close correlation found between experimentally observed and simulated crack patterns during the drying process as a whole.

Future work

It is well known that MC has a strong effect on most of the properties of wood. Certain limited results also exist indicating the effects that MC has on the tangential and radial tensile strength of wood. Knowledge of the latter is of considerable importance in analysing crack developments during the kiln-drying of wood. Another and related matter studied rather little thus far but very worthy of investigation is that of the fracture energy found under at different climatic conditions.

Another matter that should be studied is that of the stress development during the kiln-drying of timber boards showing large variations in the initial (green state) MC gradients over cross sections of the boards.

Acknowledgement

Funding:

The Danish Forest and Nature Agency, Haraldsgade 51, 2100 København Ø.

Reference

ABAQUS. *Theory manual v6.8.* Simulia, 2008.

Aramis v6 User Manual. GOM mbH, GOM Optical Measuring Techniques. (www.gom.com), 2007.

Coureau J.L., Morel S. and Gustafsson P.J.: Influence of the fracture softening behaviour of wood on load-COD curve and R-curve. Materials and Structures, 40:97-106, 2006.

Dourado N., Morel S., de Moura M.F.S.F., Valentin G. and Morais J.: Comparison of fracture properties of two wood species through cohesive crack simulations. Composites: Part A 39:415-427, 2008.

Dourado N.: R-curve behaviour and size effect of a quasibrittle material: Wood. PhD thesis. N° d'ordre: 3734. L'Université Bordeaux I, France, 2008.

Gustafsson P.J.: Timber Engineering. John Wiley & Sons Ltd. Pages 103-130, 2003. ISBN 0-470-84469-8.

Larsen F., Ormarsson S. and Olesen J.F.: *Proceedings of the 11th International IUFRO Wood Drying Conference, 2010a*. 137-144, Luleå University of Technology, Skellefteå, Sweden.

Larsen F., Ormarsson S. and Olesen J.F.: *Proceedings of the 11th World Conference on Timber Engineering, 2010b*. 449-451, Riva del Garda, Italy.

Larsen F., Ormarsson S. and Olesen J.F.: Moisture-driven fracture in solid wood. In Wood Material Science and Engineering. 6(1-2):49-57, 2011.

Larsen F. and Ormarsson S.: Numerical and experimental study of moisture-induced stress and strain field developments in timber logs. Wood Science and Technology, 2012.

Ormarsson S., Dahlblom O. and Petersson H.: A numerical study of the shape stability of sawn timber subjected to moisture variation part 1: Theory. In Wood Science and Technology 32:325-334, 1998.

S. Ormarsson, O. Dahlblom and H. Petersson: A numerical study of the shape stability of sawn timber subjected to moisture variation part 2: Simulation of drying board. In Wood Science and Technology 33:407-423, 1999.

Reiterer A. and Sinn G.: Fracture Behaviour of Modified Spruce Wood: A Study Using Linear and Non Linear Fracture Mechanics. In Holzforshung 56:191-198, 2002.

Rosner S., Karlsson B., Konnerth J. and Hansmann C.: Shrinkage processes in standard-size Norway spruce wood specimens with different vulnerability to cavitation. In Tree Physiology 29:1419-1431, 2009.

Simpson W.T.: Predicting equilibrium moisture content of wood by mathematical models. In Wood and Fiber Science 5:41-49, 1973.

Smith I., Landis E. and Gong M.: Fracture and Fatique in Wood, Wiley, 2003. ISBN 0-471-48708.

Smith I., Vasic S.: Fracture behaviour of softwood. In Mechanics of Materials 35:803-815, 2003.

Stanzl-Tschegg S.E., Tschegg E.K. and Teischinger A.: Fracture energy of spruce wood after different drying procedures. In Wood and Fiber Science, 26(4):467-478, 1994.

Stanzl-Tschegg S.E., Tan D.M. and Tschegg E.K.: New splitting method for wood fracture characterization. In Wood Science and Technology 29:31-50, 1995.

Valentin G.H., Boström L., Gustafsson P.J., Ranta-Maunus A. and Gowda S.: Application of fracture mechanics to timber structures RILEM state-of-the-art report, Statens tekniska forskningscentral, Technical Research Centre of Finland, Research Notes 1262, ESPOO 1991.

Vasic S. and Smith I.: Bridging crack model for fracture of spruce. In Engineering Fracture Mechanics 69:745-760, 2002.

Vasic S. and Stranzl-Tschegg S.: Experimental and numerical investigation of wood fracture mechanisms at different humidity levels. In Holzforschung 61:367-374, 2007.

Paper IV

”Effect of initial (green state) moisture gradients on stresses in timber boards during drying”

F. Larsen & S. Ormarsson

Submitted in Wood Science and Technology, 2012

Effect of initial (green state) moisture gradients on stresses in timber boards during drying

Finn Larsen[1#] and Sigurdur Ormarsson[1,*]

[1]Department of Civil Engineering, Technical University of Denmark, Brovej, DK-2800 Kgs. Lyngby, Denmark,

[#] Corresponding author.
E-mail: finla@byg.dtu.dk

*E-mail: sor@byg.dtu.dk

Abstract:
Timber logs are sawn into timber boards in a green condition before being kiln dried, prior to further use, to a moisture content below the fibre saturation point. The drying can easily lead to high stress levels developing during this process. For timber boards consisting of both heartwood and sapwood, a rather large initial moisture gradient over the cross sections can be present in the green condition. This variation in initial MC means that different cross sectional areas can differ considerably in the time at which the FSP is reached in the course of the drying process. This can result in strong moisture gradients developing in the transition zones between these areas. The initial moisture gradients, the differential shrinkage that occurs, and the inhomogeneity of the material make it relatively complex to simulate the stress history during the drying process as a whole. The present study reports on experimentally obtained water flux results, representing different subareas in the cross sectional plane, used as input data for stress simulations concerned with the kiln-drying of timber boards having strong initial moisture gradients in the green condition. The simulations were performed for Norway spruce timber boards having green MC levels ranging from 60 to 180% and climatic conditions of 60 °C and 80% RH. Three different sawn patterns were investigated; each cross section obtained containing heartwood, sapwood and transition zones between these. The simulations showed the initial green moisture gradient to have a marked effect on stress development in the boards during drying.

Keywords:
Wood, timber board, drying, moisture gradient, modelling, FEM

Introduction:
Timber boards are sawn from timber logs prior to kiln drying, often in patterns designed so as to obtain as large a volume of solid timber as possible. This frequently results in cuts containing both heartwood and sapwood. The drying of timber boards generally involves the presence of moisture gradients from the surface to the centre of the board during the drying process; see e.g. Ormarsson (1998, 1999), Ekevad et al. (2011) and Mounji et al. (1991). The increases in the size of these gradients that occur over the cross section due to variations in the green moisture content are seldom accounted for when evaluating kiln drying. Larsen and Ormarsson (2012) showed variations in the green MC to have a marked effect on strains, stresses and crack developments during the drying process. Mechano-sorption strains that develop during the combined occurrence of stresses and changes in moisture level can reduce the level of the stresses generated during drying. How mechano-sorption parameters affect the distortion of solid timber has been investigated numerically by Ormarsson (1999) and by Fortino et al. (2009), for example.

The surface from which water vapour evaporates also has an effect on the average drying speed since the drying speed is stronger for a small than for a larger surface/volume ratio, provided if all other climatic conditions remain constant. The drying process is also highly complicated to analyse since the MC can readily fall below FSP at different times, the frequency which this occurs depending upon the volume ratio of heartwood to sapwood, as well as the initial variation in MC in the green condition, and the associated surface areas. The drying history is likewise complex, although drying occurs faster above than below the FSP. Experiments by Wiberg et al. (2000) and by Krabbenhøft (2003) on losses in moisture above and below the FSP showed clearly that the rate of drying (the water flux) is higher above the FSP than below it. It was found that above the FSP the drying of wood is strongly dependent upon evaporation from the surface of the wood, and that below the FSP drying is strongly dependent upon moisture transport inside the wood. An overview over different drying models has been presented by Salin (2010), regarding in particular moisture transport and gradients above FSP. It was observed for materials other than wood that water can move in the form of a film or in the corners of capillaries that have polygonal cross-sections. It is possible that this phenomenon also occurs in the wood material. If it does, this would mean that links between water-filled clusters could be formed, increasing the continuity of the liquid phase. The inclusion of a film or of corner flow in modelling here was investigated by Yiotis et al. (2004). Using their method to include this phenomenon, a MC situation similar to that shown in Figure 1 would seem likely to occur.

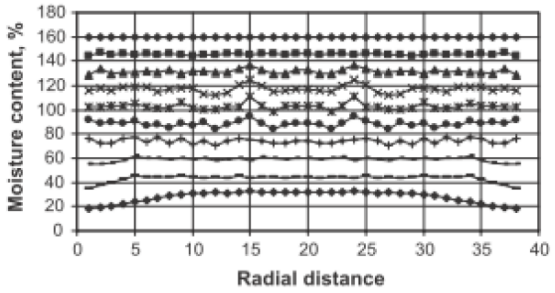

Figure 1: Moisture profiles when film flow is included in modelling (Figure from Salin (2010))

Figure 1 shows that 1-D moisture floats to the surface almost without a gradient until the MC gets down to 70%; from this stage onward a gradient beginning to arises, the MC at the surface, when it reaches FSP, becoming approximately 10-12% smaller than the MC in the material at the centre of the board. The gradient occurs at a depth of approximately 10 mm.

The present paper concerns an experimental study of water flux in Norway spruce samples exposed to climatic conditions of 60 °C and 80% RH. The experimental results were used then as input data for stress simulations of kiln-dried timber boards having large moisture gradients in the green condition. Three different board types in terms of location of the pith, all of them containing both heartwood and sapwood, were simulated. The simulations were performed for investigating the effect of the initial (green) MC gradient on stress development in the timber boards during drying. The simulation model employed was based on a 3D distortion model developed earlier by Ormarsson (1999), use being made of the moisture histories created by the experimental flux results presented here and the shrinkage properties generated from the experimental results by Larsen et al. (2010).

Materials and methods

The method employed is a combined experimental and numerical one in which the results of experimentally obtained moisture histories were used as input data for the stress simulations of different timber boards exposed to kiln drying.

Test specimens for water flux experiments

Experiments were performed to examine the water flux in Norway spruce samples during forced drying. The specimens involved were selected from the sapwood area in 20-year old Norway spruce trees from North Zealand in Denmark. The trees were felled in the winter of 2011-2012, logs having a diameter of 200-250 mm being removed from the trees. The specimens were cut out in a frozen condition, so as to avoid evaporation from the surfaces, with a band saw. The samples were 150 mm in length and had a thickness in the radial direction of 35 mm, giving them a width of 30 mm closest to pith and of 40 mm closest to bark. The specimens referred to as T1-T6 in Figure 2 were sealed with a layer of Conclad (a two component sealing layer produced by Condor Kemi A/S), both on the ends of the specimens and on the RL-surface, allowing evaporation to occur in the R direction only, the specimens referred to as R1-R6 being sealed by Conclad on the ends and on the TL-surface, allowing evaporation to only occur in the T direction. The radial and tangential surface areas are equal in size (0.0105 m^2), as are the average maximum distances from the surfaces to the centre of the specimens (0.0175 m). Figure 2 shows the principles upon which the sawing patterns to obtain samples having the same dimensions in radial as in the tangential direction

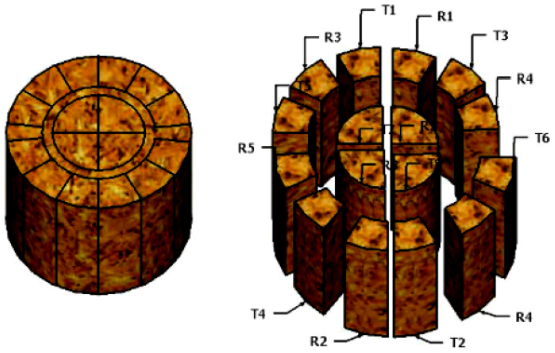

Figure 2: A sketch showing the pattern for cutting out the specimens used for to studying the radial and the tangential water flux.

Experimental setup

The water flux experiments performed during kiln-drying were conducted in a setup involving use of a climate chamber, a stand and a load cell. Further information regarding the climate chamber setup can be found in Larsen and Ormarsson (2012). The load cell built into the stand was connected to a data logger outside the chamber. The stand was so designed that the specimens touched the stand at only few points, providing for free ventilation around the specimens that were tested.

Modelling of timber boards

The simulation of the timber boards was performed by the FE softwere Abaqus (2008), a 3D stress analysis being carried out using 8-node linear brick elements of type C3D8. The type of specimens studied were rectangular timber boards containing 4 sub-volumes (parts) differing in their material properties and their drying histories, differences between the heartwood, two transition zones and

properties and their drying histories, differences between the heartwood, two transition zones and the sapwood being of particular interest. The parts were connected by a tie-constraint which allowed the board to function as an inhomogeneous continuum. Each part (sub-volume) was further partitioned into thin sub-parts close to the surface of the board, as shown in Figure 3. Each sub-parts was provided with its own set of material parameters and its own moisture and temperature history.

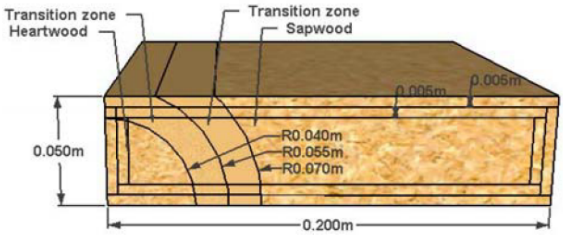

Figure 3: A simulated timber board consisting of a heartwood part, two transition zones and a sapwood part.

The thin sub-parts close to the surface enabled simple estimates of the moisture gradient over the cross section to be obtained. Three different board types were used to investigating the effects of the sawn pattern on the stress development that occurred during drying. The boards differed in the location of the pith, but each consisted of a heartwood area, a sapwood area and two transition zones in between. The heartwood area was defined as having a radius of 40 mm, the thickness of each transition zones being set to 15 mm. The timber boards had dimensions of 50x200 mm, as shown in Figure 3. The mesh of the three boards is shown in Figure 4. Note the fine mesh in the central part of board II. Since the thicknesses of the sub-parts close to the heartwood diminish down to a value of nil, so biased seeding was used to reduce singularities and make the mesh finer in these areas.

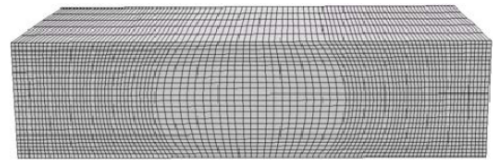

(c) Board I

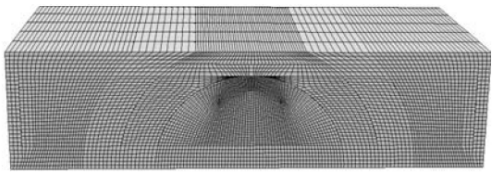

(b) Board II

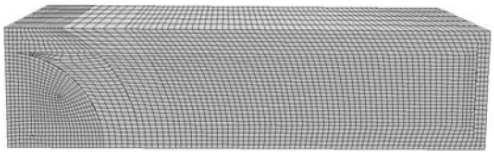

(a) Board III

Figure 4: The element mesh of the timber boards studied, where the pith being placed either (a) in the centre of the board (Board I), (b) at the centre of the lower surface of the board (Board II), or (c) at the lower left corner of the board (Board III).

Material parameters

The material parameters used in the model are the same as used in Larsen et al. (2012) and in Ormarsson (1999). The stiffness, mechano-sorption, shrinkage and temperature related parameters used are representative for Norway spruce. The different radial shrinkage coefficients for heartwood and sapwood obtained in experimental studies presented in Larsen et al. (2010, 2011) and in Rosner et al. (2009) supplements the shrinkage coefficients presented in Ormarsson (1999). The tangential shrinkage coefficient was assumed to be twice as large as the radial coefficient, both for the heartwood and the sapwood.

The moisture histories of the timber boards are based on the experimentally obtained water flux results presented in the next chapter. Each part, the sapwood part, for example, is assumed to consist of a sub-part in the centre and two outer layer sub-parts. Each sub-part has its own moisture history, in which the MC-curve for the outermost layer moves to a point 5% lower than the MC-curve for the next layer that again moves to a point 5% lower than the MC-curve for the central volume. This is a simplified estimation of the moisture gradient that exists from the centre of the board to the surface. The average of these three MCs follows the average moisture history as described in Figure 7; this implies that some of the sub-parts have an MC that is below average and others one that is above average, as shown in Figure 5.

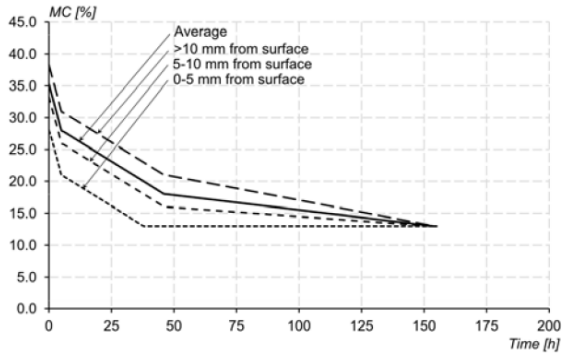

Figure 5: Examples of moisture histories within a given sub-volume (parts).

Results and discussions

The results of the water flux experiments presented below were used as an input (driving force) for the stress simulations of the kiln-dried timber boards that showed a marked variation in MC values in the green condition.

Water flux experiments for estimation of moisture histories

Several water flux tests in the tangential and the radial directions were performed in a climate chamber at three different temperatures (20, 60 and 90 °C) and three different humidity levels (70, 80 and 90% RH). The aim of these experiments was to explore the dependence of the water flux on the temperature, the humidity and the radial and the tangential material directions. Investigations of timber drying are often concerned simply with moisture related behaviour below the FSP level, but the drying history above the FSP level for board samples consisting of both heartwood and sapwood is also of considerable interest. The test specimens used for the water flux experiments are shown in Figure 2. The experiments were carried out in the climate chamber, in which a number of specimens were dried simultaneously in the tangential and the radial drying direction, respectively. This eliminated the risk of variations in climate between two similar experiments. Specimens with one drying direction (radial or tangential) were grouped and were placed separately on a stand. The temperature, humidity and air flow around the specimens were kept constant throughout the experiment. The specimens involved and the drying conditions were identical for both the drying

directions. The moisture histories obtained showed no appreciable differences in drying speed between these two directions. The water flux in the two directions is thus, insofar as one can determine, identical, although the cell structure of the softwood provides the radially directed cell sides with far more pits than the cell sides in the tangential direction. This suggests that the ray cells in the tangential direction likewise contribute to the moisture flux.

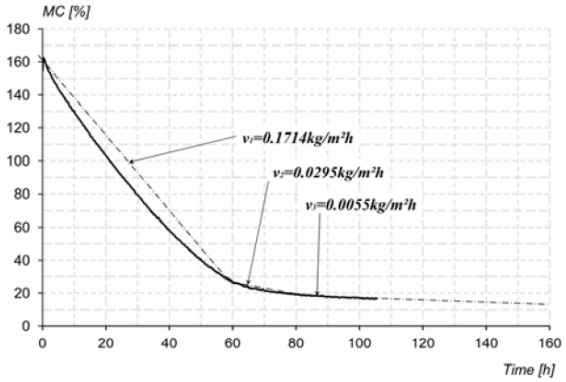

Figure 6: An experimentally obtained moisture history for sapwood at 60 °C and 80% RH and the associated water flux during the three different drying phases (that above FSP, slightly below FSP and that below FSP).

To obtain portions of both heartwood and sapwood of sufficient size in one and the same timber board, the cross section were selected as being 50x200 mm in size; see Figure 3 (and Figure 7). On the basis of the value of MC in the green condition presented in Larsen et al. (2010, 2012), the average green MC was estimated to 60% in the heartwood area and to 165% for the sapwood, whereas for the transition zones it was linearly graduated between the heart- and sapwood values. The material properties used were those representatives for Norway spruce with a density of 450 kg/m^3 at 12% MC. The moisture gradient from the surface to the centre was estimated on the basis of moisture profiles with use of film flow presented by Salin (2010); see Figure 1. Each sub-volume of the board, i.e. heartwood, transition zones and sapwood, has its own surfaces from which water can evaporate during drying. The moisture histories of these sub-volumes were estimated on the basis on the water flux measurements presented above. The moisture history of the sapwood (at 60 °C and 80% RH) and the associated water fluxes, for example, are shown in Figure 6. The water flux was determined on the basis of

$$v = \frac{\Delta m}{A_{surf} \Delta t} \tag{1}$$

where Δm is the change in weight of a sub-volume, A_{surf} is the surface area associated with this sub-volume, Δt is the time during which the weight loss occurred, and v is the water flux. It was found that the water flux started with a relatively high flux until FSP (for 25% MC) was reached, at this point the flux was reduced and then remained constant until approximately 18% MC, at which point the flux was reduced again to a constant value until 13% EMC was reached. The water flux was divided into these three MC phases, each phase involving a constant moisture loss velocity. The MC-curves in Figure 7 show the average values for each of the sub-volumes. The water content in each of the different sub-volumes of the timber board was calculated on the basis of the different sub-volume sizes, the density and the moisture content. The amount of water, m_{water}, in each sub-volume was calculated as

$$m_{water} = \frac{V \cdot \rho_{wood\_12\%} \cdot w}{k_1} \tag{2}$$

where V is the volume of the respective sub-volume of the wood, $\rho_{wood\_12\%}$ is the wood density at 12% MC, k_1 is a constant = 112 and w is the moisture content in [%]. The time needed for drying a given sub-volume within each of the drying phases i from a moisture content of w_u down to a moisture content of w_l is calculated as

$$t_i = \frac{V \cdot \rho_{wood\_12\%} \cdot (w_u - w_l)}{v_i \cdot A_{surf} \cdot k_1} \tag{3}$$

where w_u is the upper (limit) moisture content value in [%], w_l is the lower (limit) moisture content value and v_i is the water flux for the respective drying phase. The average course of drying for each of the sub-volumes starts at the green MC condition, the water flux thereafter being governed by the surface area and the average MC within each part. It was assumed that the water vapour did not move from areas of low MC to areas of higher MC. All the moisture histories were generated on basis of these conditions. Figure 7 shows the dimensions, sub-volume patterns and drying histories used for modelling of the timber boards that were studied.

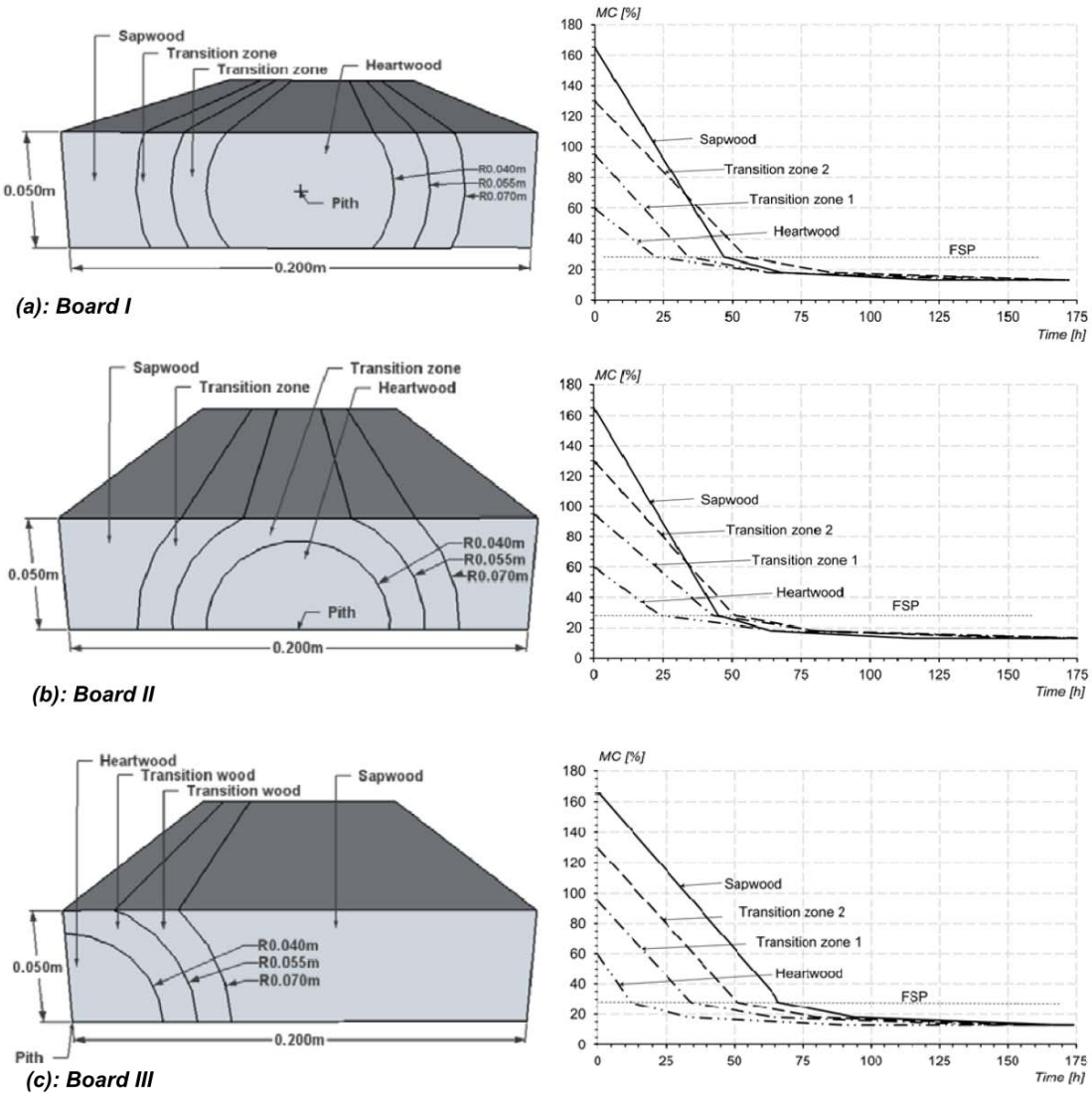

Figure 7: The geometry, sub-volume patterns and associated drying histories for the timber boards that were where the pith being placed either (a) in the centre of the board (Board I), (b) at the centre of the bottom surface (Board II), or (c) in the left corner of the bottom (Board III).

Note that the moisture histories presented in Figure 7 are based on simplifications, the water flux behaviour close to edges and the interaction between different zones in the cross section not being taken into account. The moisture histories show, even with the use of this approach, that the different parts are of value below FSP at quite different times.

Modelling of timber boards

Simulated deformations and the stress development during the drying process for each of the three timber boards are shown in Figure 8. Attention is directed here primarily at the development of tangential stress, since the strength in this direction is appreciable less than in the radial direction; see e.g. Gustafsson (2003) and Bodig et al. (1982). Climatic conditions of 60 °C and 80% RH were used here. This resulted in a FSP of approx. 28% MC and an EMC of approx. 13% MC; see e.g. Simpson (1973). The shrinkage coefficients for the transition zones were graduated between the

heartwood and sapwood values. The simulations show that each of the stresses varies markedly in the course at the drying process, the levels not necessarily being highest at the end of the process, Figure 8 showing the tangential stress distribution within boards I, II and III after 15 and 165 h of drying, and Figure 9 showing the (total) strain distribution for the boards after drying of 165 h.

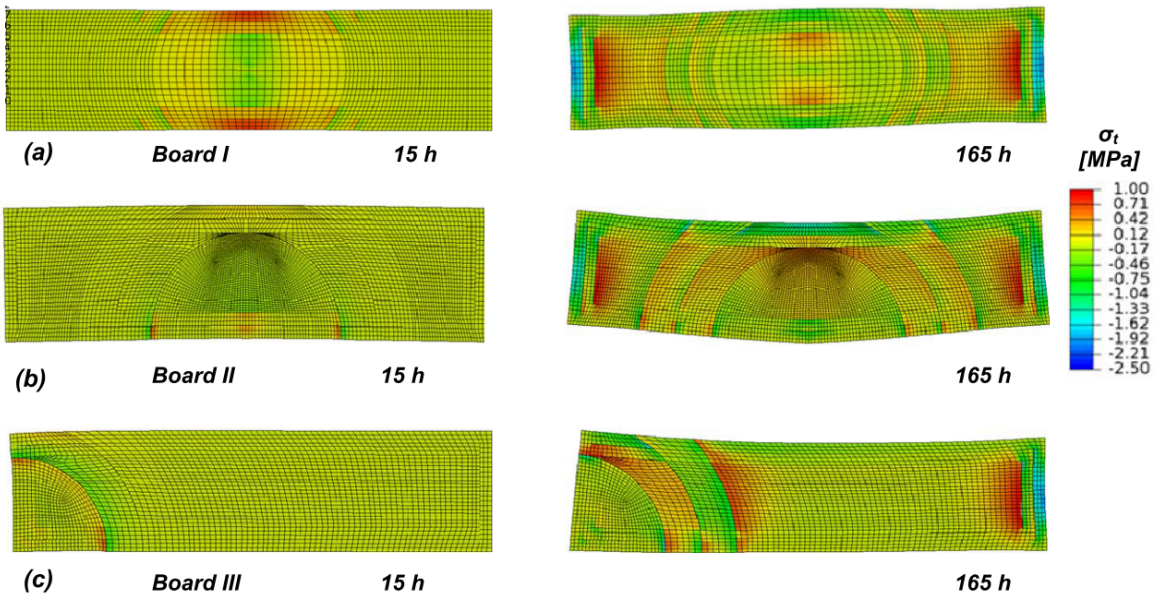

Figure 8: The simulated tangential stress distribution within the timber boards studied after 15 h and 165 h of drying at 60°C and 80% RH: (a) Board I, (b) Board II, (c) Board III.

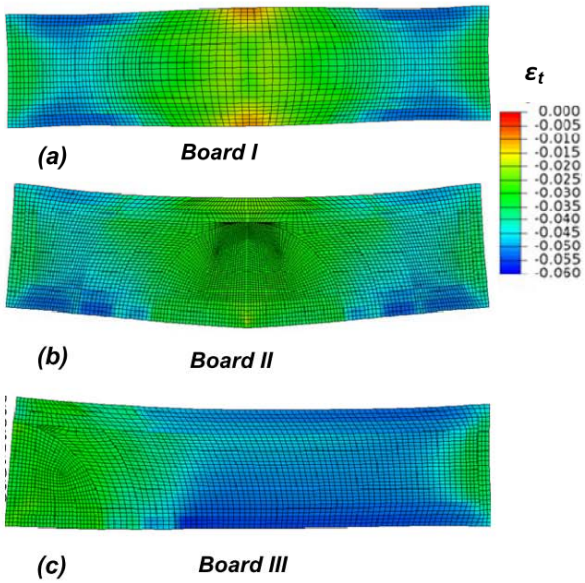

Figure 9: The simulated tangential strain distribution within the timber boards studied after 165 h of drying at 60°C and 80% RH: (a) Board I, (b) Board II, (c) Board III.

Figure 8(a) shows board I after 15 hours of drying, where only the outer layers of the heartwood zone having dried to below FSP. As can be seem, this resulted in quite strong tensile stresses of a

magnitude of up to 0.8 MPa at the centre of the top and the bottom surfaces. At the end of the drying, the stress distribution has changed markedly to a slight compression on the outer surfaces and maximum tensile stresses (of 1.0 MPa) inside the sapwood. For the final EMC state (Figure 8(a)) the strain distribution in the tangential direction shows marked mechano-sorption effects both in the heartwood and the sapwood areas, because of the strains in some sub-parts being markedly lower than in the case of free shrinkage, the stresses there being almost nil. Figure 8(b) shows the stress distribution within board II. In the early phase, only the outer layers of the heartwood zone dried to below FSP; this gave rise to tensile stresses close to the pith of 0.6 MPa in magnitude at the surface. As for board I the stress distribution changes markedly as the drying progresses. Note the large tensile stresses (of up to 1.0 MPa) at the end of the drying process at several places inside the cross section, the tangential strain distribution also showing marked mechano-sorption effects here, both in the heartwood and the sapwood areas. Figure 8(c) shows the stress distribution for board III, which in the early phase (15 h) showed the maximum tensile stresses (of 0.75 MPa) in the area between the heartwood and the first transition zone. The strongest tensile stress occurred finally in the area around the transition zones and close to the right vertical surface. The tangential strain distribution in Figure 9(c) shows lesser mechano-sorption effects within the heartwood and the sapwood areas than the two other boards do, but the strains in the transition zones are more strongly affected here. The difference is due to the heartwood area here drying down to a level close to EMC much earlier than in the other parts, resulting in a constant MC for the heartwood when the large sapwood part starts to dry.

The simulations of the boards showed the stress development for the sapwood to be quite similar in all of them. The outer layers shrink early in the drying process, due to the moisture gradient, which produces tensile stresses in the outer layers at an early stage in the drying process, and later in the drying process a small area inside these layers became in tension when the outer layers have dried down to EMC. The differences in behaviour between the boards that were studied were due primarily to how the heartwood dried, board III in which the pith was located in the corner drying much faster than the heartwood of the two other boards did. The ratio of the surface areas to the associated volumes is a good indicator of the drying speed. A larger ratio indicates faster drying of the volume involved. Table 1 lists these ratios, the relative sizes of which confirm the statements made above.

Table 1: Relation between the surface area (A) and the volume (V) for all parts of the cross sections.

Area	Board I	Board II	Board III
	A/V [m^{-1}]	A/V [m^{-1}]	A/V [m^{-1}]
Heartwood	33,6	31,8	63,7
Trans. Zone 1	45,5	36,4	46,0
Trans. Zone 2	43,3	46,9	46,9
Sapwood	67,4	71,7	48,5

A parametric study was carried out to investigate how the shrinkage coefficients affect the stress development during drying in the boards that were studied. The shrinkage coefficients were made identical for each of the four sub-volumes (just as in the case of the sapwood) and the moisture histories being identical to those of the original simulations. Second parametric study was carried out to investigate whether the displaced moisture histories had any effect on the stress development during the drying process. Each of the three boards was simulated, making use of the same moisture history for each of the sub-volumes, the drying starting simultaneously from FSP. The shrinkage coefficients were graduated from the heartwood to the sapwood, as in the original simulations. The tangential stress history at one point, located in the centre of the transition zone closest to the

heartwood, is presented for each of the three boards in Figure 10. The three curves in each subfigure represent stress results calculated with use of the three types of simulations mentioned above: Sim I) the original (reference) simulation having strong (spatial) variation in the initial MC values and different tangential shrinkage coefficients (0.2, 0.3) for the heartwood and the sapwood, Sim II) a simulation with the same initial MC variation as employed in the reference simulation (Sim II) and the same shrinkage coefficients (0.3, 0.3) for both the heartwood and the sapwood, and Sim III) a simulation with use of the same shrinkage properties as in Sim. 1 and with a constant initial MC = FSP for the cross section as a whole.

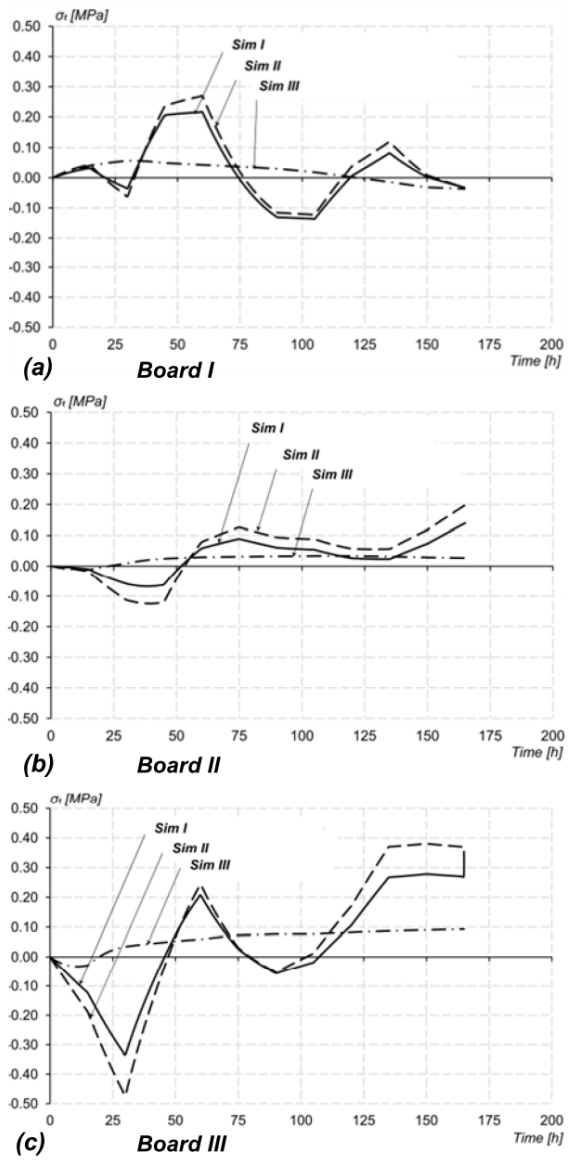

Figure 10: The simulated tangential stress history at the centre of the transition wood closest to the heartwood for each of three different material and moisture conditions, for (a) Board I, (b) Board II and (c) Board III. Sim I shows variations both in MC and in the shrinkage coefficients, Sim II shows variations in MC as for Sim I and the same shrinkage coefficients for both the cross section as a whole, Sim III shows constant initial MC=FSP overall, and the same shrinkage coefficients as in Sim I.

The figure shows clearly how variations in the initial MC over the cross-section have a strong effect on the development of stresses for each of the boards. The stresses become appreciably stronger for boards having initial variation in MC, especially boards I and III. Variations in the shrinkage parameters were also found to affect the stress development to some extent.

Conclusions

Although the fact of a moisture gradient over the cross section of timber boards being found during drying below the FSP level is well known, the initial variation in the moisture level over a cross section under green conditions is often ignored in stress simulations, the initial moisture state frequently being assumed to be equal to the MC at the FSP level. When wood dries from a green condition to a level below the FSP and variation in the initial MC is present, certain parts of the cross section dry to al level below the FSP. The fact that the times at which this occurs differ, create the risk of an increase in the moisture gradients, one that can lead to unexpected constrains. The stress simulations of the boards that were studied showed there to be variations in the green MC, variations of the shrinkage coefficients and of the sawn pattern having marked effects on the stress development occurring during the drying process. The sawn pattern in which the pith is located at the edge was found to be the one most critical in terms of a buildup of stresses. If there are large variations over a cross-section in the initial MC level found, the moisture gradient can be reduced if the humidity around the board is kept as high as possible during the initial drying phase on until the parts having the highest MC values become close to the FSP. This is illustrated in Figure 10, in which the tangential stress is shown to be less for boards having a constant initial MC over the cross section as a whole.

Future work

The stress model for timber boards presented here needs to be developed further as regards moisture related fractures. Also, the moisture and temperature flow need to be simulated with use of FEM, the initial (green) moisture gradient over the cross sections needing to be dealt with as well. Simulations could be performed at certain temperature and humidity levels that could be reproduced experimentally. With use of a climate chamber and a digital image correlation system it is possible to measure the strain field in wood specimens during drying under well-defined climatic conditions. The measured strain development could then be compared with the strain development according to the stress model, in this providing a verification of the model.

Acknowledgement

Funding:
The Danish Forest and Nature Agency, Haraldsgade 51, 2100 København Ø.

Reference

ABAQUS. *Theory manual v6.8.* Simulia, 2008.

Bodig J. and Jayne B.A.: Mechanics of wood and wood composites. Van Nostrand Reinhold Company, New York, 1982.

Ekevad M., Lundgren N. and Flodin J.: Drying shrinkage of sawn timber of Norway spruce (Picea abies): Industrial measurements and finite element simulations. Wood Material Science and Engineering. 6:41-48, 2011.

Fortino S., Mirianon F. and Toratti T.: A 3D moisture-stress FEM analysis for time dependent problems in timber structures. Mech Time-Depend Mater. 13:333-356, 2009.

Gustafsson P.J.: Timber Engineering. John Wiley & Sons Ltd. Pages 103-130, 2003. ISBN 0-470-84469-8.

Krabbenhøft K.: Chapter 4 and 5, Moisture Transport in Wood. A Study of Physical-Mathematical Models and their Numerical Implementation. Ph.D. Thesis. ISBN nr. 87-7877-225-7. Denmark, 2003.

Larsen F., Ormarsson S. and Olesen J.F.: *Proceedings of the 11th International IUFRO Wood Drying Conference, 2010*. 137-144, Luleå University of Technology, Skellefteå, Sweden.

Larsen F., Ormarsson S. and Olesen J.F.: *Proceedings of the 11th World Conference on Timber Engineering, 2010*. 449-451, Riva del Garda, Italy.

Larsen F., Ormarsson S. and Olesen J.F.: Moisture-driven fracture in solid wood. In Wood Material Science and Engineering. 6(1-2):49-57, 2011.

Larsen F. and Ormarsson S.: Numerical and experimental study of moisture-induced stress and strain field developments in timber logs. Wood Science and Technology, 2012.

Mounji H., El Kouali M., Bouzon J. and Vergnaud J.M.: Modelling of the drying process of wood in 3-dimensions. Drying Technology 9(5):1295-1314, 1991.

Ormarsson S., Dahlblom O. and Petersson H.: A numerical study of the shape stability of sawn timber subjected to moisture variation part 1: Theory. Wood Science and Technology 32:325-334, 1998.

Ormarsson S., Dahlblom O. and Petersson H.: A numerical study of the shape stability of sawn timber subjected to moisture variation part 2: Simulation of drying board. In Wood Science and Technology. 33:407-423, 1999.

Ormarsson S.: Numerical Analysis of Moisture-Related Distortions in Sawn Timber. PhD thesis. ISBN 91-7197-834-8. Göteborg, Sweden, 1999.

Rosner S., Karlsson B., Konnerth J. and Hansmann C.: Shrinkage processes in standard-size Norway spruce wood specimens with different vulnerability to cavitation. Tree Physiology 29:1419-1431, 2009.

Salin J.-G.: Problems and solutions in wood drying modelling: History and future. In Wood Material Science & Engineering. 5:123-134, 2010.

Simpson W.T.: Predicting equilibrium moisture content of wood by mathematical models. Wood and Fiber Science 5:41-49, 1973.

Wiberg P., Sehlstedt-Persson S.M.B. and More'n T.J.: Heat and Mass Transfer During Sapwood Drying Above the Fibre Saturation Point. Drying Technology 18(8):1647-1664, 2000.

Yiotis A.G., Stubos A.K., Boudouvis A.G., Tsimpanogiannis I.N. and Yortsos C.Y.: Modeling of Drying Processes in Pore Networks. Mathematics in industry 8:293-297, 2004.